UNIVERSITÀ DEGLI STUDI DI PADOVA

UNIVERSITA' DEGLI STUDI DI PADOVA

DIPARTIMENTO DI INGEGNERIA INDUSTRIALE

CORSO DI LAUREA MAGISTRALE IN CHEMICAL AND PROCESS ENGINEERING

Tesi di Laurea Magistrale in

Chemical and Process Engineering

Analysis and techno-economic comparison of bio-hydrogen production processes

Relatore: Prof.ssa Elena Barbera

Correlatore: Prof.ssa Eleonora Sforza

Laureanda: LAURA BENVENUTO

ANNO ACCADEMICO 2023 - 2024

Abstract

The objective of this thesis is to investigate two biological routes for hydrogen production, as hydrogen is considered a promising energy carrier for the future. The processes analysed are Dark Fermentation and Photofermentation: they require different type of microorganisms and distinct environmental conditions to operate efficiently. Biological processes, as the ones considered in the current study, present several challenges that make their applicability in larger scales difficult. In fact, they involve complex biological systems and are characterised by relatively low production yields compared to conventional chemical processes. In addition, these processes are highly sensitive to operating conditions and therefore require a precise control system to maintain an optimal environment, that can be complex and costly.

In the current study, process simulation is used to address material and energy balances for the dark fermentation process. The simulation of the process relies on the results of the kinetic model employed for describing the kinetics of the reactions involved. For the photofermentation process, mass balances are computed based on the literature values for the specific hydrogen production. Then, process simulation outcomes and mass balances are used to perform an economic analysis both for the single dark fermentation process and for the combined processes. Moreover, the economic results are exploited to estimate a key indicator related to the economic performance of such processes. Different scenarios are considered in order to evaluate the optimal solution in terms of the levelized cost of hydrogen (LCOH). The research focuses on a techno-economic analysis of these processes, aimed at evaluating their potential for industrialization and small-medium scale production. The results obtained highlight, on one hand, the economic advantages of employing a single-stage dark fermentation process, while, on the other hand, they emphasize the limitations related to the implementation of the photofermentation, mainly due to technologies that should be optimized for this process.

Table of Contents

Introduction

In recent decades, the rapid growth in energy demand has put significant pressure on the global energy sector, largely due to increasing daily human activities. Fossil fuels currently dominate the energy production worldwide, but the fast depletion of fossil reserves, along with the increasing population, highlights the need for alternative energy sources. Additionally, fossil fuels are major contributors to greenhouse gas (GHG) emissions, which result in global environmental issues. To meet the 2030 GHG emission targets, a substantial reduction in the use of fossil fuel is essential. Consequently, there is a strong focus on developing renewable energy technologies that should have a more sustainable impact compared to current ones. As alternative energy sources, hydrogen represents a promising biofuel for several applications that could lead to a significant contribution towards decarbonization in energy-hard-to-abate sectors, such as transportation and logistics. Hydrogen is a clean biofuel with zero CO_2 emissions, meaning it has no adverse impact on the environment. In fact, from its combustion no CO_2 is released into the atmosphere. Additionally, hydrogen has a very high energy content per unit mass, which is nearly three times greater than that of traditional fuels. Therefore, increasing hydrogen production through clean and sustainable methods is pivotal for reducing GHG emissions.

The current thesis analyses two biological processes for hydrogen production: dark fermentation and photofermentation. These processes involve the valorisation of organic substrates by specific types of microorganisms capable of converting them into biohydrogen. Both processes require distinct and specific operating conditions and are highly sensitive to slight variations of process parameters, such as temperature, pH, hydraulic retention time and, in the case of photofermentation, illumination. Additionally, biohydrogen production can be enhanced by combining these two processes in series, as the by-products of the dark fermentation process, which are primarily volatile fatty acids, serve as the substrate for the photo fermentation process.

The aim of this thesis is to investigate the economic feasibility of these two biological routes for hydrogen production on an industrial scale, considering a small-medium sized capacity plant. The processes considered in the analysis are the single-stage dark fermentation process and the combined dark and photo fermentation process. The feedstock for the process is a waste activated sludge, which is disposed by a wastewater treatment plant. The process by-products are separated and purified to enable process valorisation through sale, since they generate a revenue which may offset the overall biohydrogen production cost. A techno-economic analysis is performed to assess and compare the

values of a specific economic indicator for hydrogen production, namely the Levelized Cost of Hydrogen (LCOH).

This thesis is organized into three chapters. The first chapter provides a comprehensive overview of the state of art concerning hydrogen and the industrial processes currently employed for its production. Additionally, it describes the biological processes, including biophotolysis and fermentation processes (both dark and photo). Regarding the photofermentation process, the focus is on purple non-sulphur bacteria (PNSBs), their immobilization strategies and the experimental setup. Finally, a two-stage process combining dark and photo fermentation is introduced.

The second chapter initially presents the block flow diagram for both processes, along with the hydrogen production target for the plant. Additionally, the kinetic model employed in the dark fermentation process is introduced. Following this, the simulation performed in Aspen Plus is illustrated, detailing the various components, reactions and units involved. Moreover, the procedure and assumptions made for the photofermentation stage are described. Finally, the method used for the analysis of capital and operating costs, as well as the evaluation of the LCOH, is presented.

The third chapter shows the results of the economic analysis and consequently, of the LCOH, considering different scenarios. For the single-stage dark fermentation process, six scenarios are distinguished based on the assumption of the feedstock cost and on the possible recovery of the VFAs. Then, the best case-scenario is taken into account to evaluate the LCOH for the combined process. Finally, a sensitivity analysis is carried out to assess the effect of key variables on the LCOH.

I would like to extend my thanks to PhD student Grant Keet and Professor Robert Pott from Stellenbosch University for their collaboration on this work and for the reference they provided to me through their contribution.

Chapter 1

State of art

In this chapter, the main characteristics of hydrogen as an energy carrier alternative to conventional fuels currently in use will be outlined. Additionally, the primary processes and alternative routes by which hydrogen is produced are presented, highlighting the most significant aspects regarding energy and economic performance of each, as well as their environmental impact.

1.1 Introduction

Over the last few decades, the energy demand has increased rapidly, leading to a greater pressure on the energy sector. This trend is primarily driven by the growing energy needs of daily human activities. The current energy supply relies on fossil fuels across the world. However, due to the fast depletion of fossil reserves, along with the increasing population, there is an urgent requirement for alternative energy sources (Gürtekin, 2024). Additionally, fossil-based fuels contribute to greenhouse gas (GHG) emissions that result in global environmental challenges. Thus, a strong reduction in the use of fossil fuels must be achieved in order to meet the 2030 GHG emission targets, according to recent reports from the Intergovernmental Panel for Climate Changes (IPCC) and International Energy Agency (IEA). In this context, there is a drive to develop and promote new technologies based on renewable energies, which therefore should have a more sustainable impact compared to current ones. As alternative energy sources, bioethanol and biodiesel, obtained using chemical or biological processes, have gained particular attention due to their characteristics similar to the conventional liquid fuels. Among these biofuels, hydrogen represents a suitable energy carrier for several applications and a promising alternative fuel that could lead to a significant contribution towards decarbonization in energy-hard-to-abate sectors, such as transportation and logistics (Staffell I. et al., 2019). For this reason, its production needs to be significantly increased, through investigating clean and sustainable routes to reduce GHG emissions.

1.2 Hydrogen

Hydrogen (H_2) plays a pivotal role in the global energetic transition towards sustainability, as it emerges as a versatile and environmentally friendly energy carrier. Its inherent qualities, such as high energy density and zero greenhouse gas emissions, position it as a promising alternative to conventional fuels. Hydrogen has a very high energy content: the energetic density per unit mass of hydrogen (141.9 MJ/kg Higher Heating Value, HHV) is nearly 3 times higher compared to traditional fuel sources (gasoline 44 MJ/kg and diesel 42 MJ/kg) (Kapdan and Kargi, 2006). This can be an advantage for its application on fields where the lightness is required, as the aerospace industry. On the other hand, it has a very low volumetric energetic density at atmospheric pressure, as Figure 1.1 shows. Even when compressed or liquefied, hydrogen's volumetric energy density is significantly lower than conventional fuels. This means that to store a significant amount of energy, hydrogen requires large tanks and must be stored as compressed gas under high pressure (350-700 bar) or at cryogenic temperatures ($T_b = -252.8\,°C$) as liquid hydrogen, which involves technical issues and further costs. Additionally, hydrogen can be stored in solid materials, either absorbed or chemically bound on the surface (Møller et al., 2017).

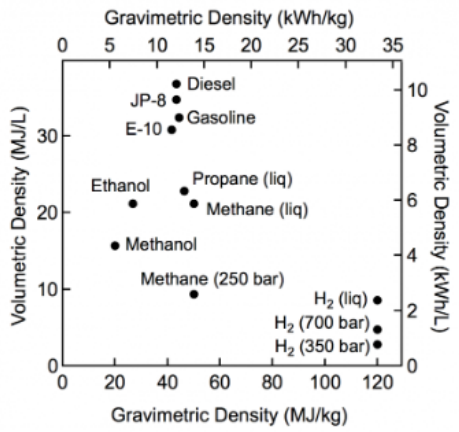

Figure 1.1: Gravimetric density [kWh/kg] and volumetric density [MJ/L] referred to different fuels (Source: U.S. Department of Energy, Fuel Cell Office, https://www.energy.gov/eere/fuelcells/hydrogen-storage)

Hydrogen is regarded as a crucial clean energy carrier because of its potential to produce energy without adverse environmental impacts. In fact, only water is produced from its combustion, thus no CO_2 is released into the atmosphere.

1.3 Processes for H_2 production

According to the industrial processes used for its production, hydrogen may be labelled using different colours: grey hydrogen produced from natural gas via Steam Methane Reforming (SMR), blue

hydrogen obtained as grey hydrogen but with additional carbon capture and storage (CCS), green and "grid" hydrogen, both produced by water electrolysis but using different sources of energy (renewable and grid electricity, respectively).

1.3.1 Steam methane reforming (SMR)

The majority of hydrogen (96%) is produced from fossil fuels, primarily through steam methane reforming (SMR) of natural gas. SMR alone accounts for roughly three-quarters of global hydrogen production. This process uses heat and pressure to convert methane from natural gas into hydrogen and carbon dioxide. The hydrogen produced via SMR is commonly referred to as "grey hydrogen," distinguishing it from "brown hydrogen," which is derived from coal gasification (Howarth and Jacobson, 2021). The SMR process consists of a catalytic conversion of methane into a mixture of CO, CO_2 and H_2 according to the following reactions:

$$CH_4 + H_2O \rightarrow CO + 3H_2 \qquad (\Delta H_R = 206 kJ/mol) \qquad (1.1)$$

$$CO + H_2O \rightarrow CO_2 + H_2 \qquad (\Delta H_R = -41\ kJ/mol) \qquad (1.2)$$

The process is mainly divided into three sections (Figure 1.2). The natural gas (NG) first undergoes a desulphurization treatment to remove sulphur, which is a poison for the catalyst. In the reforming section the desulphurized feed is converted to H_2 and carbon oxides in the presence of steam. In the catalytic reforming the main reaction (Equation (1.1)) is endothermic and requires significant amount of energy to provide the necessary heat. This energy is supplied almost entirely by the natural gas, which is burnt with air and tail gases in a furnace to provide the heat duty required in the reformer (Lee et al., 2021). The reaction occurs at high temperature and pressure (T = 500-1200 °C, P = 30 bar) over the catalysts, that can either be non-precious metals, typically nickel, or precious ones, as platinum and rhodium. However, due to the minimal effectiveness of catalyst, typically 5%, non-precious metals are mostly used (Abdalla et al., 2018). The steam to carbon molar ratio is maintained at 3 to prevent the coke deposition on the surface of the catalyst, which could eventually lead to its inactivation.

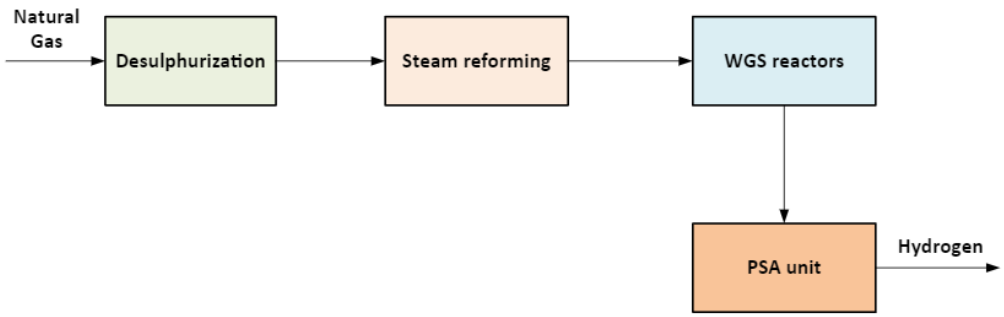

Figure 1.2: Aspen Plus process flowsheet of the SMR process.

To increase the hydrogen yield, the CO obtained in the reforming section is catalytically converted to CO_2 and H_2 according to the Water-Gas Shift (WGS) reaction (1.2), which is slightly exothermic. The reaction occurs in two stages: the first at high temperature (T = 400 °C) over iron oxide catalyst and the second at lower temperatures (T = 250 °C) over copper oxide catalyst.

The product gases are cooled down and hydrogen is purified by means of a pressure swing adsorption (PSA) unit, which allows the separation of hydrogen from the gas mixture. Almost 85% of H_2 is purified utilizing PSA, due to its high effectiveness, flexibility and low energy consumption (Shabbani et al., 2024). This method exploits the different adsorption capacities of gases on adsorbent materials at various pressures.

1.3.2 SMR with carbon capture and storage (CCS)

The SMR process can be enhanced by integrating carbon capture and storage (CCS) to manage CO_2 emissions directly associated with the process. The hydrogen produced by this method is called “blue hydrogen”. The CCS system targets two emission streams, as SMR produces two distinct types of CO_2 emissions: process emissions, originating from the SMR and WGS reactions, and combustion emissions, which come from the furnace where natural gas and tail gases are burned after H_2 purification. These two streams exhibit significant differences in CO_2 partial pressure and flow rate: tail gases, characterized by a high CO_2 concentration, present a more favourable and less energy-intensive option for capture compared to the more diluted flue gases. However, a substantial amount of CO_2 would still remain uncaptured (Meerman et al., 2012). The technique commercially available for the CO2 capture is the gas absorption, that can adopt physical or chemical solvents. Physical solvents are more suitable for high CO_2 partial pressure streams, whereas chemical solvents are more

appropriate for low CO_2 partial pressures as the loading capacity is much higher compared to the physical ones. For CO_2 absorption, a crucial class of chemical absorbents is amines, which can form carbonates-specific chemical bonds that favour absorption. These bonds are not very strong and can be broken down during stripping. Therefore, the absorption process is coupled with a stripping section to regenerate and recycle the solvent, as shown in the schematic representation in Figure 1.3. Typically, steam is used for stripping CO_2 from the amine solution. In this scenario, a reboiled stripper is utilized, where steam is generated within the reboiler itself through the recirculation of the bottom liquid (Barbera et al., 2022).

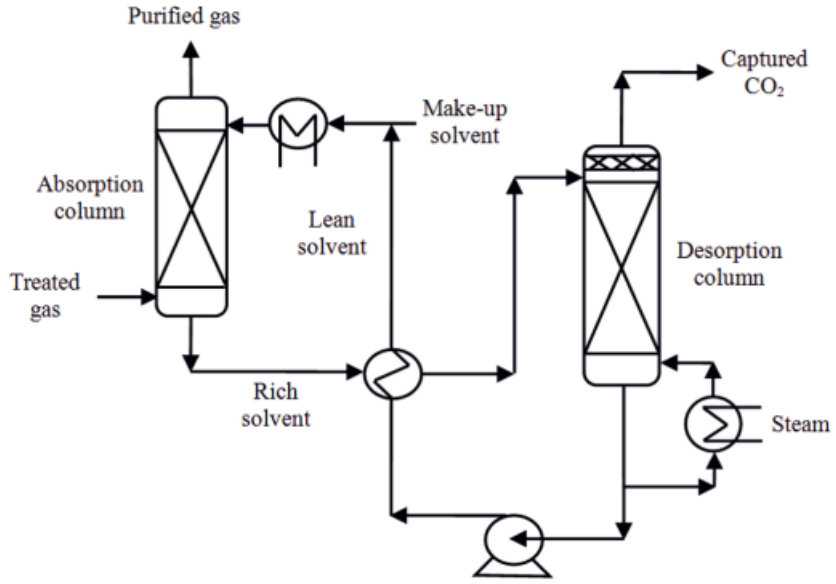

Figure 1.3: Process flowsheet of the absorption/stripping CO_2 capture process (Source: Cormos et al., 2016).

1.3.3 Water electrolysis (WE)

Water electrolysis involves the electrochemical separation of water into gaseous hydrogen and oxygen due to the application of an electrical voltage to a cell comprising electrodes, according to the following half-reactions:

$$\text{Cathode}: 2H_2O + 2e^- \rightarrow H_2 + 2OH^- \quad (1.3)$$

$$\text{Anode}: 2OH^- \rightarrow \frac{1}{2}O_2 + H_2O + 2e^- \quad (1.4)$$

Electrolysis processes comprise a cell stack, consisting of multiple electrolytic cells connected in series, which forms the core component of the system. Additionally, the balance of plant (BoP) encompasses all other necessary units for product purification, liquid purification, and related

functions. Water electrolysis systems are classified according to the operation temperature as low-temperature (ambient condition to 100 °C) and high-temperature (800-1000 °C: solid oxide electrolysis cells (SOECs)). The low-temperature systems are further categorized by the type of electrolyte used to separate the two half-reactions occurring at the cathode (hydrogen evolution reaction) and at the anode (oxygen evolution reaction). There are the alkaline electrolysis cells (AECs), proton exchange membrane electrolysis cells (PEMECs), and anion exchange membrane electrolysis cells (AEMECs), as they are illustrated in Figure 1.4 (Ham et al., 2024).

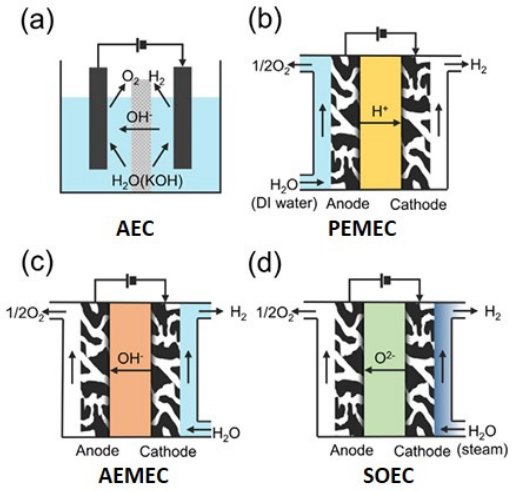

Figure 1.4: WE systems based on different type of electrolytes (Source: Ham et al., 2024).

The AEC has already reached technological maturity since it is the first-generation water electrolysis system and the most traditional one. In the stack, the electrodes are immersed in a liquid electrolyte separated by a diaphragm, characterised by porous membranes. Specifically, a high-concentration alkaline solution (20-30 wt% KOH) is used as electrolyte to reduce the electrolyte resistance. The main limitation is related to the possibility of gas crossover through the membrane, which is more pronounced at high pressure. This issue is addressed in advanced electrolysis technologies like PEMEC and AEMEC, which both utilize gas-impermeable ion exchange membranes that selectively transport only H^+ and OH^- ions. Lastly, the SOEC technologies exploits high-temperature water vapor instead of liquid water and adopts ceramic-based materials due to the severe operating conditions (Ham et al., 2024).

Green hydrogen identifies H_2 obtained from the WE process powered by renewable energy sources, including photovoltaics, wind, hydro, geothermal, biomass and urban waste incineration. Grid hydrogen is always produced by water electrolysis, but in this case the energy source is directly taken from the grid electricity mix, which currently includes both renewable and fossil sources.

1.4 Biological routes for H_2 production

The aforementioned hydrogen production methods are those currently used at an industrial level. However, these technologies rely on non-renewable sources and are not entirely sustainable, except for green hydrogen production process, which exploits renewable sources. Nevertheless, WE requires high quantity of electrical energy which may not be feasible to be implemented at a global scale. For this reason, it is needed to explore alternative hydrogen production processes which exploit different energy sources in order to complement its production. Biological processes mostly operate at ambient temperature and pressure and are expected to be less energy-intensive compared to thermochemical methods of hydrogen production. The biological processes of hydrogen production are dependent on the presence of a hydrogen promoting enzyme. These enzymes are specifically able to catalyze the chemical reaction $2H^+ + 2e^- \leftrightarrow H_2$ (Manish and Banerjee, 2008). Various microorganisms, ranging from prokaryotes (such as anaerobic or facultative aerobic bacteria, cyanobacteria) to lower eukaryotes (i.e. green algae), participate in biological H_2 production, either individually or in mixed consortia (Chandrasekhar et al., 2015). In addition, these processes can use a variety of feedstocks as carbon sources. Moreover, waste materials can also be exploited as a carbon source, thereby promoting waste recycling (Manish and Banerjee, 2008). The use of the wastes for hydrogen production offers an inexpensive source of energy while simultaneously providing waste treatment. These factors contribute to making biological processes a promising alternative to conventional methods for meeting energy demands, thereby replacing fossil fuels (Kapdan and Kargi, 2006). Biological hydrogen production methods (Figure 1.5) can be categorized into direct and indirect biophotolysis, photo fermentation, dark fermentation, a two stage process (integration of dark and photo fermentation) and biocatalyzed electrolysis (GürtekiN, 2024). Fermentation processes, both dark and photo, will be explored in greater detail in the following paragraphs, as they form the core focus of this research project. Meanwhile, a brief overview of the remaining processes will be provided.

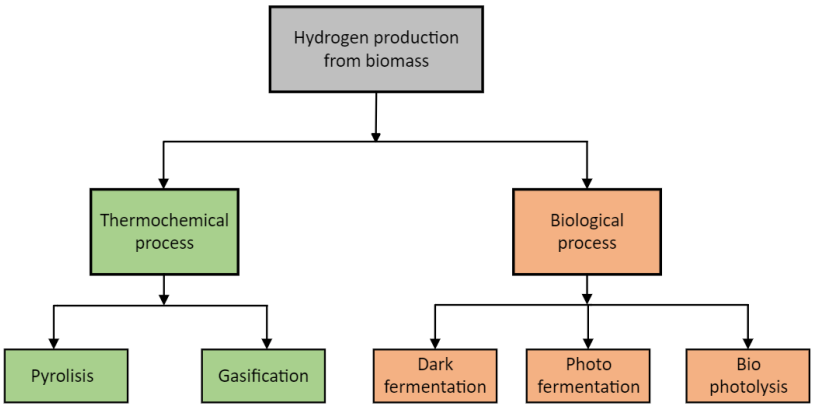

Figure 1.5: Hydrogen production processes starting from biomass (Modified from: Kamran, 2021).

1.4.1 Biophotolysis

In the biophotolysis process, solar energy is used to directly convert water into hydrogen and oxygen via photosynthetic reactions. The biophotolysis process comprises two categories: direct and indirect biophotolysis. Organic substrates undergo catabolism to produce electrons utilized in indirect biophotolysis, while direct biophotolysis uses the electrons generated from water splitting.

- Direct biophotolysis

Direct biophotolysis occurs primarily in photosystem II (PSII), the protein complex involved in the light-dependent reactions of photosynthesis, and which is responsible for the water splitting (Figure 1.6). Here the produced electrons are then transferred through an electron transport chain to reduce protons (H^+) to molecular hydrogen.

$$2H_2O + light\ energy \rightarrow 2H_2 + O_2 \qquad (1.5)$$

It represents a simpler process since it does not require the production and metabolism of intermediate organic substrates. Its limitation is due to the accumulation of oxygen, which can inhibit the enzymes responsible for hydrogen production (i.e. hydrogenase), thereby reducing the overall efficiency of the process. Green microalgae are recognized as the sole microorganisms capable of undergoing direct biophotolysis in an oxygen-free environment. Green microalgae and cyanobacteria are known as "oxygenic photosynthetic microorganisms" because they can exploit sunlight to split water molecules, converting them into chemical energy (Ahmed et al., 2021).

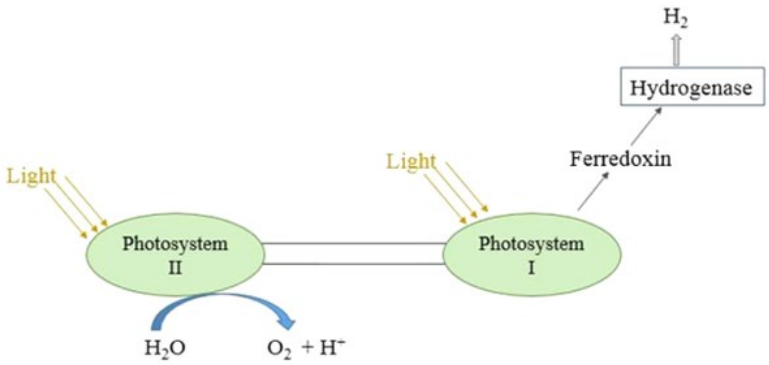

Figure 1.6: Mechanism of direct biophotolysis process (Source: Singh and Sarma, 2022).

- Indirect biophotolysis

In indirect biophotolysis, the electrons required for hydrogen production are derived from the catabolism of endogenous organic substrates produced during the initial stage of photosynthesis. These electrons, generated from the breakdown of organic substrates, are then used to reduce protons into hydrogen (Figure 1.7). This process is performed by microalgae under anoxic conditions. Cyanobacteria have the unique characteristics of fixing CO_2 in the air and using it as a carbon source, and solar energy as an energy source (GürtekiN, 2024). The overall mechanism of H_2 production in cyanobacteria can be represented as:

$$12H_2O + 6CO_2 + light\ energy \rightarrow C_6H_{12}O_6 + 6O_2 \quad (1.6)$$

$$C_6H_{12}O_6 + 12H_2O + light\ energy \rightarrow 12H_2 + 6CO_2 \quad (1.7)$$

Unlike direct biophotolysis, there is no oxygen accumulation during hydrogen production, which can enhance the efficiency of hydrogenase activity. However, the main drawback is the complexity of the process, as it involves more steps compared to direct biophotolysis (Ahmed et al., 2021).

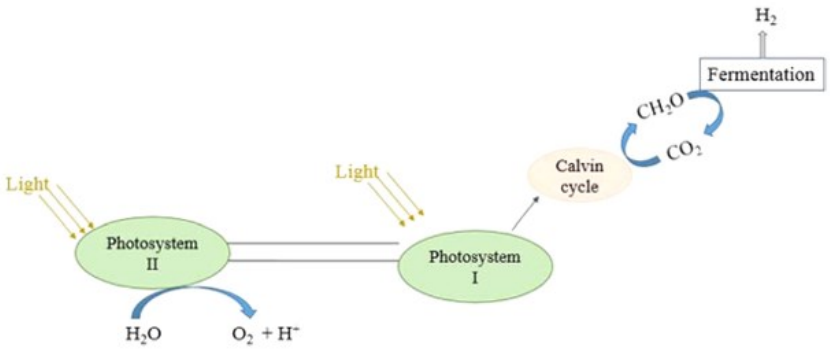

Figure 1.7: Mechanism of indirect biophotolysis process (Source: Singh and Sarma, 2022).

1.5 Dark Fermentation (DF)

Dark fermentation (DF) is a H_2 production technique that involves the valorisation of diverse organic wastes which serve as feedstock for specific microorganisms. In DF, carbohydrate-rich substrates are anaerobically decomposed by hydrogen-producing microorganisms. The bacteria involved in such processes are mainly divided into obligate anaerobes (i.e. *Clostridia*), facultative anaerobes (i.e. *Escherichia coli*) and even aerobes (*Bacillus*) (Li and Fang, 2007). Molecular hydrogen is generated during the disposal of excess electrons through the action of the hydrogenase enzyme. In anaerobic conditions, protons (H^+) serve as electron acceptors, neutralizing the electrons produced by the oxidation of organic substrates, and subsequently forming H_2. This process contrasts with aerobic respiration, where oxygen is reduced, and water is the final product. Substrates for dark fermentation can be lignocellulosic biomass, carbohydrates such as wastewater from industry, sugar-containing crop residues, and municipal solid waste. DF of complex long-chain polymers such as carbohydrates, proteins, and lipids, can result in a wide range of intermediates and by-products through various metabolic pathways, depending on the operational parameters, such as substrate type, pH, temperature, hydraulic retention time (HRT) and other environmental conditions, as they also affect the microbial population inside bioreactors. Not only the types of substrates, but also their pre-treatment methods can influence the biohydrogen production. Figure 1.8 represents the schematic depiction of the biological steps and microbiological pathways involved in the fermentative degradation of complex biomass. These pathways can lead to different theoretical yields of H_2, according to the following reactions:

$$C_6H_{12}O_6 + 2H_2O \rightarrow 2CH_3COOH + 2CO_2 + 4H_2 \quad (1.8)$$

$$C_6H_{12}O_6 \rightarrow CH_3CH_2CH_2COOH + 2CO_2 + 2H_2 \quad (1.9)$$

$$3C_6H_{12}O_6 \rightarrow 4CH_3CH_2COOH + 2CH_3COOH + 2CO_2 + 2H_2 \quad (1.10)$$

Dark fermentation processes produce a mixed biogas containing primarily H_2 and carbon dioxide CO_2, thereby the separation of hydrogen is required to recover the desired product. Acetate and butyrate are the most common products of DF, which are indicated as volatile fatty acids (VFA) (Hawkes et al., 2007). When the metabolic pathway favors the production of acetic acid, the stoichiometric yield of H_2 is 4 moles per mole of glucose, as in Equation (1.8). In contrast, when butyric acid is the final product, the yield is 2 moles of H_2 per mole of glucose. However, the actual hydrogen yield is lower than the theoretical yield because part of the substrate is used for biomass production, and substrate degradation might follow other biochemical pathways that do not produce hydrogen (Ghimire et al., 2015a). Under certain conditions, the metabolic pathways lead to ethanol and acetate production,

reducing the stoichiometric hydrogen yield to 2 moles of H_2 per mole of glucose, according to this equation:

$$C_6H_{12}O_6 + 2H_2O \rightarrow CH_3CH_2OH + CH_3COOH + 2CO_2 + 2H_2 \quad (1.11)$$

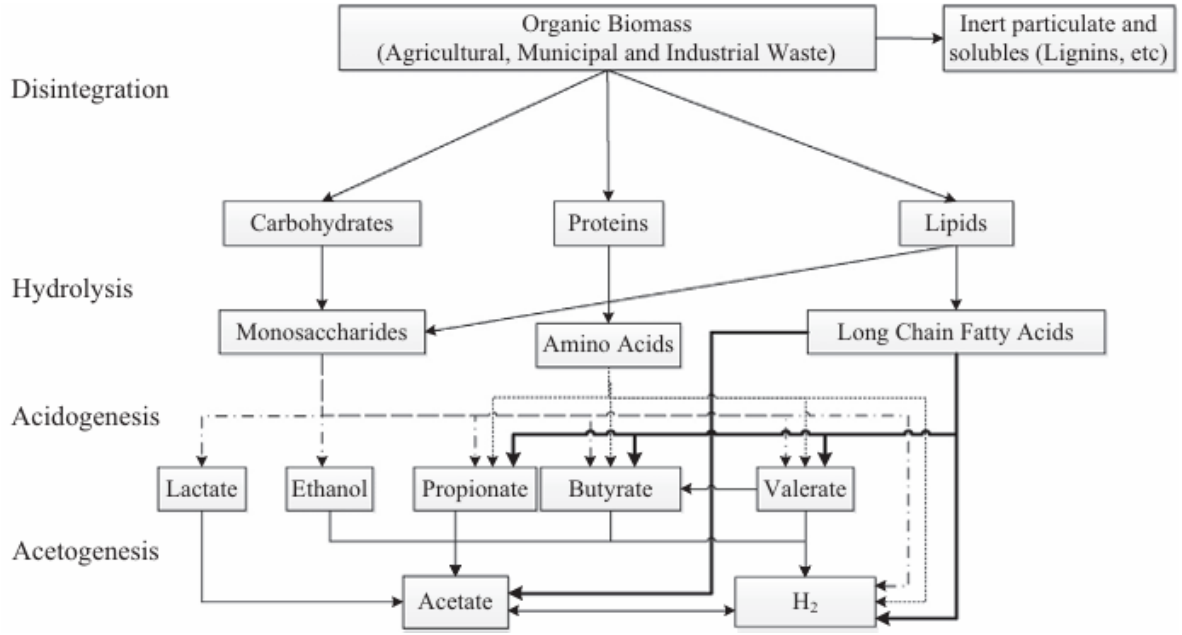

Figure 1.8: Schematic representation of the different steps and biochemical pathways in the DF of complex organic substrates (Source: Ghimire et al., 2015).

Figure 1.8 illustrates the main steps involved in the process. Most of the reactions in dark fermentation are shared with those in anaerobic digestion. Initially, complex organic substrates are hydrolysed to obtain simpler molecules, followed by the steps of acidogenesis and acetogenesis. The key difference from anaerobic digestion is that the ultimate step of methanogenesis must be avoided, as the produced hydrogen should not be further converted into methane. For this reason, in DF it is necessary to initially treat the biomass to partially inhibit or eliminate methanogenic bacteria, which degrade the hydrogen produced during fermentation.

1.5.1 Operative parameters

This process requires precise operative conditions, such as the absence of external illumination and oxygen (anaerobic environment). In addition, it is extremely sensitive to slight changes in operating conditions, such as temperature and pH. Therefore, these factors will be thoroughly examined in this section.

- Inoculum

The culture used for hydrogen production is fundamental for the startup of the process. Microorganisms that synthesize hydrogen are commonly present in environments such as soil, wastewater sludge and compost. Therefore, all these materials can be utilized as an inoculum for fermentative hydrogen production (Li and Fang, 2007). Numerous pure cultures have been employed for hydrogen production from various substrates, with *Clostridium* and *Enterobacter* being the most commonly utilized inocula for fermentative H_2 production. However, a mixed culture of H_2 producers is often favoured over a pure culture due to its practicability for environmental engineering applications and allows for a wider choice of feedstock. Nevertheless, enriching mixed cultures becomes essential to enhance biohydrogen production while inhibiting hydrogen consumers such as methanogens, commonly found in these mixed inocula (Wang and Wan, 2009). Pre-treatment of the inoculum to enhance hydrogen production often relies on the spore forming characteristics of H_2 producers such as *Clostridium*, which are commonly found in anaerobic sludge and sediments. These microorganisms are more likely to withstand the harsh conditions of the pre-treatment process compared to non-spore forming bacteria such as methanogens, since the spores can germinate again under favourable conditions (Li and Fang, 2007). The most simple and effective method for the enrichment of H_2 producers is the heat treatment of mixed culture, but also chemical and acid methods, aeration and load shock treatment can be performed. Other pre-treatment methods, such as chemical pretreatment and aeration, aim to selectively inhibit methanogens present in anaerobic sludge, as these microorganisms are highly sensitive to changes in environmental conditions.

- Substrate

There is a wide range of substrates that can be used for fermentative hydrogen production. Glucose, sucrose and starch are commonly used as substrates. However, recently several studies have started to utilize organic wastes as substrates for hydrogen production (Kapdan and Kargi, 2006). It has been demonstrated that within a suitable range, increasing substrate concentration can enhance the ability of hydrogen-producing bacteria to generate hydrogen during fermentative hydrogen production. However, at significantly higher levels, substrate inhibition could occur, leading to a decrease in H_2 production. In literature, there is no consensus on the optimal concentration of a given substrate for fermentative hydrogen production. The potential reason for this discrepancy may be attributed to variations among these studies in terms of the inoculum and substrate concentration ranges investigated (Wang and Wan, 2009). Some complex substrates are not appropriate for fermentation

processes due to the complexity of their structure; however, after being properly pretreated, hydrogen-producing bacteria can use them. Waste activated sludge from wastewater treatment plants contains significant amounts of organic matter, making it a promising substrate for hydrogen production.

DF processes exhibit low substrate conversion efficiencies: this is partially due to the requirement to regenerate nicotinamide adenine dinucleotide hydride (NADH) from NAD^+ (Ahmed et al., 2021). NADH and NAD^+ are pivotal molecules involved in the biochemical reactions of the cellular energy metabolism. NADH supplies the electrons required for the energy production, whereas NAD^+ acts as electron acceptor during catabolic reactions. In fact, NAD^+ is the oxidized form of the molecule and accepts protons to regenerate NADH, which promote the ATP production through the oxidative phosphorylation. The regeneration of NADH results in only about 33% of the electrons available being diverted towards the H_2 production (De Gioannis et al., 2013). It has been shown (Hallenbeck and Ghosh, 2009) that fermentation processes in nature are optimized not for hydrogen production but to support microbial growth, satisfying their metabolic needs. Consequently, hydrogen is considered a metabolic waste product and is often recycled within metabolic pathways. This recycling leads to the formation of several reduced products, such as ethanol, butanol, butyrate, and lactate, which facilitate NADH re-oxidation. Therefore, even under optimal process conditions, achieving conversion efficiencies to hydrogen higher than 15% of the original electrons in the substrate is rarely possible.

- Reactor type

Most studies on fermentative hydrogen production were conducted in batch mode due to its simple operation and control. However, for practical engineering purposes, large-scale operations would necessitate continuous production processes. The most widely used reactor for continuous hydrogen production is the continuous stirred tank reactor (CSTR). In this reactor, biomass is well suspended by means of mechanic agitation in the mixed liquid, which has the same composition as the effluent. Since biomass has the same retention time as the liquid (SRT is equal to HRT), the phenomenon of cell washout may occur at shorter HRT. It has been noted that in a proper range, increasing HRT could lead to an enhancement of hydrogen production. However, there is a threshold value for HRT beyond which inhibition occurs, and the evolution of H_2 decreases accordingly (Chen et al., 2008). The HRT can also be used as control parameter of the methanogenic activity. Low HRT values favour hydrogen production as methanogenic biomass are washed out from the inoculum. However, the optimal HRT for biohydrogen production relies on the type of substrates used since the hydrolysis stage, which is

the rate-limiting step in dark fermentation, depends on the biodegradability of the substrates (Kim et al., 2006).

In addition to CSTR, numerous studies have explored the use of anaerobic fluidized bed reactors, fixed or packed bed reactors, anaerobic baffled reactors, plug flow reactors (PFR), and membrane bioreactors, with the objective of enhancing biohydrogen yield and productivity.

- pH and temperature

The operational pH and temperature are pivotal parameters that affect the activity of hydrogen-producing bacteria and the metabolic pathways of fermentative hydrogen production, as well as the inhibition of the H_2 consuming processes which may occur simultaneously. Thus, the control of the process pH and temperature plays an important role in achieving high conversion rates by minimizing the activity of the hydrogen degraders.

The pH is a critical parameter that can influence the metabolic pathways since it directly affects the hydrogenase activity, which is the key enzyme involved in the DF processes. In fact, the activity of hydrogenase enzyme begins to decrease as the pH starts increasing. In most of the studies, it is noted that the optimum range for operating pH in DF is between 5.5 and 7 (Ghimire et al., 2015a). Considering acetate and butyrate as the major end products of hydrogen synthesis, it can be shown that a neutral pH favours the acetate pathways, whereas acidic pH conditions favours the butyrate pathways (Ghimire et al., 2015a). The choice of the operational pH also depends on the type of substrate and on the organic loading rate (OLR), which determines the VFA concentration. Many studies have demonstrated that increasing pH results in a lower hydrogen production (Ferchichi et al., 2005).

The DF process can be conducted at different operating temperatures, depending on the range considered. In particular, it can be carried out under mesophilic (35 °C), thermophilic (55 °C) or hyper-thermophilic (70 °C) conditions. In the latter case, the high temperatures favour the thermodynamics of the process and guarantee a reaction environment that is less prone to contamination by methanogenic bacteria. The operating temperature can influence the metabolic pathways, thus shifting the composition of the by-products (Ghimire et al., 2015a).

1.6 Photofermentation

Photofermentation (PF) refers to the photoheterotrophic process where organic substrates are converted into hydrogen by photosynthetic bacteria under anaerobic conditions, utilizing light as the

primary energy source. As for dark fermentation, also photo fermentative microorganisms are able to convert various organic compounds as feedstocks for the production of H_2. The most common microorganisms that can produce H_2 through photofermentation are the pigmented purple non-sulfur bacteria (PNSB), which are facultative anoxygenic phototrophs. Generally, PNSBs perform anoxygenic photosynthesis to produce ATP molecules driven by light under anoxic conditions. Nitrogenase is the key biocatalyst involved in PNSBs which mediates the production of hydrogen. Its activity mainly depends on the availability of molecular nitrogen (N_2) (McKinlay and Harwood, 2010). In presence of N_2, nitrogenase has the ability to fix it at the expense of the ATP molecules produced through photosynthesis, according to the following reaction:

$$N_2 + 8H^+ + 8e^- + 16ATP \rightarrow 2NH_3 + H_2 + 16ADP + 16P_i \quad (1.12)$$

Under N_2 limited conditions, nitrogenase loses its nitrogen-fixing capacity and catalyses an alternative reaction that leads to H_2 production as following:

$$8H^+ + 8e^- + 16ATP \rightarrow 4H_2 + 16ADP + 16P_i \quad (1.13)$$

Both reactions require a high expenditure of intracellular energy in the form of ATP molecules. However, the second reaction is more favourable for hydrogen production since all available protons are converted to H_2. Nitrogenase is highly sensitive to oxygen, which inactivates it in an irreversible manner. Therefore, maintaining anaerobic conditions by excluding oxygen and nitrogen from the reaction environment significantly enhances the photofermentative yield of H_2 in PNSBs (Deo et al., 2012). PNSBs can produce H_2 only under strictly anaerobic heterotrophic conditions in the presence of either solar or artificial light. These bacteria show a clear preference for short-chain fatty acids (SCFAs) or volatile fatty acids (VFAs), such as acetate, butyrate, lactate, malate, propionate, succinate etc. The growth rate of PNSBs, substrate conversion efficiency, and rate of H_2 production vary significantly depending on the type of substrate used. It is documented that PNSBs produce hydrogen at higher rates from organic acids compared to pure sugars (Tao, 2008). The stoichiometric equations that illustrate the theoretical yields of hydrogen produced through the complete photo-conversion of commonly used organic substrates by PNSBs are as follows:

$$C_6H_{12}O_6 + 6H_2O + Light \rightarrow 12H_2 + 6CO_2 \quad (1.14)$$

$$CH_3COOH + 2H_2O + Light \rightarrow 4H_2 + 2CO_2 \quad (1.15)$$

$$CH_3CH_2CH_2COOH + 6H_2O + Light \rightarrow 10H_2 + 4CO_2 \quad (1.16)$$

$$CH_3CH(OH)COOH + 3H_2O + Light \rightarrow 6H_2 + 3CO_2 \quad (1.17)$$

$$HO_2CCH(OH)CH_2COOH + 3H_2O + Light \rightarrow 6H_2 + 4CO_2 \quad (1.18)$$

Equation 1.14 illustrates the production of hydrogen starting from the simple sugar glucose. The series of Equations 1.15-1.18 show the H_2 production from various VFAs, in order acetate, butyrate, lactate and malate. From these equations it can be clearly noted the variability in the hydrogen yield with variation of type of substrates. Generally, malate and lactate are considered the most suitable VFAs for enhancing the rate and yield of H_2 production by PNSBs, whereas acetate and butyrate have a more significant impact on the formation of poly-hydroxyalkanoic acids (PHAs) than on H_2 production (Carlozzi and Lambardi, 2009). However, this observation may vary with the specific strain of PNSB used.

1.6.1 Purple Non-Sulphur Bacteria (PNSB)

Photosynthetic microorganisms have a wide variety of biotechnological applications due to their versatile metabolisms. PSNBs are pigmented nitrogen-fixing bacteria that carry out anoxygenic photosynthesis to produce ATP molecules. In presence of light, PNSBs absorb solar energy with wavelengths in the visible and near-infrared spectrum and metabolically synthetise hydrogen starting from organic compounds. Both light source and light intensity play an important role on the growth of PNSB and consequently, on hydrogen production. One of the most common photosynthetic bacterial strains investigated in PF processes is *Rhodopseudomonas palustris*, which has emerged as a promising organism for waste valorisation and for biohydrogen production. *R. palustris* has the ability to generate H_2 without producing O_2, allowing for purer hydrogen fuel production (Brown et al., 2022). Moreover, significantly higher H_2 yields are reported from *R. palustris* when limited N_2 condition are guaranteed in the growth media and thus cells use available electrons to synthesize H_2 as the only product of nitrogenase (McKinlay et al., 2014). *R. palustris* is an appealing microbial biocatalyst for commercial hydrogen production because it can generate ATP from light and obtain reductants necessary for nitrogen fixation from a wide range of compounds, including aromatic ones, industrial wastes, etc. For example, it has been shown that *R. palustris* can produce biohydrogen from crude glycerol (a by-product from biodiesel production) obtaining higher yields than other photosynthetic bacteria (Ghosh et al., 2012).

Thus far, the most attractive biohydrogen production strategy is the syntrophic metabolism of co-cultures. The development of co-culture systems with *R. palustris* allows for the degradation of inhibitory compounds or metabolic by-products that are resistant to degradation by other microbes. This approach enhances the growth of biomass in the organisms involved and promoted more efficient

utilization of feedstocks. However, further research and development are required to explore hydrogen production from renewable and economically viable substrates.

1.6.2 Cell growth

PNSBs require specific conditions and a proper environment for their growth. The culture medium is mainly composed of acid-base buffers (i.e. K_2HPO_4/KH_2PO_4), bulk nutrients (i.e. sulphates), trace elements, carbon and nitrogen sources. PNSBs require organic substrates such as acetate, malate, lactate, glycerol for growth. Additionally, the presence of yeast or glutamate as nitrogen sources enhances culture development. PNSBs are capable of growing under strictly anaerobic conditions, as oxygen is not involved in the photosynthetic process, but only when properly illuminated (Van Niel, 1944). PNSBs utilize infra-red radiation (780-1000 nm) for growth, necessitating continuous illumination with these wavelengths. Research has shown that cells cultivated under increased light intensities exhibit higher biomass concentrations (Nath and Das, 2009). To ensure anaerobic conditions, the injection of argon into the inoculum is required. Cell growth occurs at ambient temperatures (25-30 °C) and pressure, with pH maintained neutral (pH = 7) through adjustments using NaOH and HCl. Due to continuous illumination, optimal cultures are usually obtained in 4-5 days.

1.6.3 Immobilization techniques

Currently, photofermentation has low production rates compared to industrial hydrogen production processes. In addition, the use of photosynthetic microorganisms in industry is limited, partially because of the additional complexity of their cultivation. Therefore, improvements and strategies are required to enhance hydrogen productivity. One approach involves the advancement of enhanced photobioreactor (PBR) systems. A PBR is a specialized reactor designed for properly growing and controlling phototrophic bacteria that produce valuable biological products. At present there exist various PBRs adopted in research and, less frequently, in industry and they can be placed either indoor or outdoor. PBRs are properly equipped with systems that provide sufficient lighting to microorganisms, mixing of the medium, removal of oxygen and recovery of the product. Since PF necessitates light penetration, both the light source and light intensity are critical factors to monitor during operation to ensure optimal performance of photosynthetic microorganism growth within the photobioreactor. Most PBRs are configured for batch cultivation of the microorganisms which generally perform adequately if the biomass itself is the desired product of the process. Batch

conditions are typically considered not optimal in the biological processes due to the reduced overall productivity. However, there are several cases where the system would operate more effectively if the biomass were retained within the reactor while the media flows through it (Srivastava and Gupta, 2011). A critical limitation for this type of continuous operation is the phenomenon of cell washout, which occurs when the dilution rate exceeds the capacity of cells to grow and reproduce, namely the growth rate of the microorganisms. At dilution rate higher than the reproductive one, the microorganisms are flushed out of the system, resulting in the expulsion of the cells from the system more quickly than they can proliferate. This leads to a reduction in cell concentration within the bioreactor, until their complete removal, and consequently to a decline in productivity. Thus, the cell washout is a critical phenomenon in biological processes operated in continuous and constantly requires a control of operational parameters. Biomass retention can be obtained by designing a system that decouples solid retention time and hydraulic retention time of the bacteria and liquid media in the process. The SRT of a system indicates the average time that a solid particle, in this case the microorganism cell, spend inside the reactor. Similarly, the HRT is the average amount of time that a volume of process liquid, in this case the medium used, remains inside the PBR. Thus, the separation of the SRT and HRT within a PBR can promote an efficient continuous operation and prevention of cell washout, which represents a common issue when operating with planktonic cultures. A strategy increasingly developed to achieve this goal is to adopt cell immobilisation techniques. Biomass immobilisation involves the physical entrapment of a microorganism into a localized area without losing its biological activity (Keet et al., 2024). Thus, the substrates are still able to diffuse to the microorganisms, which is partially separated from the bulk fluid medium. Different immobilisation method currently exists; among these, confinement within a solid matrix, adsorption on carriers, entrapment behind a barrier and self-aggregation of the microorganisms. These techniques aim to isolate the biocatalyst from the media and concentrate it into a specific volume, allowing for an easy separation of the microorganisms from the liquid bulk.

Another issue that must be addressed when managing PBRs is the effect of mutual shading. This phenomenon occurs when photosynthetic microorganisms absorb light for themselves, thereby shading microorganisms situated further from the light source. The impact of mutual shading is more pronounced at higher biomass concentrations, potentially leading to large parts of the reactor volume being entirely shaded. The use of immobilised cells within solid matrices is intended to address the challenges encountered in planktonic cell systems, such as mutual shading of microorganisms and biomass washout (Wang et al., 2010).

1.6.4 Experimental setup

- Growth phase

When applying the immobilization technique in PF processes, cells are initially cultivated in a culture medium, followed by their isolation for immobilization. In contact with nutrients, bacteria grow following the typical curve as the one reported in Figure 1.9. The logistic kinetic model is widely used to describe the growth characteristics of photosynthetic bacteria (Gilbert et al., 2011). The model is described as follows:

$$\frac{dx}{dt} = k_c X \left(1 - \frac{X}{X_{max}}\right) \qquad (1.\ 19)$$

where dx/dt is the bacterial growth rate, X is the cell dry weight (g/L), X_{max} is the maximum cell concentration produced (g/L) and k_c is the apparent kinetic constant (h^{-1}) for the logistic model.

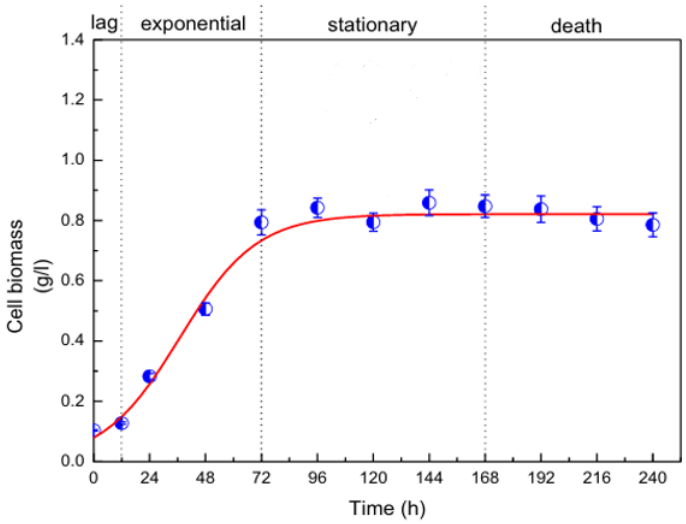

Figure 1.9: Cell growth characterization of a specific microorganism (Source: Xie et al., 2012).

The typical growth curve of bacteria (Figure 1.9) represents the cell concentration variation over the time and can be divided into four different phases: the lag phase, the exponential growth phase, the stationary phase and the death phase (Boran et al., 2010). The lag phase represents the period during which photofermentative bacteria initially adapt themselves to growth conditions. During this stage, cells may increase in size without undergoing division, resulting in a nearly constant cell concentration. The duration of this phase relies on the characteristics of bacterial species and culture conditions. Subsequently, cell biomass increases sharply during the exponential phase. Bacterial growth ceases

when the maximum biomass concentration is reached during the stationary phase. Finally, when all nutrients in the PBR are depleted, bacteria can no longer reproduce and enter the death phase.

In PF processes, hydrogen productivity of bacteria is closely related to the growth phase. It can be demonstrated that Table 1.1: Relationship between cell growth and hydrogen production (Source: Xie et al., 2012).hydrogen is mainly produced during the stationary phase, making the bacteria in this stage most effective for H_2 production (Xie et al., 2012). Table 1.1 shows the relationship among the growth of bacteria, H_2 production and substrate consumption. During exponential phase, 51.25% of substrate is consumed for cell growth and correspondingly, 89% of biomass is produced, while the H_2 yield is only 1.82 mol H_2/mol acetate. Most of H_2 is accumulated during stationary phase, where the maximum yield is reached, and the synthesis of cells is minimal.

Growth phase	Cell growth (%)	H_2 production (%)	Substrate consumption (%)	H_2 yield ($mol_{H2}/mol_{acetate}$)
Lag	3.19 ± 0.11	0.00 ± 0.00	6.42 ± 0.28	0.00 ± 0.00
Exponential	89.30 ± 4.69	38.87 ± 2.45	51.25 ± 3.47	1.82 ± 0.12
Stationary	7.51 ± 0.33	59.19 ± 3.48	38.17 ± 2.69	3.67 ± 0.26
Death	-6.40 ± 0.32	1.94 ± 0.12	4.16 ± 0.23	1.12 ± 0.07

Table 1.1: Relationship between cell growth and hydrogen production (Source: Xie et al., 2012).

- H_2 production

As it is shown that bacteria in stationary phase are the most effective for H_2 production, they are separated from the culture medium and immobilized to produce H_2. The immobilized cells are introduced into a culture medium primarily composed of acid-base buffers (K_2HPO_4/KH_2PO_4), bulk nutrients, trace elements and a carbon source. For the hydrogen production phase, the culture medium is deprived of nitrogen sources, such as yeast or glutamate, which are present in the medium used for cell growth. Ensuring nitrogen-limited conditions is essential to promote the capacity of the nitrogenase enzyme to catalyse the reaction for H_2 formation, which otherwise would be suppressed. In many studies, acetate results as the best carbon source for H_2 production, since higher production rate can be achieved (Barbosa et al., 2001). The pH is adjusted to a neutral value (7±0.2) using NaOH and HCl. Light plays a pivotal role in such processes: a continuous illumination is required, with favourable wavelengths in the visible and near-infrared spectrum (600-800 nm). Each type of bacteria

preferably absorbs light energy with a specific wavelength range for the stimulation of photo-hydrogen production (Tian et al., 2010). Not only the light source, but also the light intensity significantly impacts the production of H_2. The optimal light intensity typically ranges from 200 to 300 W/m^2, with a saturation at approximately 300 W/m^2, beyond which no further effects are observed (Abdalla et al., 2018).

On the other hand, an increase in light intensity has a negative effect on the light conversion efficiency (LCE). The LCE is defined as the efficiency with which the light energy is converted into hydrogen energy. The light conversion efficiency is calculated according to Equation 1.20 (Tian et al., 2010):

$$LCE\ (\%) = \frac{H_2\ ouput \times H_2\ energy\ content}{light\ energy\ input} \times 100 \qquad (1.20)$$

where it is assumed that all the incident light is absorbed. The decrease in LCE arises from the high incident light intensity (I), as outlined in the alternative definition of LCE provided below (Uyar et al., 2007):

$$LCE(\%) = \frac{33.61 \cdot \rho_{H_2} \cdot V_{H_2}}{I \cdot A \cdot t} \times 100 \qquad (1.21)$$

where ρ_{H_2} and V_{H_2} are respectively the density and the volume of H_2 produced expressed in g/l and l, A is the irradiated area (m^2) and t is the time required for H_2 production (h). The factor 33.61 indicates the energy content per mass of hydrogen, specifically 121 MJ/kg, which is converted to J/g in order to correspond the unit of measures.

In conclusion, assessing the optimal light intensity and wavelength that are compatible with the absorption maxima of a specific bacteria is necessary to ensure an efficient photo-H_2 production and to prevent wasting light energy as well.

1.6.5 Reactor configuration

The structure and operational methods of various photobioreactors significantly impact the light, heat, and mass transfer properties, thereby influencing the photo-fermentative H_2 production process. Different studies have identified that the design of PBRs should exhibit specific characteristics to optimize the PF process effectively (Akkerman et al., 2002; Dasgupta et al., 2010). First, a PBR should be an enclosed system that avoids hydrogen leakage. It should be constructed with transparent and durable materials to allow for light penetration and photo-permeability. PBRs should be designed to provide effective mixing performances and facilitate the light-heat-mass transfer.

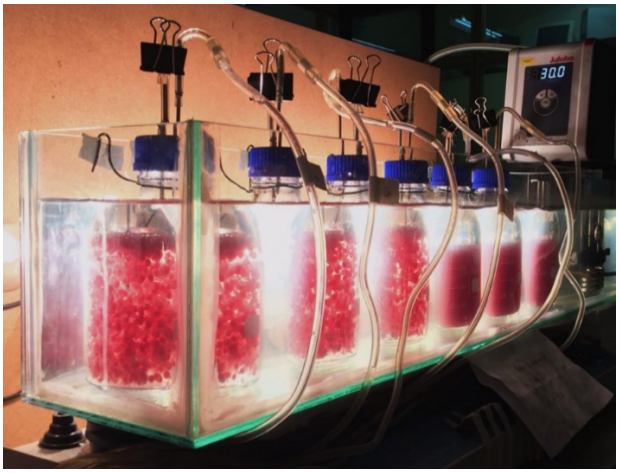

Figure 1.10: A photobioreactor (PBR) with immobilized cells of PNSB in polyvinyl-alcohol (PVA) cryogel beads.

There are diverse types of photobioreactors, such as CSTRs, flat panel reactor, outdoor stacked-tubular reactor, etc. A common type of PBR configuration is the fluidized bed (FB) reactor, which is particularly utilized with immobilized cells serving like a biocatalyst within the reactor. A comparison between the FB and packed bed (PB) configuration of the column when loaded with immobilized cells can be done by evaluating the hydrogen production kinetics (Ross and Pott, 2021).

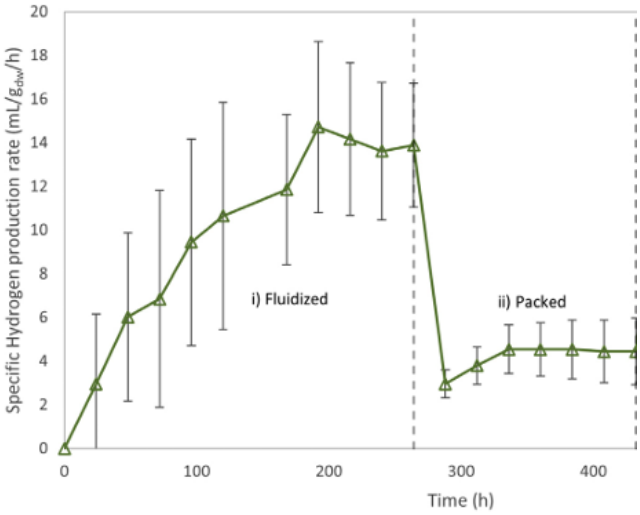

Figure 1.11: Specific hydrogen production rate by immobilized cells in the PBR operated as a fluidized (i) or packed (ii) bed reactor (Source: Ross and Pott, 2021).

From a qualitative perspective, Figure 1.11 shows that when operated as a fluidized bed the H_2 production rate increases linearly and then steadies to higher values than the one obtained with PB configuration. The lower specific hydrogen production rate observed in section ii) of Figure 1.11 can likely be attributed to reduced light attenuation within the PBR. When operated as a fluidized bed, the reactor exhibits enhanced mixing and distribution of the immobilized cells, which results in increased

light exposure. On the other hand, in the PB configuration light attenuation may be constrained, as most of the incoming light is absorbed or scattered by the beads closest to the reactor surface, limiting light availability for the cells at the rear of the reactor (Ross and Pott, 2021).

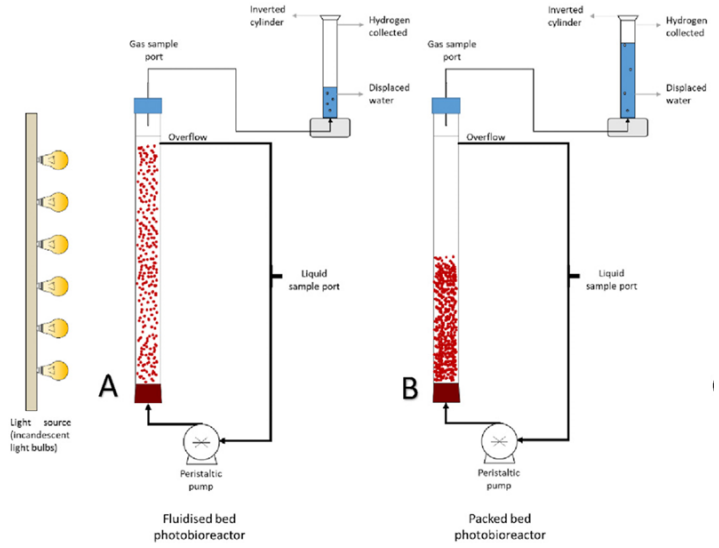

Figure 1.12: A PBR operated in different configurations: as a fluidised bed PBR (A) and as a packed bed PBR (B) (Source: Ross and Pott, 2021).

1.7 Two-stage process

One way to improve the efficiency of H_2 production processes is the two-stage system which is the combination of dark fermentative and photofermentative processes. A combined process in enabled by the fact that the effluents from the DF process, which are primarily volatile fatty acids, serve as the feedstock for the photofermentation process. In this case, sugar monomers are initially converted into VFAs and H_2 by facultative anaerobes. Subsequently, the organic by-products of this process are then further converted into H_2 from photosynthetic bacteria according to photofermentation reactions. The primary limitation of DF is the partial breakdown of sugars into CO_2 and water, leading to low H_2 yields per mole of substrate. Organic compounds present in the DF effluents, mainly acetic, butyric, lactic and propionic acids, can be readily fermented by photosynthetic microorganisms, thereby enhancing the H_2 yield. The two stages are carried out in two separate reactors, which can be controlled and manipulated separately thus allowing for the optimization of each single stage. A combination of dark fermentation phase and photofermentation phase can potentially offer a solution for converting organic acids obtained in the DF and providing more flexibility in the use of renewable and cost-effective feedstocks. Additionally, the PF process needs to be optimized to enhance the growth rates of photosynthetic bacteria and improve light conversion efficiencies (Das et al., 2008). Biological H_2 production through the sequential stages of DF and PF represents a favourable approach to bio-

hydrogen generation as it achieves higher yields compared to single-step methods (Özgür et al., 2010). It is worth noting that potential contamination between stages can occur in the two-stage process. PNSBs require strict conditions to produce hydrogen, which limits the types of substrate and streams that can be used as input for the combined process. These conditions comprise a relatively high-quality stream with low concentrations of contaminating microorganisms, minimal or no toxic contaminants and free of nitrogen. One suitable input stream is the waste glycerol generated as a by-product of the biodiesel production industry, as glycerol is an appropriate substrate for PNSBs to produce hydrogen. However, this crude glycerol requires pre-treatment to meet the upgraded quality required (Pott et al., 2014).

Figure 1.13 clearly illustrates the formation of VFAs as extracellular metabolic end products of microorganisms involved in the dark fermentation. These VFAs subsequently enter the succeeding photofermentative pathway as nutrients for PNSBs. The H_2 yields from the two metabolic pathways contribute to the overall higher cumulative hydrogen production achievable through the combined dark-photofermentation process. The most common approach for integration is the hybrid system, which is made up of the connection in series of DF and PF processes. This method involves conducting the two phases in separate reactors, thereby avoiding the contamination of the bacterial cultures and ensuring optimal process conditions for both processes.

As stated in §1.5.1, the low substrate conversion efficiencies observed in DF processes can be attributed, in part, to the necessity of regenerating NAD^+ from NADH. This results in only about 33% of the electrons being directed toward hydrogen production. In contrast, the photosynthetic process involves the absorption of light energy in the electron chain, converting $NADP^+$ to NADPH (analogous to NADH), which enhances substrate conversion efficiencies to hydrogen. This is because a greater portion of cellular energy is diverted towards its production rather than to NADH generation.

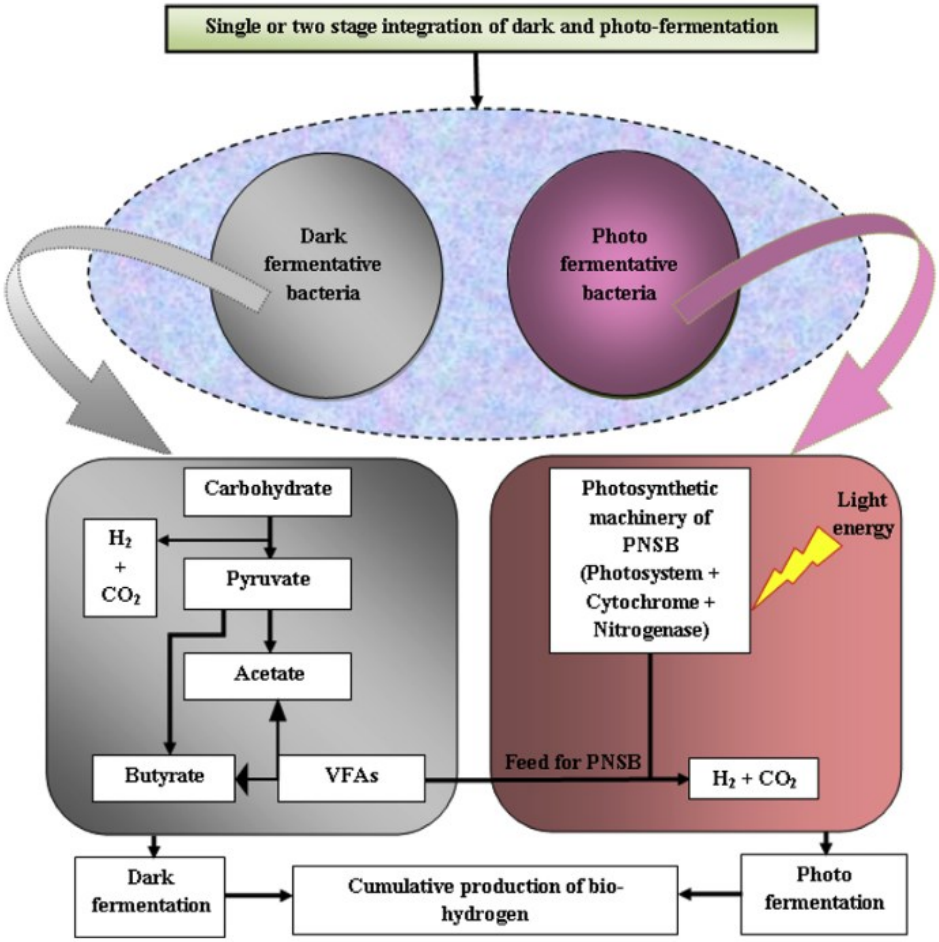

Figure 1.13: Integration of dark and photo fermentation for H_2 production via VFAs acting as intermediate metabolic linker (Ghosh et al., 2018).

1.8 Aim of the thesis

The current study focuses on the biological processes regarding the H_2 production, specifically Dark Fermentation and Photo Fermentation. The aim of the current thesis is to assess the feasibility of these processes on an industrial scale (small-medium sized plant) and to understand which are the main issues related to their implementation and the sources of major costs, which need to be improved in the future analysis. This is obtained by performing a techno-economic analysis on the single and the combined processes. In the Dark Fermentation process, the feed considered is a waste activated sludge that can be obtained from a wastewater treatment plant. The DF process is simulated using Aspen Plus, which allows for obtaining rigorous mass and energy balances. The vapor phase is sent to an absorption column where H_2 is separated from CO_2, which is then captured in a stripping column. Simultaneously, the liquid phase undergoes a series of purification steps to separate the organic acids and recycle the sludge and water. The separation of the organic acids is performed as it might decrease the overall production costs of the biohydrogen, since their selling generate a revenue which might increases the

valorisation of the process itself. The material balances of the DF process are computed by means of the process simulator Aspen Plus V14. In addition, for Dark Fermentation process, the kinetic model is preliminary implemented in MATLAB R2023b, and the results are elaborated using Excel. Finally, capital and operating costs are evaluated using CAPCOST 2017 and starting from them, a specific key indicator for hydrogen production is used to assess the economic performance of the process, namely the Levelized Cost of Hydrogen (LCOH). Various scenarios are analysed, including the single-stage DF process and the integrated DF and PF processes. The LCOH results are compared to identify the most optimal scenario in terms of economic performance of the process.

Chapter 2

Methods

Chapter 2 details the methods employed to carry out the simulations using Aspen Plus. Initially, it explains the model used to describe the kinetics of the dark fermentation process and specifically, how this model was implemented in MATLAB to solve its differential equations. Furthermore, the chapter explains how the simulation was performed in Aspen Plus for the dark fermentation process and how the calculations were based for the photo fermentation process. In this chapter, the process flowsheets are presented with a focus on the operating units used for the gas upgrading.

2.1 Block Flow Diagram of the processes

This paragraph presents the two BFDs (Block Flow Diagrams) of the processes of Dark Fermentation and the combined processes of Dark and Photo fermentation. Regarding the Dark Fermentation process (Figure 2. 1), it is considered that the inlet flowrate is a waste activated sludge which is sent to the bioreactor operating under thermophilic conditions (T = 35°C), where fermentation reactions occur.

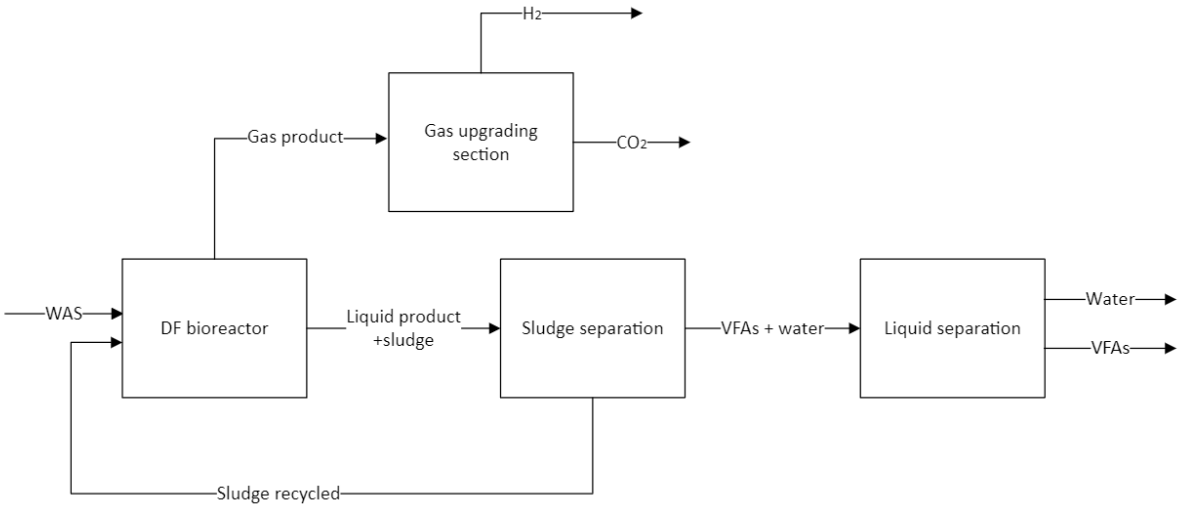

Figure 2. 1: BFD of the single-stage dark fermentation process.

From this unit, two product streams are obtained: one in the gas phase, containing H_2, CO_2 and water vapour, and the other in the liquid phase, consisting of an aqueous solution of volatile fatty acids with a solid fraction of sludge. The solid fraction is separated and recycled though a settler, while the liquid

stream is concentrated and sent to a separation unit, where the single components are recovered. The gas product stream is sent to a gas upgrading section to enrich the hydrogen stream and separate the CO_2. It is assumed that the target for H_2 production is equal to 33 kg/h, which corresponds to a small to medium-sized plant capacity, equivalent to that of an electrolyser of approximately 1.8 MW.

Regarding the combined process, the bioreactor where the DF process takes place is maintained, and once the sludge is separated, the liquid effluent from DF is sent to the photofermentation unit, which involves a photobioreactor. From this unit, two product streams are obtained: one in the gas phase, involving the formation of H_2 and CO_2, and one in the liquid phase, containing VFAs and water. The gas phase product stream in this case is mixed with that coming from the DF unit for the separation to obtain an enriched H_2 stream.

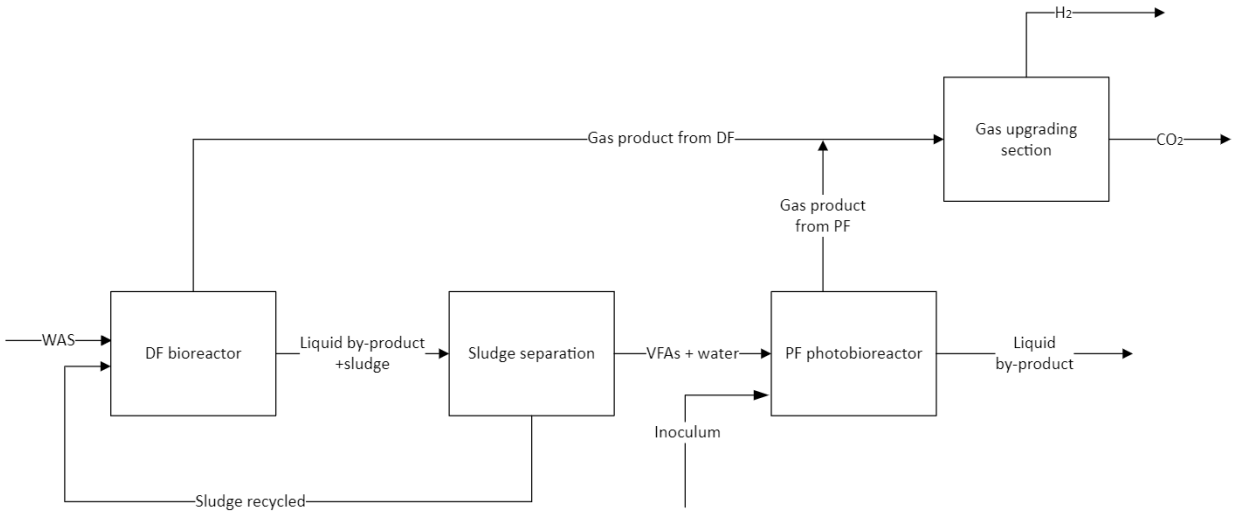

Figure 2. 2: BFD of the 2-stage process combining dark and photo fermentation processes.

2.2 Modified Anaerobic Digestion Model 1 (ADM1)

The IWA Anaerobic Digestion Model 1 (ADM1) is a mechanistic model developed to describe methane production during anaerobic digestion process (Gadhamshetty et al., 2010). This structured model includes multiple steps which integrate the biokinetics with the physico-chemical processes, as illustrated in Figure 2. 3.

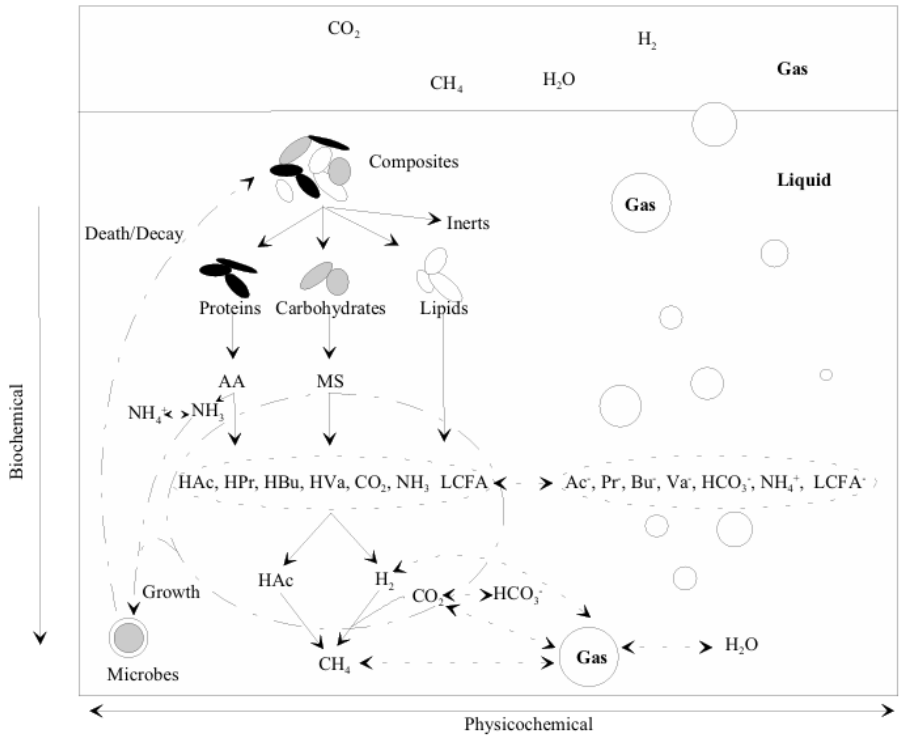

Figure 2. 3: Conversion processes in anaerobic digestion included in the model ADM1 (Batstone et al., 2002).

The biochemical steps involve disintegration and metabolises of organic carbon-containing homogeneous particulates to carbohydrates, proteins and lipids. Following, the hydrolysis of these compounds to sugars, amino acids and long chain fatty acids (LCFA), respectively; then, acidogenesis from sugars and amino acids to VFAs and hydrogen; acetogenesis of LCFA and VFAs to acetate; and finally, methanogenesis from acetate and hydrogen/CO_2. The physico-chemical processes are not biologically driven, and they include ion association-dissociation and gas-liquid transfer. The ADM1 framework can be adapted to predict the hydrogen and VFAs production through dark fermentation, by neglecting the final step of methanogenesis.

The unit commonly selected as the base unit for organic compounds is the chemical oxygen demand (COD) due to its wide application in characterizing the organic carbon concentration in wastewater streams. COD measures the total amount of oxygen being consumed during the degradation of organic matter by strong oxidizing agents. COD is used to identify the amount of organic compounds in aquatic systems and to assess the response of particulate matter toward the oxidation process (Sharma and Dahiya, 2023). Components with no COD such as inorganic carbon (CO_2 and HCO_3^-) and inorganic nitrogen (NH_4^+ and NH_3) are described on a molar basis (kmole m^{-3} ≡ M). All the units adopted in the model are summarized in Table 2.1, unless otherwise stated.

Measure	Units
Concentration	kgCOD m^{-3}
Concentration (non-COD)	kmole m^{-3}
Pressure	bar
Temperature	K
Distance	m
Volume	m^3
Energy	J
Time	d (day)

Table 2.1: Units of measure of the ADM1 model (Batstone et al., 2002).

2.2.1 Nomenclature and description of parameters and variables

There are four main categories of parameters and variables: stoichiometric coefficients (Table 2.2), equilibrium coefficients (Table 2.3), kinetic parameters (Table 2.4), and dynamics state and algebraic variables (Table 2.5). All parameters and variables with their corresponding nomenclature are listed in the following tables.

Symbol	Description	Units
C_i	Carbon content of component i	kmoleC $kgCOD^{-1}$
N_i	Nitrogen content of component i	kmoleN $kgCOD^{-1}$
$\nu_{i,j}$	Rate coefficients for component i on process j	nominally kgCOD m^{-3}
$f_{product,substrate}$	Yield (catabolism only) of product on substrate	kgCOD $kgCOD^{-1}$

Table 2.2: Stoichiometric coefficients (Batstone et al., 2002).

Symbol	Description	Units
H_{gas}	Gas law constant (equal to K_H^{-1})	bar M^{-1}
$K_{a,acid}$	Acid-base equilibrium coefficient	M
K_H	Henry's law coefficient	M bar^{-1}
pK_a	$-log_{10}[K_a]$	-
R	Gas law constant (8.3134×10^{-2})	bar M^{-1} K^{-1}

Table 2.3: Equilibrium coefficients and constants (Batstone et al., 2002).

Symbol	Description	Units
$k_{A/Bi}$	Acid-base kinetic parameter	M^{-1}
k_{dec}	First order decay rate	d^{-1}
$I_{inhibitor,process}$	Inhibition function (see K_I)	-
$k_{process}$	First order parameter (for hydrolysis)	d^{-1}
k_La	Gas-liquid transfer coefficient	d^{-1}
$K_{I,inhibit,substrate}$	50% inhibitory concentration	kgCOD m^{-3}
$k_{m,process}$	Monod maximum specific uptake rate	$kgCOD_S$ $kgCOD_X^{-1}$ d^{-1}
$K_{S,process}$	Half saturation value	$kgCOD_S$ m^{-3}
ρ_j	Kinetic rate of process j	$kgCOD_S$ m^{-3} d^{-1}
$Y_{substrate}$	Yield of biomass on substrate	$kgCOD_S$ $kgCOD_X^{-1}$
μ_{max}	Monod maximum specific growth rate	d^{-1}

Table 2.4: Kinetic parameters and rates. The subscript S indicates a dissolved substrate, whereas the subscript X a particulate subscript (Batstone et al., 2002).

Symbol	Description	Units
pH	$-\log_{10}[H^+]$	-
$p_{gas,i}$	Pressure of gas i	M
P_{gas}	Total gas pressure	M bar^{-1}
S_i	Soluble component i	$kgCOD_S$ m^{-3}
X_i	Particulate component i	$kgCOD_X$ m^{-3}

Table 2.5: Dynamic state and algebraic variables (Batstone et al., 2002).

2.2.2 Dynamic state variables

The model is implemented as a set of differential equations (DEs), with 32 dynamic concentration state variables. Dynamic state variables are those computed at a specific time *t* by solving the set of differential equations as defined by the ADM1 process rates, the modelled process configuration, inputs and initial conditions (i.e., the values of these variables at t=0). Consequently, when a set of DEs is implemented, the state of the system at time *t* is entirely determined by the values of these variables. The characteristics of the dynamic state variables are reported in Table 2.6, with the corresponding molecular weights and the conversion factor for COD unit, namely gCOD $mole^{-1}$. This

factor is used to convert the concentration of components from kgCOD m^{-3} to g/l or the mass flowrates in kg/h, which are useful for further calculations.

Name	i	Description	MW	gCOD $mole^{-1}$
X_c	13	composite	varies	varies
X_{ch}	14	carbohydrates	180	192
X_{pr}	15	proteins	113	160
X_{li}	16	lipids	806	2560
X_I	24	particulate inerts	varies	varies
S_I	12	soluble inerts	varies	varies
S_{su}	1	monosaccharides	180	192
S_{aa}	2	amino acids	varies	211
S_{fa}	3	total LCFA	256	736
S_{va}	4	total valerate	102	208
S_{bu}	5	total butyrate	88	160
S_{pro}	6	total proprionate	74	112
S_{ac}	7	total acetate	60	64
S_{h2}	8	hydrogen	2	16
S_{ch4}	9	methane	16	64
S_{IC}	10	inorganic carbon	44	0
S_{IN}	11	inorganic nitrogen	17	0
$X_{su\text{-}h2}$	17-23	biomass	113	160
S_{cat}	-	cations	varies	0
S_{an}	-	anions	varies	0

Table 2.6: Dynamic state variables and their molecular weight and conversion factor from COD to SI (Batstone et al., 2002).

All the units for the state variables reported in Table 2.6 are kgCOD m^{-3}, with the exception for S_{IC}, S_{IN}, S_{cat} and S_{an} that are expressed as M.

2.2.3 Biochemical reactions

The structured model includes the three overall biochemical steps, which refer to the acidogenesis (fermentation), acetogenesis (organic acids oxidation) and methanogenesis phases, but also

disintegration and hydrolysis steps, which are extracellular and partly non-biological processes (Batstone et al., 2002).

All extracellular processes are described using first order equations, as it reflects the cumulative effect of a process involving multiple steps (Eastman and Ferguson, 1981) and all the biochemical conversions are implemented as irreversible. Cellular processes are described by three expressions that represent the uptake, the growth and the decay kinetics. The substrate uptake is the pivotal rate equation and is based on Monod-type kinetics. In the substrate uptake equations, the biomass growth is not explicit. Death of biomass is expressed by first order kinetics and the spent biomass remains in the system as composite particulate material. It is assumed that complex composite particulate waste is homogeneous and disintegrates into carbohydrates, protein, and lipids. This assumption is useful when modelling the digestion of activated sludge, since the disintegration step should precede the more complex hydrolytic step. Thus, the disintegration step includes multiple processes such as lysis, non-enzymatic decay, phase separation and physical breakdown (i.e. shearing).

In Figure 2. 4, a schematic representation of all biochemical processes included in the modified ADM1 is reported. Processes 6 and 7 correspond to the methanogenic steps included in the original ADM1. However, these steps have been neglected in this study, since the H_2 produced cannot be degraded into methane when methanogenic bacteria are not present. The biological kinetic rate expression and coefficients are expressed in the form of Peterson matrices, which are reported in Appendix A (Tables A.1 and A.2). These tables do not include physico-chemical rate equations, as liquid-gas transfer and ion dissociation, since they do not take part to the metabolic and biochemical steps of the process.

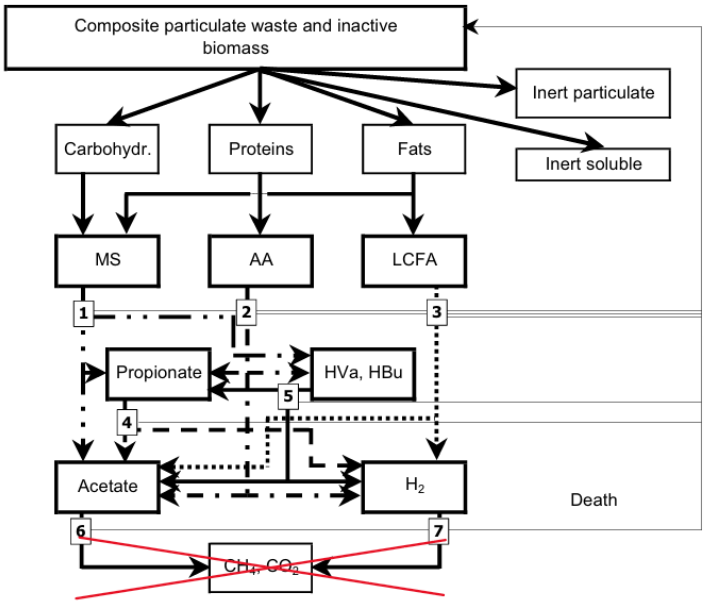

Figure 2. 4: Biochemical steps included in the modified ADM1 (Modified from: Batstone et al., 2002).

2.2.4 Physico-chemical processes

The physico-chemical reactions refer to those where microorganisms are not involved, such as liquid-liquid reactions (i.e. ion association/dissociation), gas-liquid exchange (i.e. gas transfer) and liquid-solid transformation (i.e. precipitation and solubilisation of ions). Due to the difficulty in modelling liquid-solid transformation, precipitation is not included in the ADM1, and so neither in the modified model.

The physico-chemical reactions are fundamental in modelling anaerobic systems for several reasons. They allow for the expression of various biological inhibition factors, including pH and dissolved gas concentrations. In addition, some key performance variables such as gas flow depend on the estimation of physico-chemical transformations. Moreover, pH control with a strong acid or base in such processes often represents the major operating cost and the setpoint is determined from the physico-chemical state (Batstone et al., 2002).

The acid-base pairs considered in this model, which are the most important in anaerobic systems, are presented in Table 2.7 (Lide, 2001).

Acid-base pair	pK_a
NH_4^+/NH_3	9.25
CO_2/HCO_3^-	6.35
VFA/VFA^-	4.8
$H_2O/OH^-/H^+$	14

Table 2. 7: Acid-base pairs considered in the physico-chemical processes and their corresponding pKa values (at 298 K) (Batstone et al., 2002).

The transfer rates of gas i, $\rho_{T,i}$ (where i = H_2, CO_2) are evaluated as follows, represented by equation 2.1 below:

$$\rho_{T,i} = k_L a\left(S_{liq,i} - K_{H,i} p_{gas,i}\right) \quad (2.1)$$

Where $k_L a$ is the gas-liquid transfer coefficient (d^{-1}), $K_{H,i}$ is the Henry's law equilibrium constant (M bar^{-1}), $p_{gas,i}$ is the partial pressure of component i in the gas phase (bar) and $S_{liq,i}$ is the concentration of i in the liquid (M). The partial pressure of a component in the gas phase can be evaluated with the ideal gas law as follows:

$$p_{gas,i} = S_{gas,i} RT \quad (2.2)$$

Where $S_{gas,i}$ indicates the molar concentration of component i in the gas phase (kmole m^{-3}).

2.2.5 Implementation

The system in which the process takes place comprises a reactor (fermenter) containing a liquid volume, with a sealed gas headspace at atmospheric pressure (Figure 2. 5). In this space, gas accumulates and is subsequently removed continuously for downstream processing or utilisation. The system is modelled as a continuously stirred tank reactor that guarantees sufficient mixing and contact between the phases, as to not impose significant mass transfer limitations between phases. It is assumed that the liquid volume is constant and incompressible, meaning that the outlet volumetric flowrate is equal to the inlet flowrate ($q_{out} = q_{in}$).

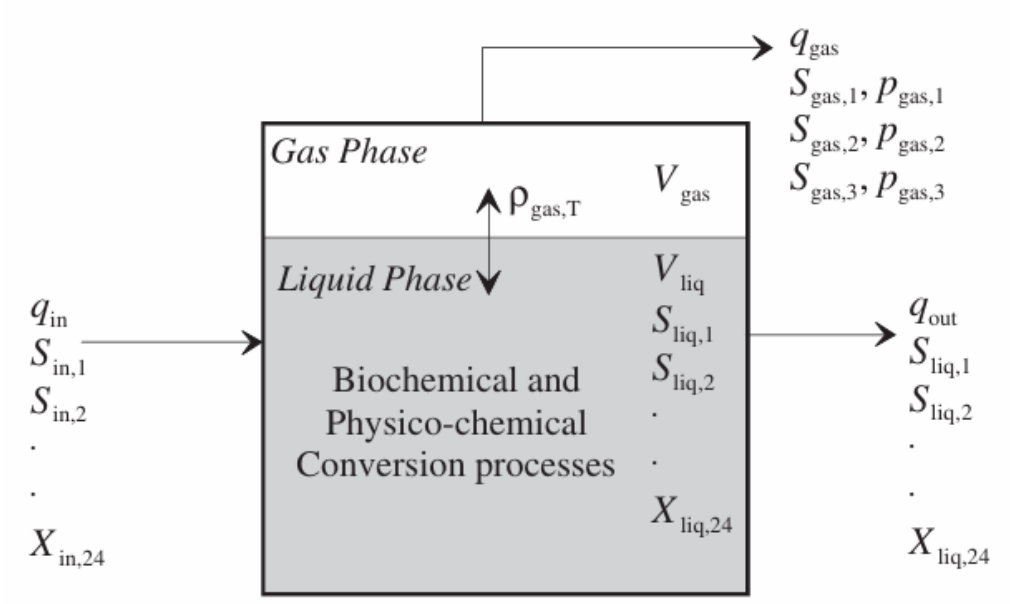

Figure 2. 5: Schematic representation of a stirred tank reactor (q = volumetric flowrate; V = volume; $S_{liq,i}$ = concentration of dissolved liquid components; $X_{liq,i}$ = concentration of particulate components; i is the component index) (Batstone et al., 2002).

The mass balance for each component in the liquid phase is expressed as:

$$\frac{dS_{liq}}{dt} = \frac{q_{in}S_{in,i}}{V_{liq}} - \frac{S_{liq,i}q_{out}}{V_{liq}} + \sum_{j=1-19}\rho_j\nu_{i,j} \qquad (2.\ 3)$$

Where the term $\sum_{j=1-19}\rho_j\nu_{i,j}$ is the sum of the kinetic rates for process j multiplied by the reaction parameters $\nu_{i,j}$. In cases where inorganic carbon (column 10 of the matrix in Table A.1) is used as carbon source for catabolism or anabolism (i.e. uptake of sugars, amino acids, propionate, acetate and hydrogen; j = 5,6,10,11,12), the inorganic carbon rate coefficient can be expressed as a carbon balance, as follows:

$$\nu_{10,j} = -\sum_{i=1-9,11-24} C_i\nu_{i,j} \qquad (2.\ 4)$$

For example, the inorganic carbon coefficient for the uptake of sugars (j = 5) is expressed as:

$$\nu_{10,5} = -\left[C_{su} + (1 - Y_{su})f_{bu,su}C_{bu} + (1 - Y_{su})f_{pro,su}C_{pro} + (1 - Y_{su})f_{ac,su}C_{ac} + Y_{su}N_{bac}\right] \quad (2.5)$$

where C_i is the carbon content of component i (kmoleC kgCOD^{-1}), $f_{product,substrate}$ is the yield of product with respect to substrate and N_{bac} is the carbon content of biomass (N_{bac} = 0.0313 moleC gCOD^{-1}).

The gas phase mass balances are similar to the liquid phase equations, but the inlet term is represented by the mass transfer rate from the liquid phase. They are expressed as follow:

$$\frac{dS_{gas.i}}{dt} = -\frac{S_{gas,i}q_{gas}}{V_{gas}} + \rho_{T,i}\frac{V_{liq}}{V_{gas}} \quad (2.6)$$

The term V_{liq}/V_{gas} is required since the gas transfer kinetic rate are referred to liquid volume. The reactor headspace is assumed to be saturated with water vapour. The Van't Hoff equation can be adopted in order to evaluate the temperature dependence of water vapour pressure, considering a partial pressure of 0.0313 bar at 298 K and $\Delta H^0_{vap} = 43{,}980$ J mole^{-1} (Lide 2001):

$$p_{gas,H_2O} = 0.0313\ exp\left(\frac{43{,}980}{8.324}\left(\frac{1}{298} - \frac{1}{T}\right)\right) \quad (2.7)$$

Where a value of R = 8.324 J mol^{-1} K^{-1} is used to be consistent with the units of J mol^{-1} and K.

The gas flow is calculated by equating it to the total gas transfer, corrected for water vapour, as follows:

$$q_{gas} = \frac{RT}{P_{gas} - p_{gas,H_2O}}V_{liq}\left(\frac{\rho_{T,H_2}}{16} + \frac{\rho_{T,CH_4}}{64} + \rho_{T,CO_2}\right) \quad (2.8)$$

Where P_{gas} is the set headspace total pressure (1.013 bar), calculated as the sum of each gas components partial pressure. The terms 16 and 64 in the denominator positions are the corrective factors to account for COD equivalent of the gases.

To solve the set of differential equations, a vector of initial values for all state variables is defined, by considering that the feed to the process is an activated sludge waste. All parameters are estimated based on the specific type of feed considered and are retrieved from literature (Rosen and Jeppsson, n.d.). They are reported in Table A.3-A.7 in Appendix A. Initially, a value for the liquid volumetric flow rate and the liquid volume is assumed. The solution is then obtained as a function of a time interval of 200 days, which is initially an indicative large time period for the process, thus ensuring that during this period, the concentration profiles of each component reach the steady-state and attain a constant value. Afterwards, the initial liquid flowrate is varied to ensure that *HRT* = 1-20 d. In this case, the script is executed multiple times to solve the set of equations for different liquid flow rates (i.e., *HRT*), by means of a "*for*" cycle reported in Appendix B. For each run of the simulation, it stores in a separate

matrix only the concentration values at the final iteration (the one at t = 200 d), corresponding to their steady-state values. The H_2 production rate is obtained by considering the molar flowrate of H_2 produced divided by the liquid volume and the curve obtained is plotted in Figure 2.6.

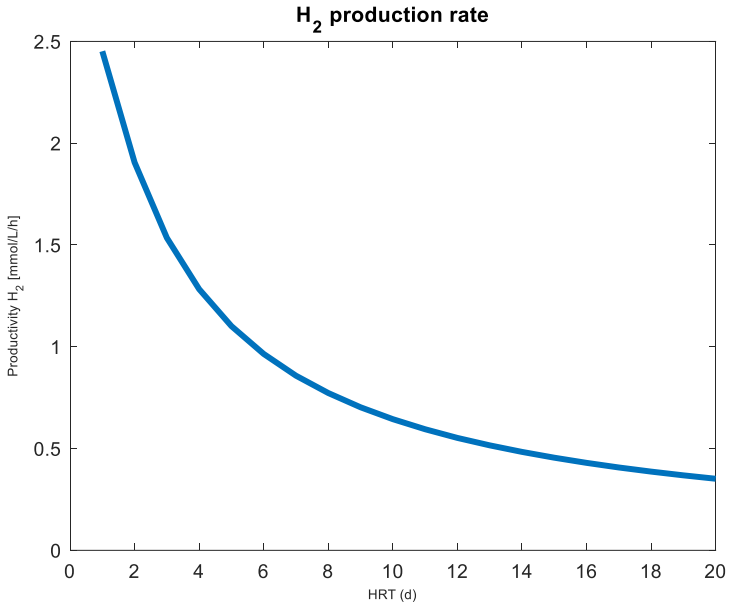

Figure 2.6: Plot of the H_2 production rate (mmol/L/h) as a function of the HRT (d) in the range 0-20 d.

To more accurately evaluate the trend of this variable, the *HRT* is restricted to 0.1-2 d (Figure 2. 7). Within this range, it is possible to assess the trend of the H_2 production rate and identify the maximum point as well as how drastically the production rate varies around the maximum point. Based on this consideration, an optimal *HRT* suitable for the operational conditions is adopted equal to 1 d. The low value of *HRT* can also be used as a control parameter of the methanogenic activity, since it avoids that the methanogenic bacteria have enough time to grow and consume the H_2 produced (Ghimire et al., 2015b). The plots representing the trend of the concentration of both the VFAs and the macromolecules (carbohydrates, proteins and lipids), the gas product composition and the pH as a function of the HRT are reported in Appendix B.

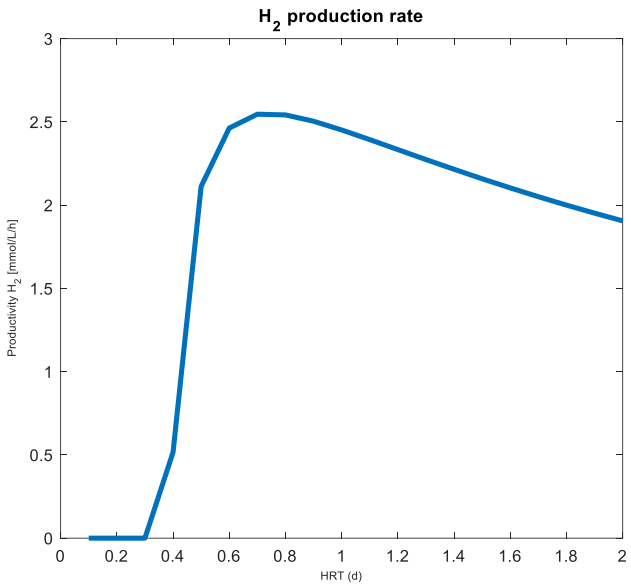

Figure 2. 7: Plot of the H_2 production rate (mmol/L/h) as a function of the HRT (d) in the range of 0-2 d.

Once the optimum *HRT* is determined, all material balances are evaluated on the basis of this value. The waste activated sludge is considered as the feedstock for the process, which is a by-product of the wastewater treatment plant (WWTP). The waste activated sludge can be used as waste biomass for DF process, as it represents a valuable substrate with carbohydrate content. In addition, DF also offers biological treatment of the organic waste that otherwise would generate WWT costs. The waste activated sludge is already used as feed for the anaerobic digestion process, with which DF shares part of the steps involved (Appels et al., 2008).

The yield of H_2 is defined as:

$$y_{H_2} = \frac{P_{H_2}}{Q_{sludge}^{in}} \quad (2.\ 9)$$

Where P_{H2} is the desired H_2 production (the target value considered is equal to 33 kg/h), and Q_{sludge}^{in} is the inlet flowrate of waste activated sludge (kg/h), estimated considering the concentration of carbohydrates, lipids and proteins present in the inlet liquid flowrate Q^{in}, representing approximately only 0.001 of the mass fraction of the total flowrate. At *HRT* = 1 d, the H_2 yield corresponds to 0.116 g_{H2}/g_{sludge} and from Equation 2.9, the required inlet flowrate of sludge is obtained as well as the inlet liquid flowrate (Q_{in}, m^3/h). From Q_{in}, it is possible to obtain the value of the liquid volume V_{liq} (l) required to obtain the target H_2 production of 33 kg/h, following the equation:

$$V_{liq} = HRT_{opt} \cdot Q_{in} \quad (2.\ 10)$$

The species involved in the process include the sludge (carbohydrates, lipids and proteins), water, gas components (H_2 and CO_2), and VFAs (acetic, propionic and butyric acids). Table 2. 8 summarizes the concentration of species present in the MATLAB code and the corresponding mass flowrates. To obtain the mass flowrate of each component, the concentrations, which are expressed as kgCOD m^{-3}, are initially converted into mass concentrations (kg/m^3) by means of the corresponding conversion factors. The calculated mass concentration is multiplied by the volumetric flowrate of the liquid feed ($Q^{in} = 315.4\ ton/h$) to obtain the mass flowrates. This is done both for the inlet and outlet concentrations and starting from that the yields are evaluated as follows:

$$Y_i = \frac{Q_i^{out}}{Q^{in}} \qquad (2.\ 11)$$

where Q_i^{out} is the mass flowrate (kg/h) of the component i in the outlet (at HRT = 1 d) and Q^{in} is the liquid flowrate (kg/h) of the waste activated sludge. The yield values for each component are useful for the simulation in Aspen Plus, where a Yield Reactor unit is adopted to simulate the DF process.

Species	Concentration ($kgCOD/m^3$)	Conversion factor	MW (kg/kmol)	Concentration (kg/m^3)	Flowrate (kg/h)
Carbohydrates	0.6	1.067 kgCOD/kg	180	0.5623	161.25
Proteins	0.6	1.416 kgCOD/kg	113	0.4237	121.51
Lipids	0.6	2.896 kgCOD/kg	884	0.2072	59.41
Propionic acid	0.1	112 kgCOD/kmol	74	0.0661	18.95
Butyric acid	0.1	160 kgCOD/kmol	88	0.0550	15.77
Acetic acid	0.1	64 kgCOD/kmol	60	0.0938	26.88

Table 2. 8: Inlet concentrations and mass flowrates of each component present in the feed.

2.3 DF simulation on Aspen Plus

2.3.1 Components and the thermodynamic model

Table 2. 9 reports the components used in the Aspen simulation. In Aspen Plus the components can be defined as conventional or non-conventional components. The non-conventional components are those which are not included in the databases available within Aspen Plus. In the simulation, the non-conventional component is called SLUDGE and refers to the waste activated sludge that enters the process. The non-conventional component is treated as solids within the Aspen Plus simulation and is defined using the GENANAL component attributes, HCOALGEN as an enthalpy model and

DCOALIGT as a density model. The property model adopted is NRTL model, a local composition model which considers non-ideality in the liquid phase (Figure 2.8).

Chemical species	Component name	Aspen type	Henry Component
CO_2	Carbon dioxide	Conventional	Yes
H_2O	Water	Conventional	No
H_2	Hydrogen	Conventional	Yes
$C_3H_6O_2$	Propionic acid	Conventional	No
$C_2H_4O_2$	Acetic acid	Conventional	No
$C_4H_8O_2$	Butyric acid	Conventional	No
SLUDGE	-	Non-conventional	No

Table 2. 9: Chemical species defined in the Aspen Plus simulation.

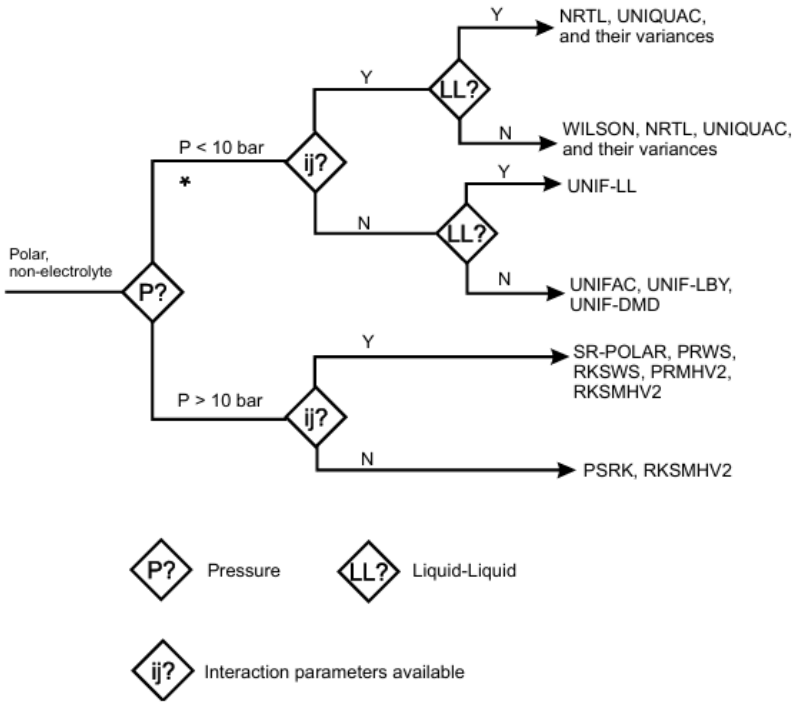

Figure 2.8: Guidelines for choosing a property model (Aspen Technology, Inc. 2000).

Table 2.10 defines the critical temperature provided in the Aspen Plus database for the species that are defined as Henry components. The components in the gas phase are defined as Henry components, which means that their vapor-liquid equilibrium behaviour is calculated according to the Henry's law. One species is defined as Henry component when it is in supercritical condition with respect to the temperature range of the process (which is higher than ambient temperature).

Chemical species	Critical Temperature (°C)
CO_2	31.06
H_2	-239.96

Table 2.10: Critical temperatures (°C) of the Henry components retrieved by Aspen Plus database

.

2.3.2 Simulation flowsheet

The simulation is divided into two sections: the dark fermentation section and the gas upgrading section. The DF section comprises the bioreactor, where the DF takes place, and the separation of the VFAs in the liquid phase. The gas upgrading section involves the separation of H_2 produced with the subsequent carbon capture. The method used to upgrade this gas stream and to produce an enriched hydrogen gas stream is through the combination of absorption and stripping using a chemical solvent (i.e., amines solution).

2.3.2.1 Dark Fermentation section

The process flowsheet detailing the dark fermentation section is reported by Figure 2. 9. The system is fed with 7570 ton/d of waste activated sludge. It is assumed that the feed enters the system at a temperature of 25 °C. The composition of the feed is reported in Table 2.11. For the evaluation of the sludge composition, it is considered the concentration of macromolecules such as carbohydrates, proteins and lipids, as well as propionic acid, butyric acid and acetic acid evaluated from the results obtained from the kinetic model.

Component	Mass fraction
Water	0.9987
Sludge	0.0013

Table 2.11: Composition of the feed.

The feed is mixed with the liquid sludge from stream SLUDGE-R that is recycled back to the system. Since the reactor operates under mesophilic conditions, the influent stream is heated up to 35 °C prior to employment in the bioreactor.

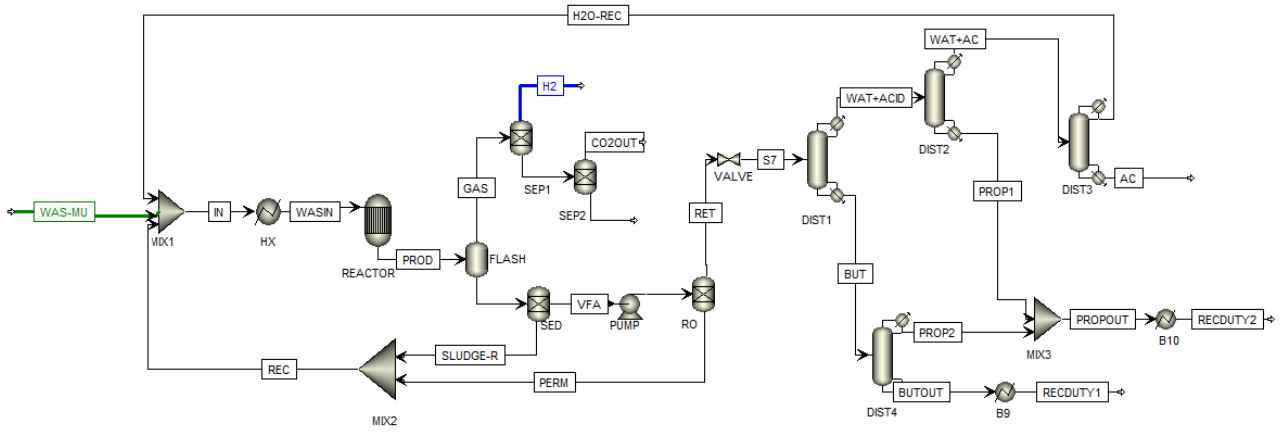

Figure 2. 9: Process flowsheet of Aspen simulation of DF.

The reactor is modelled using a RYield block. This type of reactor is based on mass balances and for this reason, it requires the specification of yield values for each component, both reactant and product, as well as the temperature and pressure at which the reactor operates. The pressure is set to 1 bar, as the process occurs at ambient pressure condition. The yield is evaluated considering the mass of waste sludge fed to the reactor, comprising both the water and the solid sludge. The yields (on mass basis) are expressed as:

$$Y_i = \frac{Q_i^{out}}{Q^{in}} \qquad (2.\ 12)$$

Where Q_i^{out} is the mass flowrate (kg/h) of the component i in the outlet (at HRT = 1 d) and Q^{in} is the liquid flowrate (kg/h) of the waste activated sludge. Table 2. 12 summarizes the yields of each component specified in the Aspen simulation.

Species	Q_i^{in} (kg/h)	Q_i^{out} (kg/h)	Yield (g/g)
Solid sludge	342.2	270.3	0.00086
Water	315034	313058	0.99246
H_2	0	33.75	0.00011
CO_2	0	932.7	0.00296
Propionic acid	18.95	210.8	0.00067
Butyric acid	15.77	212.1	0.00067
Acetic acid	26.88	719.9	0.00228

Table 2. 12: Mass flowrates of each component and the corresponding yield.

The DF reactions occur in a fermenter which is simulated in Aspen as a reactor and a flash unit, operating at the same temperature of the reactor (T=35°C) since in reality the separation of the gas and

liquid phases occur in the same environment, within the digestor. The liquid phase is comprised of the water with solid sludge and the organic acids. The solid sludge is completely separated from the liquid stream by means of sedimentation, which is simulated in Aspen as a separator where the split fraction of the SLUDGE is set equal to 1. The flowrate of solid sludge represents only 10 wt% of this stream, and the remaining fraction is water.

The liquid stream without sludge represents a very diluted aqueous solution of organic acids, with a small fraction of solubilized CO_2. The valorisation of the organic acids may represent an increase in revenues for the process. Accordingly, it is necessary to concentrate the organic acids before they are sent to purification since the high amount of water would require the use of distillation columns with large capacities and consequently, higher capital and operating costs. To produce an enriched organic acid stream by removing most of the water, a reverse osmosis (RO) membrane is adopted, which is a commonly employed method of industrial water purification (Werber et al., 2016). The RO membrane is a pressure driven process which operates through the application of a pressure higher than the osmotic one of the solution, and this generates a reverse flux from the more concentrated side to the most diluted one, i.e. the "fresh" water one. The osmotic pressure (π) is defined as the pressure that must be applied to a given solution to prevent water from moving through a semipermeable membrane by osmosis. It is a thermodynamic property and as such, it is a state variable that depends on temperature, pressure and concentration ($\pi = f(T, P, c)$). The osmotic pressure is related to the chemical potential (μ) and at equilibrium, the chemical potential of water in the two sides of the membrane must be equal ($\mu_w^\alpha = \mu_w^\beta$) (H. Strathmann, 2004). Since the chemical potential of water in the concentrated solution is different from that of pure water, the difference between the two sides is balanced by the pressure difference. Thus, the osmotic pressure is the pressure that must be applied to a given solution to make the chemical potential of the solvent in the solution equal to that of pure solvent at a given temperature. The RO membrane block is simulated and designed by means of the flux model, which defines the water flux according to (Khraisheh et al., 2020):

$$J_w = A_m(\Delta P - \Delta\pi) \qquad (2.13)$$

Where A_m is the water permeability constant and is determined experimentally for a specific type of membrane. In this case an average value for a thin-film composite (TFC) membrane of 3 L $(m^2\ h\ bar)^{-1}$ is adopted (Werber et al., 2016). The TFC involves a very thin dense layer of a polymerized polyamide on a porous structure.

The differences in pressure are defined as:

$$\Delta P = \frac{P_f + P_r}{2} - P_p \quad (2.\ 14)$$

$$\Delta \pi = \frac{\pi_f + \pi_r}{2} - \pi_p \quad (2.\ 15)$$

Where the subscripts *f*, *p* and *r* indicate the pressures at the different sides of the membrane, namely feed, permeate and retentate, as illustrated in Figure 2. 10.

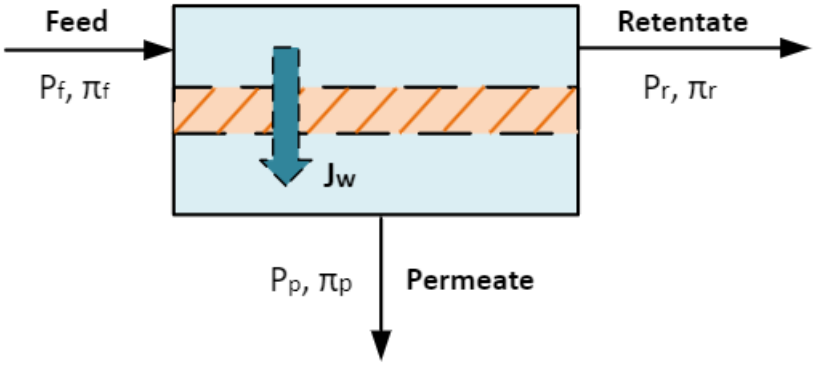

Figure 2. 10: Schematic representation of a RO membrane, with feed, permeate and retentate sides.

In the Aspen simulation, the osmotic pressure is overcome by increasing the hydraulic pressure of the feed side to 80 bar (which is currently the upper operating limit of commercial RO membranes), using a high-pressure pump. The composition of the retentate is calculated using an iterative approach with final values obtained at the point where the osmotic pressure of the retentate side is equal to 75 bar (i.e., the highest concentration achievable). The procedure involves modifying the split fraction of water and CO_2 in the permeate side equally, since both permeate through the membrane, thus they have the same split fraction. Then, the concentration of the solutes, i.e. the organic acids, in the retentate and in the permeate is determined.

From the material balances for the overall system and for the solute, the volumetric flowrates are evaluated. Particularly, the volumetric flowrate of the permeate (Q_p) is calculated, which is necessary to determine the total area (A_t) of the membrane as follows:

$$A_t = \frac{Q_p}{J_w} \quad (2.\ 16)$$

Since commercial membrane modules have standard sizes, the number of parallel modules can be evaluated starting from the total area and they are useful for the cost estimation of the total membrane.

Once the water and CO_2 are separated from the permeate side, they are mixed with the sludge exiting from the sedimentation and are recycled back to the reactor. On the retentate side, an enriched solution of organic acids is obtained which are sent to a series of distillation columns in order to be separated and purified. A preliminary analysis on the binary mixtures of these components (water, acetic acid, propionic acid and butyric acid) is conducted to find out the existence of azeotropes. All parameters of the NRTL model are present in the Aspen Plus databank for each binary pairs of the components that constitute the mixture. Only the binary mixture of water and butyric acid exhibits an azeotrope at 99.8 °C with 81.5% weight of water, shown by the T-x diagram in Figure 2. 11. The boiling temperatures of these components are retrieved from the Aspen Plus database and are reported in Table 2. 13.

Component	Boiling temperature [°C]
Water	100.0
Acetic acid	117.9
Propionic acid	141.2
Butyric acid	163.3

Table 2. 13: Boiling temperature (°C) of pure components to be separated.

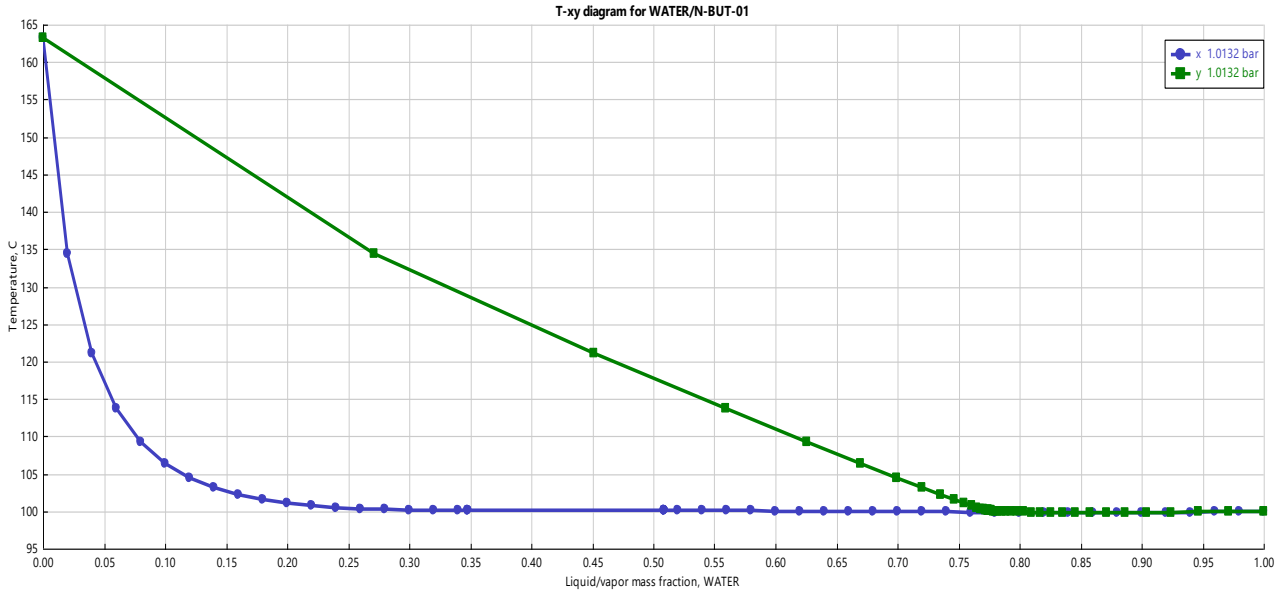

Figure 2. 11: T-x diagram for binary mixture water/butyric acid.

All four distillation columns are simulated using RadFrac unit in Aspen, which models a rigorous column assuming equilibrium between each stage. The first distillation column operates at conditions under the azeotropic point, in order to avoid the requirement of alternative separation techniques for azeotropic mixtures. Butyric acid is separated from the bottom of the first distillation column (DIST1), without reaching the purity required from the market (77.2% wt). For this reason, the bottom stream

is sent to another distillation column (DIST4) that recovers propionic acid from the top and butyric acid from the bottom and the corresponding mass fractions are 99.8% and 98.7%. The specifications of these two columns are reported in Table 2. 14.

Parameters	Column 1	Column 2	Column 3	Column 4
Reflux ratio	2	0.6	2.2	11.5
Number of stages	18	25	30	23
Distillate rate [kmol/h]	323	321	309	0.82
Bottom rate [kmol/h]	3.27	2.26	12	8.96
Top temperature [°C]	101	100	61.7	141
Bottom temperature [°C]	156	135	117	162

Table 2. 14: Specifications of the four distillation columns separating butyric acid and water (Column 1), propionic acid and water (Column 2), acetic acid and water (Column 3) and butyric acid and propionic acid (Column 4).

The stream obtained from the top of the first distillation column consists of a solution of water (86.4% wt), acetic acid (11.3% wt), and propionic acid (2.3% wt), which is further separated in two additional distillation columns. In the second column (DIST2), propionic acid is recovered as the bottom product (94.4% wt) and is subsequently mixed with the distillate stream from the column DIST4. The overhead stream from DIST2, containing a mixture of water and acetic acid (88.5% wt. and 11.5% wt, respectively), is sent to the last column (DIST3). In DIST3, water is recovered as the distillate and recycled back to the reactor, while acetic acid is withdrawn as the bottom product, meeting the required purity specifications for market sale. The integrated operation of these four distillation columns enables process valorisation through the efficient recovery of by-products. Additionally, the removal of water through both membrane separation and distillation reduces the makeup requirement. The mass flowrates and the mass fractions of the by-products recovered from the distillation columns are reported in Table 2.15.

Component	Mass flowrate [kg/h]	Mass fraction [-]
Acetic acid	712	0.995
Propionic acid	219	0.96
Butyric acid	215	0.99

Table 2. 15: Mass flowrates and mass fraction of the recovered by-products.

2.3.2.2 Gas upgrading section

This section involves the treatment of the gas stream exiting the fermenter, and the removal of carbon dioxide to produce an enriched hydrogen stream. The desired product of the process is hydrogen, which accumulates in the headspace above the reactor and is separated as a gaseous mixture from the liquid product that has been treated as described in the previous section. The method used to capture CO_2 from the gaseous stream is the reactive absorption and stripping (Madeddu et al., 2019). The process flowsheet is illustrated in Figure 2. 12. The composition of the gaseous product (FLUEGAS) exiting the reactor is reported in Table 2. 16, where the percentage of organic acids is minimal and can be assumed to be negligible. The primary component present in this stream is CO_2, which must be separated from H_2.

Component	Mole flowrate [kg/h]	Mole fraction [-]
H_2	16.8	0.46
CO_2	17.4	0.48
H_2O	2.33	0.06

Table 2. 16: Composition of the gaseous product stream (FLUEGAS).

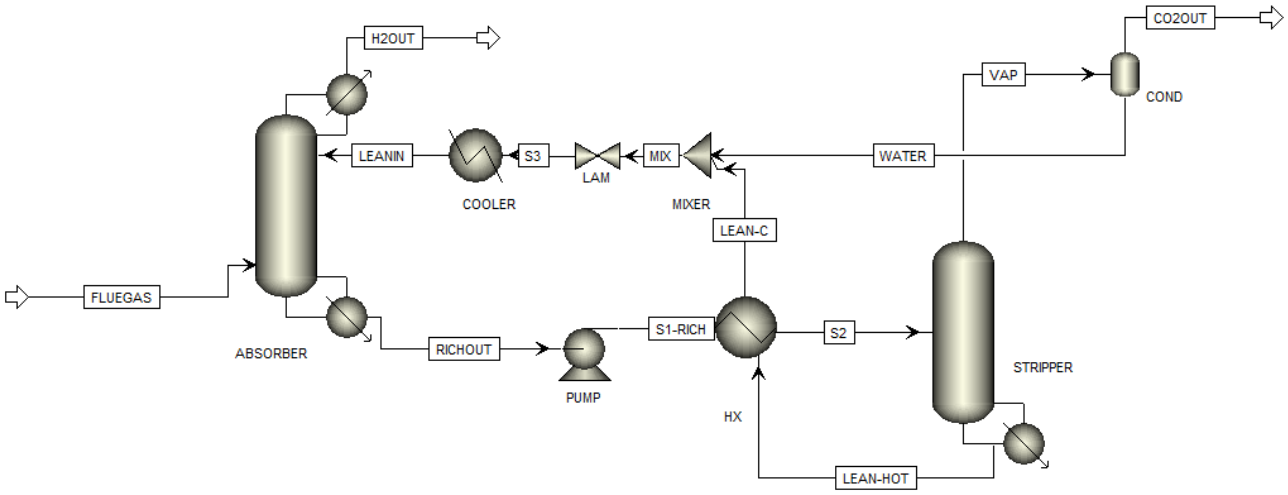

Figure 2. 12: Process flowsheet of Aspen Plus simulation of absorption and stripping of CO_2 from gaseous stream (FLUEGAS).

Chemical absorbents are an important class of liquid solvents used to absorb CO_2, since they facilitate the formation of carbonate bonds, which favours absorption. Specifically, an aqueous solution of monoethanolamine (MEA) is used in the simulation and its composition (LEANIN) is reported in Table 2. 17: Composition of the liquid solvent stream (LEANIN).. The flowrate of solvent necessary to achieve the desired level of CO_2 absorption is determined through a procedure that is explored in a further section.

Component	Mass fraction [-]	Mass flowrate [kg/h]
MEA	0.335	5206
H_2O	0.6	9325
CO_2	0.065	1010

Table 2. 17: Composition of the liquid solvent stream (LEANIN).

Once the main components of LEANIN and FLUEGAS are specified, the ionic equilibrium reactions involved in the liquid phase of the process are defined, as illustrated in Table 2. 18.

Reaction	Stoichiometry
1	$2H_2O \leftrightarrow H_3O^+ + OH^-$
2	$CO_2 + 2H_2O \leftrightarrow HCO_3^- + H_3O^+$
3	$HCO_3^- + H_2O \leftrightarrow CO_3^{2-} + H_3O^+$
4	$MEAH^+ + H_2O \leftrightarrow MEA + H_3O^+$
5	$MEACOO^- + H_2O \leftrightarrow MEA + HCO_3^-$

Table 2. 18: Equilibrium reactions for the MEA-H_2O-CO_2 system (Madeddu et al., 2019).

The thermodynamic model used for the estimation of properties in the liquid phase is the Electrolyte Non-Random Two Liquid (ELEC-NRTL), which is the most suitable to describe the electrolytic interactions present in the MEA-CO_2-H_2O system due to the presence of ions (Madeddu et al., 2019). Moreover, this model is combined with the Redlich-Kwong Equation of State (RKEOS) for the estimation of properties in the gas phase.

In the Simulation environment, it is necessary to specify a set of reactions in the Reactions panel due to the reactive nature of the process. Specifically, a set with three ionic equilibrium reactions and four kinetic reversible reactions are determined (Table 2. 19).

Reaction	Type	Stoichiometry
1	Equilibrium	$2H_2O \leftrightarrow H_3O^+ + OH^-$
2	Equilibrium	$MEAH^+ + H_2O \leftrightarrow MEA + H_3O^+$
3	Equilibrium	$HCO_3^- + H_2O \leftrightarrow CO_3^{2-} + H_3O^+$
4	Kinetic	$MEA + CO_2 + H_2O \rightarrow MEACOO^- + H_3O^+$
5	Kinetic	$MEACOO^- + H_2O \leftrightarrow MEA + HCO_3^-$
6	Kinetic	$HCO_3^- \rightarrow CO_2 + OH^-$
7	Kinetic	$CO_2 + OH^- \rightarrow HCO_3^-$

Table 2. 19: Set of reactions involved in the process: ionic equilibrium reactions (1-3) and kinetic reversible reactions (4-7).

For the equilibrium reactions, the equilibrium constants are determined from the standard Gibbs free-energy change equation:

$$K_{eq} = exp\left(-\frac{\Delta G^0}{RT^L}\right) \quad (2.\ 17)$$

Where the values of ΔG^0 are retrieved from the Aspen Properties database. Instead, for the kinetic reactions, the kinetic constants are obtained from the Arrhenius law:

$$k = k_0\left(-\frac{E_a}{RT^L}\right) \quad (2.\ 18)$$

Where the parameters k_0 and E_a are reported in Table 2. 20.

Kinetic reaction	k_0 [-]	E_a [cal/mol]
4	9.77e+10	9855.8
5	3.23e+19	15655
6	2.38e+17	29451
7	4.32e+13	13249

Table 2. 20: Kinetic parameters for the kinetic reactions (4-7) of the reactive columns.

Both the absorption and the stripping columns are simulated as packed columns by means of the RadFrac model, employing the rate-based approach. In this case, the height of the column is discretized in several segments that define the precision with which the calculations are made. The rate-based approach is useful to model such processes since it takes into account the mass transfer limitations due to the occurrence of chemical reactions inside the column (Madeddu et al., 2019). This model is based on the two-film theory that describes the mass transfer of gas across a liquid film during absorption (Lewis and Whitman, 1924). A schematic representation of the segment in the rate-based approach is illustrated in Figure 2.13: Schematic representation of a column segment in the rate-based approach (Madeddu et al., 2019).Figure 2.13.

Initially, a theoretically infinite packing height is used to determine the minimum solvent flowrate. To design the packed column in Aspen, the *Packing Rating-Design Mode* option allows to determine the column diameter. In this case it is required to specify the base stage, namely the specific point at which the evaluation of the column diameter is performed, which corresponds to the part of the column where most vapour is present. To monitor the location of the base stage, it is necessary to plot the trend of the vapor flowrate inside the column and assess at which stage its maximum value is located. The absorption column is designed such that at least 90% of the CO_2 entering the system in the stream FLUEGAS is absorbed in the first column.

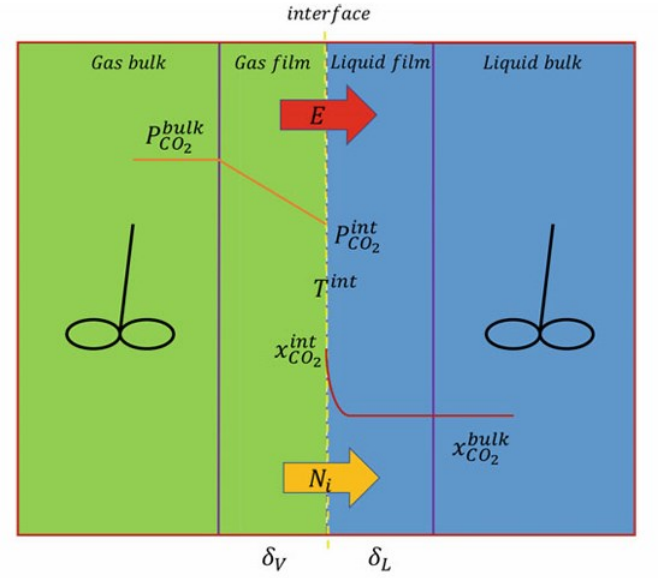

Figure 2.13: Schematic representation of a column segment in the rate-based approach (Madeddu et al., 2019).

Once the H_2 is separated and recovered from the top of the absorption column, the stream exiting from the bottom of the column is sent to the stripping section where the regeneration of the solvent rich in CO_2 occurs. In the stripper the CO_2 is separated from the amine solution due to the vapor flowrate produced in the reboiler. Generally, the stripping process is favoured by high temperatures and it must be operated at pressures higher compared than that of the absorber to ensure the transfer of CO_2 to the gas phase (Madeddu et al., 2019). However, the pressure cannot exceed an upper limit imposed by the degradation of amines. Thus, the stream RICHOUT is pumped to 1.8 bar that is the operating pressure of the stripper.

The condenser of the stripping column is designed to condense the water from the vapour phase to its liquid phase, effectively separating the CO_2 from H_2O and producing a CO_2 rich gas stream. The condensed water is not sent back to the column as a reflux to avoid a decrease of the top column temperature that would require a higher duty from the reboiler and consequently, a larger diameter. Thus, the liquid water stream recovered from the condenser is then mixed with the lean solvent coming from the reboiler. The link between the two columns is represented by the cross heat-exchanger, where the lean solvent (LEAN-HOT) releases the heat required to heat up the rich solvent coming from the bottom of the absorption column. The lean solvent is then mixed with the water coming from the condenser and the stream is brought to its initial temperature and pressure by means of a heat exchanger and a valve. The final size of the absorption and stripping columns are reported in Table 2.20.

	Absorption column	Stripping column
Height [m]	12	3
Diameter [m]	0.66	0.55

Table 2. 21: Specifications of the absorption and stripping columns in terms of design parameters.

2.4 PF simulation

As far as Photofermentation is concerned, it is considered to couple this method with the Dark Fermentation process, as simulated in the previous section. In this case, the combination of Dark and Photo fermentation allows the use of the VFAs stream produced by the first process as a substrate for the second process. By doing so, the liquid product stream leaving the first fermenter can be recovered and used as the feed for the second process. The liquid stream considered for the feed of the photobioreactor is the diluted aqueous solution of the organic acids that leaves the sedimentation unit in the DF simulation. The composition and concentration of this stream is reported in Table 2.22.

Component	Molar flowrate [kmol/h]	Concentration [g/L]
Water	17 906	993
Acetic acid	12.26	2.23
Butyric acid	2.47	0.66
Propionic acid	2.92	0.67

Table 2.22: Feed liquid stream for the Photofermentation process.

It is assumed that the microorganisms involved in the photofermentative H_2 production process is the PNSB-*Rhodopseudomonas palustris*, which under anaerobic and nitrogen free conditions, in presence of light and an organic source of carbon is able to produce high purity hydrogen (Ross and Pott, 2021). It is assumed that the acetic acid is the carbon source utilised by the PNSB for H_2 production, according to the following reaction:

$$CH_3COOH + 2H_2O \rightarrow 4H_2 + 2CO_2 \quad (2.19)$$

The production of H_2 is calculated based on experimental values found on literature, since no kinetic model is applied to predict the H_2 production though PF, unlike the approach used for DF, due to the lack of a suitable model. The experimental values adopted as basis for the calculations are reported in Table 2. 23.

Parameter	Value	Unit
Volumetric production rate	44	mL/L/h
Hydrogen yield	3.56	$mol_{H2}/mol_{acetate}$
HRT	36	h
Cell concentration	6.13	g/L
Specific hydrogen production	7.18	$mL/g_{CDW}/h$

Table 2. 23: Literature results used as reference basis for calculations (Chen and Chang, 2006).

The mass of bacteria required is determined by multiplying the cell concentration by the volume of the PBRs, which is based on the volumetric flowrate of the effluent from DF and the adopted HRT. The overall volume of the PBR is divided in a certain number of reactors, such that the dimension of each reactor lies within a reasonable range. Thus, it is assumed that the radius of each photobioreactor is equal to 0.1 m, which ensures that the PBR is not too thick, resulting in mutual shading issues. The volume of each PBR is equal to approximately 0.4 m^3 and the total number of PBRs results as 31027. The values obtained for the PBRs and the mass of bacteria are reported in Table 2. 24.

Parameters	Values	Unit
Cell concentration	6.13	g/l
Total volume PBRs	11,697	m^3
Single PBR volume	0.38	m^3
Height PBR	12	m
Radius PBR	0.1	m
Number of PBRs	31027	-
Total area PBRs	74,465	m^2
Biomass	93	tons

Table 2. 24: Parameters specifications for the PBRs and the biomass required for the photofermentation process.

The block flow diagram of the process is reported in Figure 2. 14.

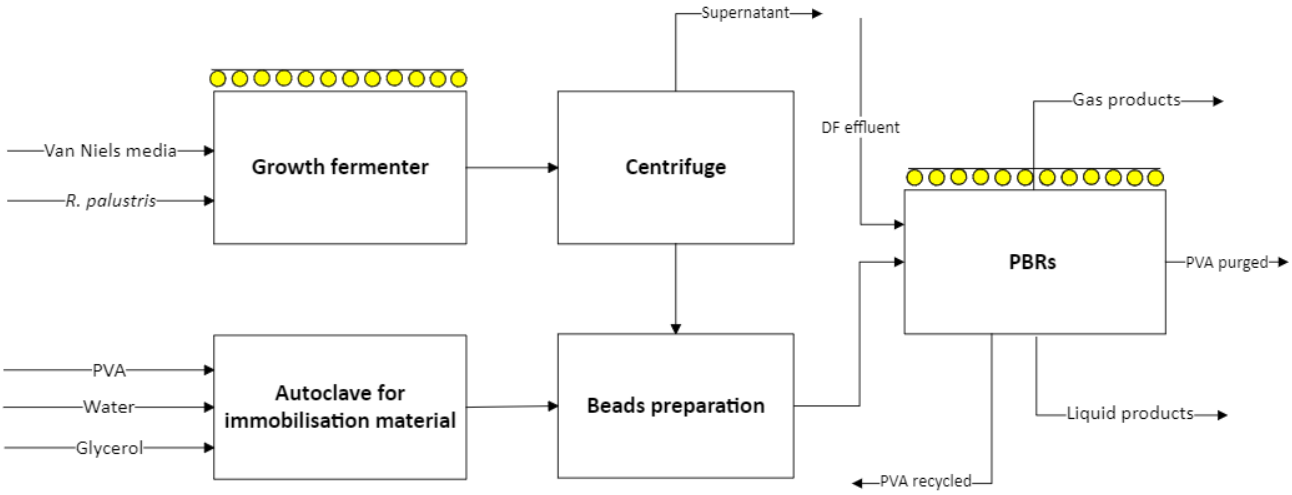

Figure 2. 14: BFD of the Photofermentation process with the immobilisation technique.

It is assumed that the effluent from DF is sent directly to the PBRs where the PF occurs. It is considered that the biomass is immobilized in a solid matrix made of PVA hydrogels. In this case, the process comprises an initial stage where the bacteria are grown in a proper media to produce the inoculum, and subsequentially the bacteria in the stationary phase are separated and then immobilised in the PVA beads. The photosynthetic bacteria are grown in a proper media, specifically in a Van Niels medium, which comprises 10 g/L of yeast extract, 0.5 g/L of $MgSO_4 \cdot 7H_2O$ and 1 g/L of K_2HPO_4. The bacteria are grown in fermenters with a sufficient source of illumination. Once they reach the stationary phase, or mid-late logarithmic phase, they are separated through centrifugation and immobilised in a solid matrix. In this state, the bacteria inside the PBRs can be considered as a constant biocatalyst which can be completely replaced annually, since preliminary data show that a high percentage of intact cells remains viable for about 9 months (personal communication). The bacteria are immobilized using PVA hydrogels, with a biomass concentration, expressed as a mass fraction of the bacteria to hydrogel material, equal to 1.5% wt. The immobilisation material is 11 wt/v% PVA dissolved in a solution containing 50 v/v% water and 50 v/v% glycerol. It is assumed that a portion of beads within the PBRs is replaced twice a month, with a total replacement rate of once every 9 months. In this scenario, the total amount of PVA required is split up to 24 replacements occurring in the 1-year period, which results in approximately 130 tons of PVA hydrogels replaced every 2 weeks. In these 130 tons of hydrogels, there are about 2 tons of bacteria. Considering that *R. palustris* grows to approximately 5 g/l after a period of 5 days in Van Niels growth media (Ross and Pott, 2022), it is required a volume of 390 m^3 to obtain the required amount of bacteria after 15 days. The fermenter volume is split up to 260 fermenters for them to be within a reasonable size range. An autoclave for the immobilisation material is required, and its volume is evaluated considering that 130 tons of hydrogels corresponds to

approximately 108 m^3. Due to the large volume requirements for the PVA, it is assumed that 50% of the PVA discharged from the PBRs is recycled and the other half is purged. The light requirement for the reactors is calculated considering as a design case 150 W halogen light bulbs, which are then converted to the equivalent LED light of approximately 19 W (Figure 2. 15). The number of total lights required, and the corresponding electrical requirements, are evaluated considering the total area of the reactor and the surface area covered by a light bulb which supplies an average of approximately 200 W/m^2.

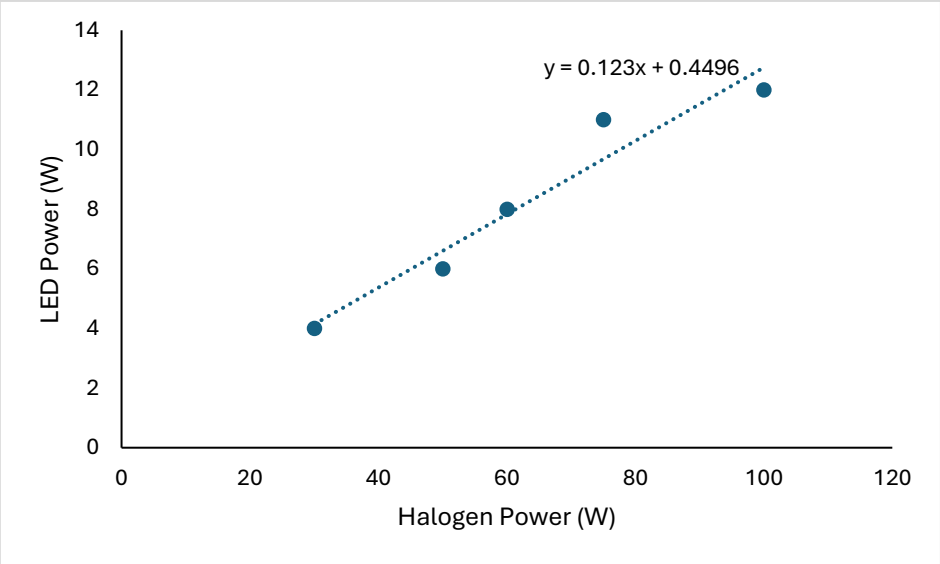

Figure 2. 15: Correlation between the power of halogen and LED light to obtain the conversion of the light power from halogen to LED (https://ledhut.co.uk/blogs/news/led-equivalent-wattages-against-traditional-lighting).

The same procedure is adopted to evaluate the light requirements for the PBRs where the PF process is facilitated. The two streams leaving the reactors are the gas product stream and the liquid effluent stream. In the gas phase, H_2 and CO_2 are produced according to the stoichiometric reaction, and they represent the 67% and 33% molar fraction of such stream, respectively. It is assumed that the gas products from DF and PF are mixed and sent to the gas upgrading section to separate H_2 and to capture CO_2. The total amount of H_2 produced from the combined processes is 76 kg/h. The composition of the mixed gaseous stream is different from the one leaving the DF process, as can be noted in Table 2. 25.

Process	Component	Molar flowrate [kmol/h]	Molar fraction [-]
DF	H_2	16.8	0.46
	CO_2	17.4	0.48

	H_2O	2.0	0.06
Combined process	H_2	21.4	0.67
	CO_2	10.7	0.33
	H_2O	-	-

Table 2. 25: Composition of the gas product from DF and combined process.

The liquid stream products contain the water, butyric and propionic acid and the unreacted acetic acid. This stream can be sent to a membrane separation process to recover the water which can be recycled back to the DF reactor and to separate the mixture of organic acids, as it was done for the DF simulation case (Paragraph §2.3.2 **Simulation flowsheet**). In order to obtain the mass balances, the RO membrane is simulated using Aspen Plus with the same procedure adopted for DF.

2.5 Techno-economic analysis

Once the flowsheet of the process has been obtained, an economic analysis can be performed to assess the capital and operating costs of the hydrogen production process, with the aim of assessing the Levelized Cost of Hydrogen of the two bio-processes analysed.

2.5.1 Capital costs

Capital costs (CAPEX) are evaluated directly from the output of the Aspen Plus Economic Analyser (APEA), which allows to retrieve the sizing and operative specification of each piece of equipment. To perform the cost estimation, the computer program CAPCOST from Turton book (Turton et al., 2018) is exploited, which eases the calculation with less chance of errors. All data considered in CAPCOST are retrieved from the correlations present in Turton's book (Turton et al., 2018) which are provided as approximate costs in 2001 with a Chemical Engineering Plant Cost Index (CEPCI) equal to 397. To adjust the cost data for inflation, the current CEPCI value, updated to June 2024 (798.8), is used (Chemical Engineering, Plant Cost Index, https://www.chemengonline.com/site/plant-cost-index/).

The program requires specific input depending on the type of equipment, as for example the heat transfer area for the heat exchangers or the diameter and height of the columns and vessels. Since it is a new chemical plant, the method used for cost estimation is the module costing technique. This method accounts for the purchased cost of equipment evaluated at a base condition and eventual

deviations, such as specific material of construction, are considered by means of multiplying factors. The bare module cost is expressed as:

$$C_{BM} = C_p^0 F_{BM} \quad (2.20)$$

where C_{BM} accounts for both direct and indirect costs for each unit, C_p^0 is the purchased cost at base conditions (generally, made of carbon steel and operating at ambient pressure) and F_{BM} is the deviation factor.

The total capital investment (TCI), or CAPEX, is the sum of the FCI, the working capital (WC) and the start-up costs (StC), as indicated by Equation 2.21.

$$TCI = FCI + WC + StC \quad (2.21)$$

The outputs from CAPCOST are considered as the fixed capital investment (FCI) which accounts for the so-called inside battery limits (ISBL), the offsite battery limits (OSBL) and the indirect costs (IC) (equation 2.22). Most of ISBL costs are associated with process equipment, including the purchased and installation costs, instrumentation and control systems, piping and related components. The off-site battery limits (OSBL) costs cover direct expenses related to auxiliary buildings and land. The IC are not directly related to manufacturing capital investment and can include supervision and engineering expenses and contingencies.

$$FCI = ISBL + OSBL + IC \quad (2.22)$$

The WC is the capital required in the first months of plant operations to cover raw-material purchases, salaries and contingencies, before the plant starts to generate revenues. It is fully recoverable at the end of the project; thus, it cannot be depreciated. It can be estimated as a fraction (20%) of the fixed capital investment.

The StC accounts for further modifications that can be applied to the process and is related to the cost required to cover the start-up labour and any loss in production that could occur once the process is started-up.

2.5.2 Operating costs

The Cost of Manufacturing (COM) for a chemical production, also known as operating costs, are related to the day-to-day operation of a chemical plant. There are many factors that influence the cost of manufacturing chemicals, and they can be divided into 3 categories (Turton et al., 2018): direct manufacturing costs (DMC), fixed manufacturing costs (FMC) and general expenses (GE), according to Equation (2.23):

$$COM = DMC + FMC + GE \quad (2.\ 23)$$

Where the general expenses (GE) cover the costs related to management, sales, research and development. For the purpose of this analysis, they were neglected.

The DMC represents the variable costs of production, namely they vary depending on the production rate of the plant. They include the costs of:

- Raw materials fed to the process
- Utilities (steam, cooling water, electricity…)
- Consumables (solvents, catalysts…)
- Effluent treatment (i.e. wastewater)
- Operating labour
- Supervision
- Labour overheads

The operating costs are expressed in terms of €/y. For this reason, it is necessary to fix the amount of time that the plant is operating during the year. Generally, plants in continuous operations are designed to run 24 hours a day for 7 days a week. However, due to necessary maintenance and other interruptions, plants do not operate continuously for the entire year. Thus, a stream factor is used which reflects the actual operating time. In this case, the stream factor is 93% which corresponds to a plant which operates for 8150 h/y.

The FMC are fixed costs of production and as such, they are independent of changes in production rate. They include:

- Maintenance
- Local taxes and insurance
- Plant overhead costs

Table 2. 26 summarizes the components of the utilities and the fixed manufacturing costs, with the corresponding unit price.

Components	Unit cost
Electricity	0.112 €/kWh (https://www.statista.com/statistics/1267500/eu-monthly-wholesale-electricity-price-country/)

Low-Pressure Steam	0.4338 €/Smc (https://www.arera.it/consumatori/valori-della-materia-gas-per-il-servizio-di-tutela-della-vulnerabilita)
Cooling water	2.63 €/m^3 (https://altotrevigianoservizi.it/files/filemanager/source/utenti/Tariffe%202024/Tariffe_servizio_idrico_integrato_in%20attesa_mti4_2024.pdf)
Operating labour	40 k€/y (Turton et al., 2018)
Supervision	25% of operating labour
Overhead	35% of the sum of operating labour and supervision
Local taxes	1% of the FCI
Maintenance	3% of the FCI
Plant overhead	65% of the sum of maintenance and operating labour

Table 2. 26: Components of the operating costs with the associated unit cost.

2.5.3 Levelized cost of hydrogen (LCOH)

Levelized costs are effective indicators used to assess the economic efficiency of a production process as they measure the feasibility, in terms of economic performance, of a specific technology. The levelized cost of hydrogen (LCOH) is a specific indicator for H_2 production as an energy vector and represent the present value since it takes into account the discounted rates. It is evaluated according to the equation 2.24 (Fan et al., 2022):

$$LCOH = \frac{CAPEX + OPEX_{year} \sum_{t=1}^{N} \frac{1}{(1+r)^t}}{HP \sum_{t=1}^{N} \frac{1}{(1+r)^t}} \quad (2.\ 24)$$

where N (years) is the lifetime of the project, r (%) is the discount rate and HP is the yearly H_2 production (kg). It can be assumed that OPEX and HP remain constant over the years, thus they are outside the summation term. The value of this indicator reflects the market price that hydrogen must

reach to match the average production costs over the project's lifetime. In other words, it is the price at which, by the end of the N-year project, the investment at least breaks even.

CAPEX and OPEX are evaluated using the methodology described in §2.4.1 and §2.4.2. The annual hydrogen production (HP) is given by the total H_2 produced in a year, considering a stream factor of 93%. The lifetime of the project is considered to be 20 years, and the discount rate is equal to 10%. In addition, the revenues from the by-products selling are taken into account in the evaluation of the LCOH, and specifically they are subtracted from the operating costs (OPEX) present in the equation 2.24.

The production cost of biohydrogen can be partially mitigated by selling the by-products generated through the separation and purification stages following the DF process unit. The unit costs of each compound are based on the current market price of the compound and are reported in Table 2. 27.

By-products	**Market price [€/ton]**	**Reference**
Propionic acid	903	[4] https://www.intratec.us/chemical-markets/propionic-acid-price
Acetic acid	450	[5] https://www.echemi.com/pip/acetic-acid-temppid160628000977.html
Butyric acid	1339	[6] https://www.chemanalyst.com/Pricing-data/butyric-acid-1250
CO_2	314	[7] https://www.oecd.org/content/dam/oecd/en/topics/policy-sub-issues/carbon-pricing-and-energy-taxes/effective-carbon-rates-2021-brochure.pdf

Table 2. 27: Unit cost for the by-products (VFAs and CO2) of the DF process.

It is assumed that CO_2 can also generate revenue considering that it is sold within the food industry, where it is applied for beverages or for food processing.

Chapter 3

Results and discussion

The following section presents the results of the economic analysis, focusing on capital and operating costs for the single-stage dark fermentation and the two-stage dark-photo fermentation processes. Various scenarios are analysed to evaluate the levelized cost of hydrogen (LCOH), which in this study serves as an indicative measure of the economic performance for each developed technology. Additionally, a sensitivity analysis is performed on the best-case scenarios to assess the effect of different key factors on the LCOH.

3.1 Results of the economic analysis

The results of the economic analysis are presented for the base case of the dark fermentation plant, which comprises both the fermentation section, the gas upgrading section and the liquid product separation section. The variations from this case study that will be presented later involve adjustments to the costs outlined below and will be explained in the corresponding analysis. Table 3. 1 summarizes the installation equipment cost for the dark fermentation plant.

	Equipment	**Installation cost 2024 [k€]**
Dark fermentation unit	Bioreactor	1,815
	Flash	237
	Sedimentation	237
	RO vessel	198
	Cooler	126
VFAs separation	Towers	4,228
	Reboilers	920
	Condensers	630
Gas upgrading	Absorption column	62
	Stripping column	23

	Cooler	98
	Reboiler	211
	Condenser	36
Total equipment cost		8,821

Table 3. 1: Total equipment cost for the dark fermentation plant, including the fermentation unit, the liquid separation and the gas upgrading.

All equipment costs are retrieved from the CAPCOST software, with the specifications for the equipment derived from APEA. The only exception is the cost for the bioreactor, as the correlation provided in Turton's book offers a capacity parameter range which is too narrow for the case under consideration and would lead to an overestimation of the cost. Instead, the bioreactor cost is based on the data found on a techno-economic analysis of dark fermentative hydrogen production from molasses (Han et al., 2016). It can be noted that more than half of the Fixed Capital Investment (ISBL) is given by the equipment related to the liquid separation section, namely the towers for the distillation, the reboilers and the condensers. The liquid product separation unit involves energy-intensive processes which are more complex and costly than the only production methods of hydrogen.

The various components of the capital cost of the plant are presented in Table 3. 2, which shows that the total capital investment for the plant is approximately 11,500 million €.

Capital cost components	**Value [k€]**
FCI	8,821
Start-up costs	882
Working capital	1,764
TCI (CAPEX)	11,466

Table 3. 2: Components of the capital cost for the dark fermentation plant.

Regarding the annual plant operating costs, they include the cost for the feedstock and raw materials, the utilities cost, the operating labour, supervision and overhead, and indirect costs such as local taxes, maintenance and plant overhead. Table 3.3 illustrates the composition of the various operating costs for the plant. The raw materials cost also considers the RO membrane, since it is assumed that, due to fouling, the membrane may need to be replaced once a year, making it a recurrent expense. In fact, fouling issues in the RO unit must be accounted since they reduce the water permeability by partially clogging the membrane pores. This can result in increased flow resistances, either by reducing the permeability of water at constant pressure or requiring higher pressure to maintain a constant flux

(Ahmed et al., 2023). The membrane cost is estimated considering a unit cost for the membrane module (250 €/module, (El-Gendi et al., 2021)), which is then multiplied by the number of total modules constituting the membrane.

Components	Unit cost	Total cost [€]
Feedstock	15 €/kg (Domini et al., 2022)	1,956
Raw material	-	25,973
Utility		
Electricity	0.112 €/kWh (https://www.statista.com/statistics/1267500/eu-monthly-wholesale-electricity-price-country/)	818,486
Natural gas (for Low-Pressure Steam production)	0.4338 €/Smc (https://www.arera.it/consumatori/valori-della-materia-gas-per-il-servizio-di-tutela-della-vulnerabilita)	8,653,816
Cooling water	2.63 €/m^3 (https://altotrevigianoservizi.it/files/filemanager/source/utenti/Tariffe%202024/Tariffe_servizio_idrico_integrato_in%20attesa_mti4_2024.pdf)	815,710
Operating labour	40 k€/y (Turton et al., 2018)	600,000
Supervision	25% of operating labour	150,000
Overhead	35% of the sum of operating labour and supervision	262,500
Local taxes	1% of the FCI	88,198
Maintenance	3% of the FCI	264,596
Plant overhead	65% of the sum of maintenance and operating labour	561,986
OPEX		12,243,221

Table 3.3: Components of the total operating costs of the dark fermentation plant, with the unit cost related to each category.

The cost for the operating labour is evaluated assuming a total number of operators equal to 15, with an annual operator cost equal to 40 k€/y. The cooling water cost considers the unit cost per cubic meter

of water required in the condensers. Consequently, the total cost is based on a single-use water flow, which is a conservative estimation, considering that this water could potentially be recovered through a cooling tower system.

The annual revenues obtained from the selling of the by-products are reported in Table 3. 4. It is assumed that the selling cost for propionic acid, butyric acid and CO_2 is 85% of their market price, since they do not have the high purity required by the market. In fact, the composition of such compounds may result in a lower market value, with the only exception is made for acetic acid, since it is recovered at a very high purity (99.5% in mole fraction). In addition, these results do not take into account the fact that the market for such compounds may be saturated, and therefore not all the quantity produced can be accepted for sale. Thus, the annual revenue generated from selling the by-products may be lower and the cost for their storage must be taken into account.

By-product	**Annual income [€/y]**
Acetic acid	2,611,260
Propionic acid	1,611,184
Butyric acid	2,345,824
CO_2	1,922,298
Total annual revenues	8,490,566

Table 3. 4: Total annual revenues generated from the sale of by-products: acetic acid, propionic acid, butyric acid and CO_2.

Regarding the photo fermentation process, the capital costs related to the equipment for the inoculum preparation and the material for bacteria immobilisation are considered. The new capital cost sources in addition to the DF process are related to the preparation of the inoculum and the immobilised cells. Specifically, the fermenter where the bacteria are grown, the autoclave used for the immobilisation material, the centrifuge to separate the bacteria and the PBRs where the photofermentation process takes place. The corresponding installation costs are reported in **Errore. L'origine riferimento non è stata trovata.**5, where the costs are all referred to the 2024 by means of the updated CEPCI.

Equipment type	**Cost [k€]**
PBRs	1,116
Growth fermenter	19
Autoclave	5,582
Centrifuge	65

Table 3. 5: Installation costs related to the piece of equipment required by the PF process, expressed in terms of k€ (2024).

For the cost estimation of the PBRs, a 2019 NREL techno-economic study is considered (Clippinger and Davis, 2019), where the cost for a horizontal tubular PBR is estimated at 61 k€/acre (2024), which corresponds to approximately 15 €/m^2. The installation costs for the autoclave and for the centrifuge are estimated using the correlations from Turton's book (Turton et al., 2018). In the case of the autoclave, the purchased cost is scaled through the six-tenth's rule (equation 3.1), since the capacity parameter exceeds the upper limit imposed by the correlation.

$$C_a = C_b \left(\frac{A_a}{A_b}\right)^{0.6} \quad (3.1)$$

Where C is the purchased cost and A is the capacity parameter related to a specific piece of equipment. The value of the cost esponent can vary depending on the class of equipment considered, but 0.6 can fit well for this purpose. Neverthless, it should be noted that estimating the cost using this correlation could significantly overestimate the total cost of the autoclave, which effectively results in a very high expense. The composition of the total capital costs (CAPEX) for the combined processes are reported in Table 3. 6.

Capital cost components	**Value [k€]**
FCI	9,823
Start-up costs	982
Working capital	1,965
TCI (CAPEX)	12,770

Table 3. 6: Components of the total capital costs (CAPEX) correlated to the combined processes (dark and photo fermentation).

Since in this study the PBRs are assumed as made of plastic tubes, 20% of the reactor cost is included in the operating cost for maintenance, in order to consider that part of the plastic tubes may be replaced once a year. In fact, plastic tubes undergo a steady loss of transparency that might affect the light penetration within the reactors, and negatively impact the H_2 production efficiency. Thus, the use of cheaper materials for the PBRs such as LDPE (Low Density Poly-Ethylene) is favoured compared to glass-like materials since it reduces the capital cost related to the reactor.

As far as operating costs are concerned, in this process one has to consider the cost of utilities related to the consumption of electricity for the demand of light both in the growth phase of the bacteria and for the PBRs of photofermentation. The electricity consumption for the light requirements results in an annual operating cost equal to 820,590 €. In addition, the cost for the immobilisation materials

(PVA, glycerol and water) and for the Van Niels media nutrients must be taken into account, as shown in Table 3. 7.

Component	Unit cost	Value [€]
PVA	1.8 €/kg (https://www.intratec.us/chemical-markets/polyvinyl-alcohol-price)	5,592,586
Glycerol	0.783 €/kg (https://www.intratec.us/chemical-markets/glycerol-price)	85,147
Water	0.013 €/kg ((Turton et al., 2018)	1,123
Van Niels media		
K_2HPO_4	0.72 €/kg (https://www.alibaba.com/product-detail/Dipotassium-hydrogen-phosphate-DKP-98-K2HPO4_60606530182.html)	559
$MgSO_4 \cdot 7H_2O$	0.116 €/kg (https://www.alibaba.com/product-detail/Wholesale-Price-99-White-Crytal-MgSO4_1601095208094.html)	45
Yeast extract	4.5 €/kg (https://www.chemicalbook.com/ProductDetail_EN_yeast-extract_2805126.htm)	34,954
Total material costs (inoculum+immobilisation)		5,714,414

Table 3. 7: Composition of the raw materials costs related to the inoculum preparation and the immobilisation material.

3.2 LCOH results

3.2.1 Dark Fermentation process

To evaluate the LCOH related to DF process, six different scenarios are investigated. Initially, the main distinction is made between the cost related to the feedstock of the process. The waste activated sludge can be retrieved from a wastewater treatment plant (WWTP) located near the plant of DF, since it is a

by-product of the wastewater treatment process. Thus, in terms of feedstock cost two different cases are considered: in the first case, only the cost for transportation of the sludge from the WWTP to the DF facility is taken into account and is evaluated as 15 €/kg (Domini et al., 2022). The other possibility is to consider that the sludge disposal and recovery from the WWTP generates an income for the process itself. In this case, the WWTP compensates the DF plant for treating its wastewater stream with a revenue of 100 €/kg (Domini et al., 2022). Thus, considering an annual operating period of 8150 h (stream factor ~ 93%), the cost for transportation results as 2 k€/y. On the other hand, the recovery of waste activated sludge generates an income of 13 k€/y. A third scenario assumes that no costs are generated for either the feedstock or for the effluent treatment. Thus, in this case there is a balance between the DF process, which offsets the costs of sludge treatment, and the effluent produced by the plant that still requires to be treated.

The other key difference between the scenarios for the DF process is the separation and sales of the organic acids. In order to evaluate whether the recovery of organic acids is a factor that positively affects the LCOH, it is distinguished among the two cases. On one hand, capital and operating costs related to the four distillation columns are taken into account. On the other hand, the effluent leaving the RO membrane from the retentate side, which comprises an aqueous solution of organic acids, is not sent to purification but it is treated as a wastewater stream that generates a cost for the plant, specifically 0.04 €/m^3 (Turton et al., 2018).

Table 3. 8 summarizes the results obtained for the LCOH, with the corresponding CAPEX, OPEX and the annual revenues.

	Case 1a	**Case 2a**	**Case 3a**	**Case 1b**	**Case 2b**	**Case 3b**
CAPEX [k€]	11,466	11,466	11,466	3,954	3,954	3,954
OPEX [k€]	12,243	12,228	12,241	2,655	2,640	2,653
Revenues [k€]	8,491	8,491	8,491	1,922	1,922	1,922
HP [tons/y]	269.3	269.3	269.3	269.3	269.3	269.3
LCOH [€/kg]	18.94	18.88	18.93	4.45	4.39	4.44

Table 3. 8: Results of the LCOH for the 6 scenario for DF process.

Case a) (1-3) refers to the scenario where the liquid by-products are separated, whereas case b) (1-3) refers to the scenario where the separation is neglected, and the effluent is treated. Moreover, case 1

takes into account the cost for the activated sludge feedstock, case 2 considers the sludge as an income, whereas case 3 does not take into account either the cost or profit related to the feedstock, nor the cost of treating wastewater. CAPEX for case a) is much higher compared to the one resulted from case b) since major contribution to capital investment is given by the cost of the columns for the separation of the VFAs by-products. In fact, Figure 3. 1 shows that the 66% of the fixed capital investment (FCI) for the case a) is related to the equipment for the liquid separation, while the remaining 34% is directly allocated to the core of the process and the gas upgrading section.

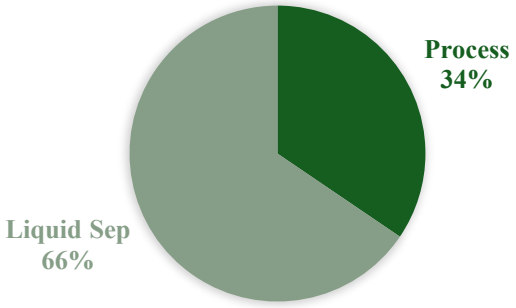

Figure 3. 1: FCI composition for the case a).

Figure 3. 2 further breaks down these percentages to illustrate the cost distribution for each type of equipment.

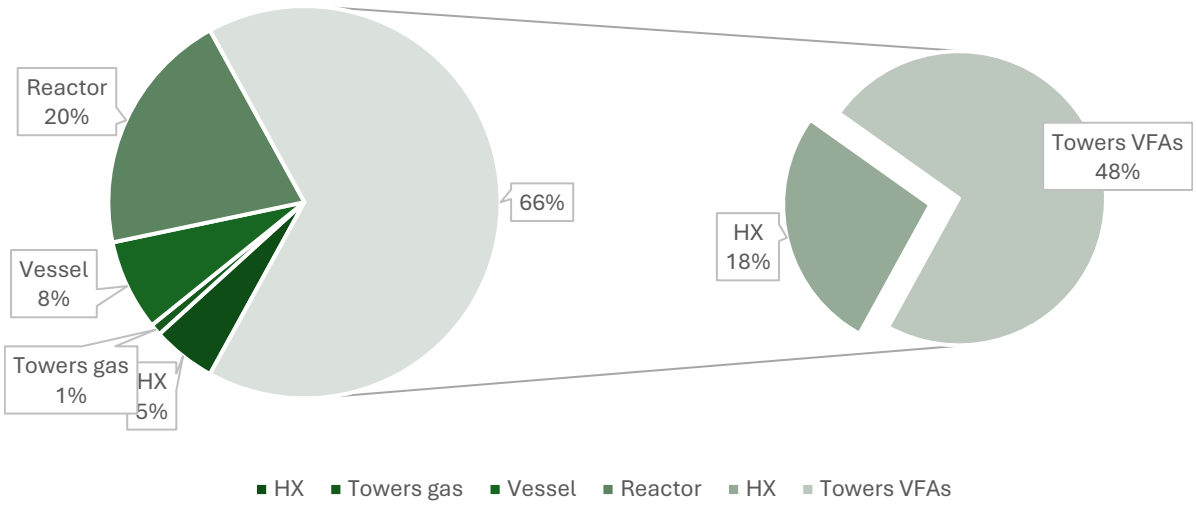

Figure 3. 2: Cost break-down for the FCI of the case a).

On the other hand, the difference among cases 1-3 lies in the operating costs (namely, the cost related to the activated sludge feedstock), where cases a) have higher expenses due to increased utility costs

associated with the distillation columns (mainly the steam for the reboilers) and higher labour costs, as more shift positions would be required. In Figure 3.3 the utilities costs are compared for cases a) and b): it is worth noting that in case a) more than half of the utilities are related to the steam consumption for the reboilers, whereas when the distillation columns are neglected, almost 60% of the utilities cost are related to the electricity, which is consumed by the pumps, specifically the one required by the RO membrane.

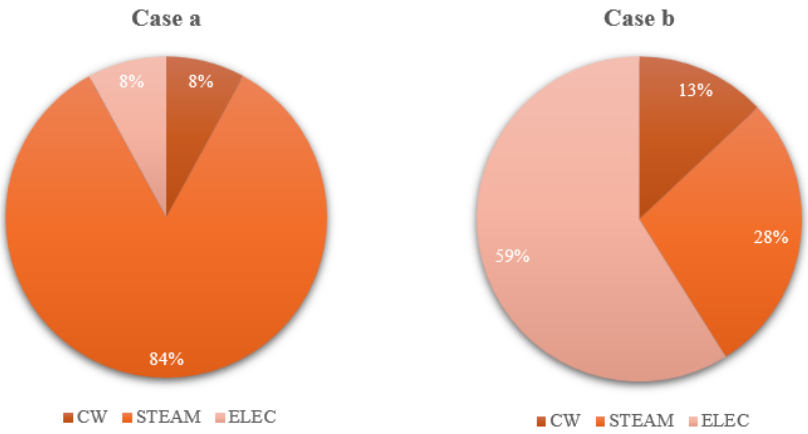

Figure 3.3: Utilities cost break-down for cases a) and b).

By evaluating the values obtained for the LCOH, it can be noted that there is no such variation between cases 1-3: this is mainly due to the fact the the impact of the feedstock cost is negligible compared to other operating costs. As a result, it does not cause a notable variation on the overall OPEX and, consequently, on the LCOH. However, a decrease is observed when the separation of the by-products is not accounted for in the process. Even though the sale of the organic acids might enhance the process's profitability, the separation techinques adopted in this study do not reveal as the more optimized method since they generate significantly higher costs, leading to a unit cost for H_2 that is approximately 19 €/kg. Therefore, based on the results obtained for the LCOH values for these scenarios, the most favourable case relates to the scenario in which the separation of organis acids is not performed. Thus, the optimal case (i.e., the one with the lower LCOH) is taken as the basis for obtaining the results related to the two-stage process.

3.2.2 Combined processes

When considering the two-stage process, the most optimal scenario obtained from the analysis of the DF process in terms of LCOH is taken as the basis for the evaluation of the capital and operating costs.

Thus, the separation of the organic acids is neglected and it is assumed that the feedstock represents an income for the plant and the effluent is treated as wastewater (i.e., case 2b).

Table 3. 9 summarizes the LCOH value obtained for the two-stage process, with the corresponding capital and operating costs, the annual revenues generated and the annual hydrogen production.

	Combined processes
CAPEX [k€]	12,770
OPEX [k€]	9,762
Revenues [k€]	3,144
HP [tons/y]	619.4
LCOH [€/kg]	13.11

Table 3. 9: Results of the LCOH for the combined processes (DF+PF).

The total capital investment related to the installed equipment is illustrated in the Figure 3.4, where the costs are allocated based on the specific section and it can be noted that most of the installed equipment costs are related to the photofermentation process.

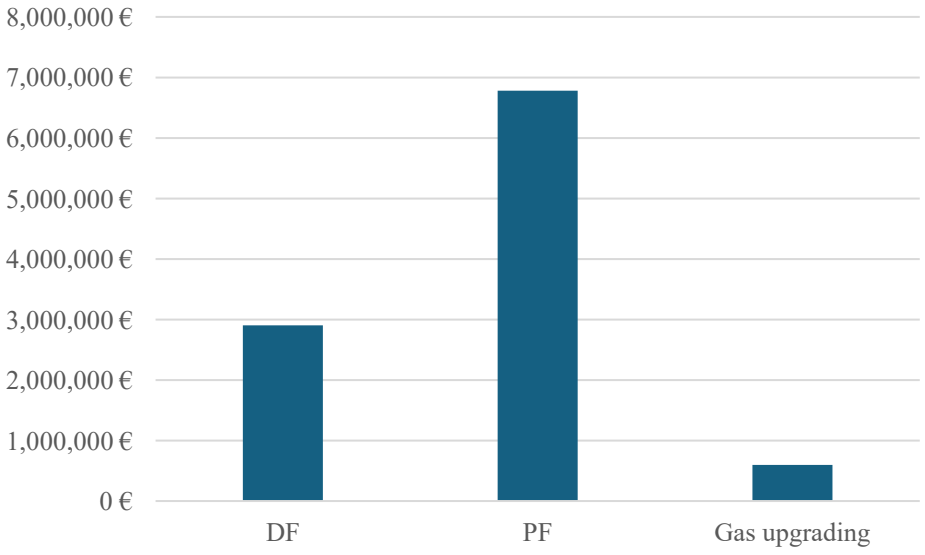

Figure 3. 4: Composition of the capital investment related to the installed equipment for the two-stage process.

Figure 3. 5 represents the breakdown of the OPEX (both direct and indirect costs), where it can be highlighted that more than 75% of such expenses are related to the raw material and utilities cost. Among these, the cost for PVA represents the major contribution since a large amount is required for the cell immobilisation due to the large capacity of the PBRs. Thus, a sensitivity analysis should be performed in order to investigate the variation of the LCOH value with respect to a change in the cost

of the raw materials (specifically, the PVA used for the cells immobilisation) and of the unit price of electricity.

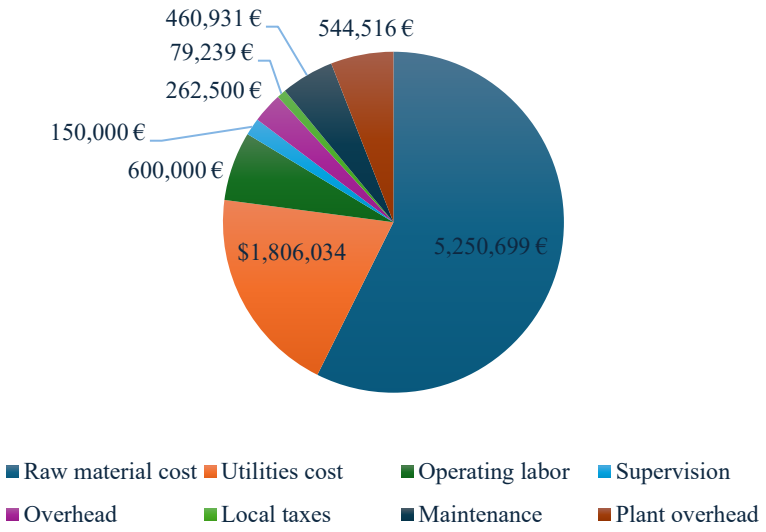

Figure 3. 5: Operating costs (OPEX) related to the combined processes.

The composition of the utilities cost for the combined processes is illustrated in Figure 3. 6. It is clear that the major source of cost is related to the electricity consumption, accounting for 68% of the total expense. This electricity consumption is evenly split between powering the pump for the RO process and supplying the light required in the PBRs and in the growth fermenters.

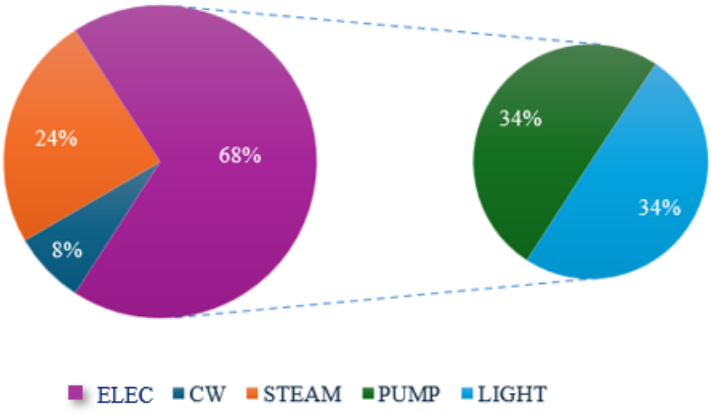

Figure 3. 6: Utilities cost breakdown for 2-stage process.

3.3 Sensitivity analysis

Once the LCOH values are obtained for all the cases analysed, the best scenario with a lower unit cost per kg of hydrogen is identified. The case of not separating the individual organic acids and then selling them separately turned out to be the most promising in economic terms, as the capital and operating costs associated with their separation greatly increase the production cost for hydrogen. In this scenario, the most favoured case, although the difference in terms of LCOH was not so marked, is the one in which the sludge disposal from the WWTP generates an income, while the outlet stream from the process generates a cost for its treatment. From this case, a sensitivity analysis was performed to assess the effect that specific cost components within the cost sources have on production cost of the biohydrogen. The key variables included in the sensitivity analysis for the DF process are the unit price for the steam (i.e. natural gas), electricity and cooling water and the annual hydrogen production. Figure 3. 7 illustrates the fluctuation in the LCOH for a ±20% variation in the cost parameters.

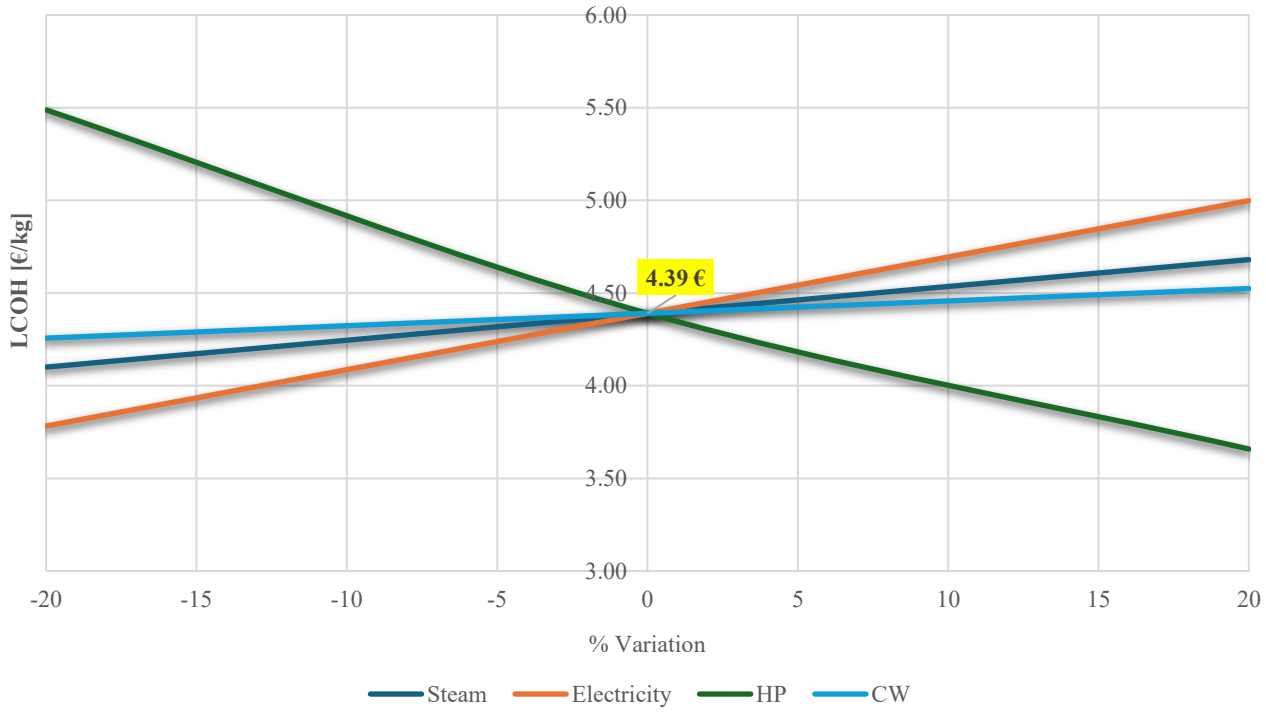

Figure 3. 7: Sensitivity analysis performed for LCOH on the case 2b for a ± 20% variation of four different factors: the unit price of steam, electricity and cooling water and the annual hydrogen production (HP).

The most significant parameter is the annual hydrogen production (HP) which causes a LCOH change of 25% and 16% for a variation of respectively ±20% in this parameter. This result highlights the fact that increasing the annual hydrogen production is important to reduce the production cost of biohydrogen. However, this variable is closely dependent on the performance of the process, such as

the hydrogen yield. Therefore, to achieve a higher hydrogen production, the development of more efficient solutions in terms of operative parameters for the dark fermentation process is necessary. For example, the development of genetically modified microorganisms could lead to improved process performance as they result in higher H_2 production. Additionally, enhancing process performance, such as increasing the H_2 production, could reduce the required capacity of the fermenter since a lower feedstock flowrate would be required. This, in turn, would lead to a reduction in the capital costs associated with the bioreactor.

The variation in the unit price of electricity, steam and cooling water leads to a less significant change compared to hydrogen production. However, in the case of cooling water and steam, a ±20% change in its unit price would not result in a substantial variation in biohydrogen production cost. This is because steam consumption is not a determining factor in the total operating costs, similarly to the consumption of cooling water. Regarding the cost of electricity, it can be noted that this parameter has a more pronounced effect compared to steam and cooling water, as the production cost of hydrogen would be more impacted by changes in the electricity costs. This is mainly due to the electricity consumption of the pump required for the RO membrane separation process. However, given the energy consumption related to this technology, an alternative, more energy-efficient option for the concentration of organic acid solution should be evaluated.

A similar sensitivity analysis is performed for the two-stage process, in order to assess how certain key variables influence the biohydrogen production cost in this scenario as well, and the results are plotted in Figure 3. 8. In this case, the factors that are varied in a range of ±20% are the unitary cost for PVA, used for the cell immobilisation, the unit cost of electricity and steam, and the annual hydrogen production. Similarly to the previous case, the annual HP results as the most important influential parameter in the LCOH determination, since its variation leads to a greater change in the biohydrogen production cost.

Regarding the unit cost of electricity and steam, the effect is minor, as a variation of ±20% results in a respective change of approximately 0.20-0.50 €/kg, both positively and negatively. However, electricity consumption represents a significant cost factor in this scenario due to the light requirements of the photobioreactors, and for this reason its slope is higher than that related to the steam. In this case, the cooling water is disregarded, since the operating cost associated with its consumption are the lowest compared to others. Finally, it can be observed that the variation in the unit cost of PVA shows a steeper slope, leading to a greater fluctuation in the biohydrogen cost. PVA consumption is quite high, and this corresponds to a considerably large cost associated with its use for the immobilization

technique. By reducing the unit cost of PVA, the operational costs would be optimized, significantly lowering the expenses related to immobilization and, consequently, the overall operating costs.

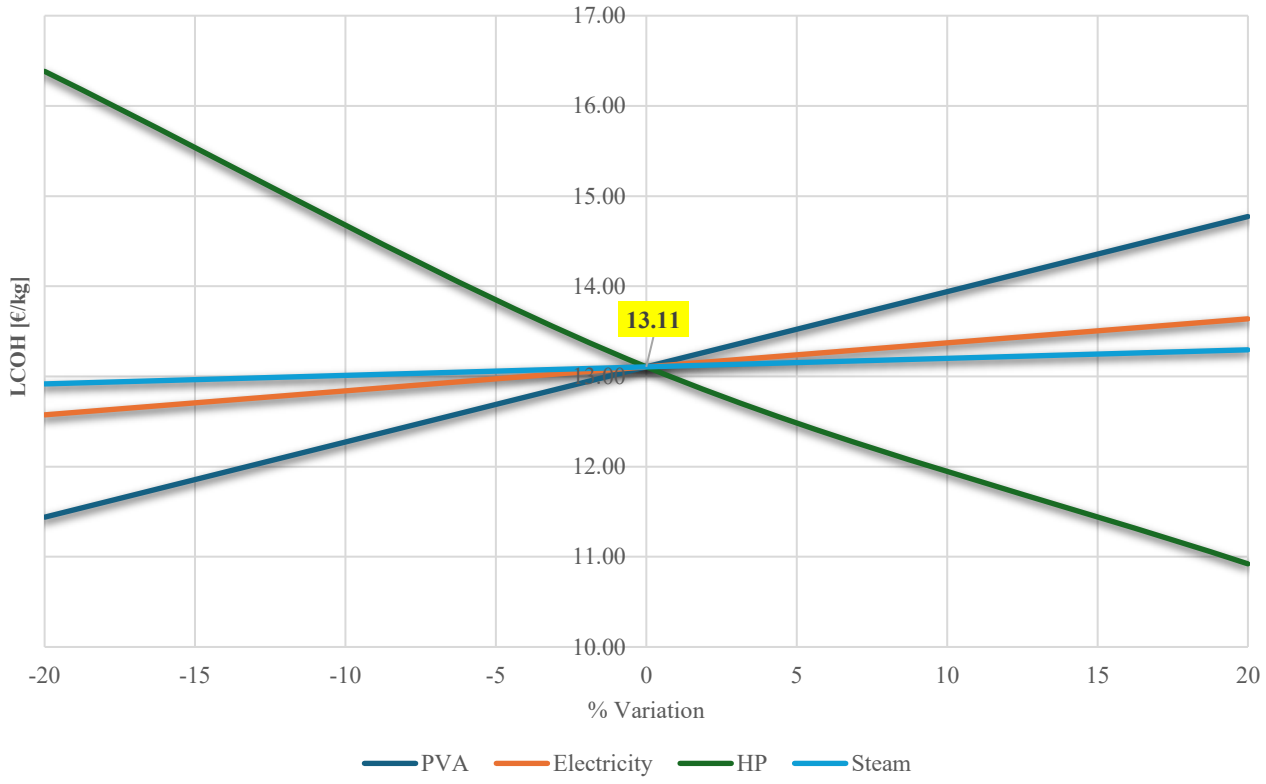

Figure 3. 8: Sensitivity analysis performed for the LCOH on the combined processes for a ±20% variation of 3 different factors: the unit price of PVA and electricity and the annual hydrogen production (HP).

Another key factor considered in the sensitivity analysis is the percentage of bacteria immobilized in the PVA hydrogels. In the case study, a value of 1.5% wt biomass concentration was considered, expressed as the mass fraction of bacteria to hydrogel material. Therefore, the effect on the LOCH is evaluated assuming that this value is increased to 3.0 wt%. The amount of PVA material required is lower in this scenario, as the concentration of entrapped biomass is higher, thus less PVA is used for this purpose. As a result, the capital cost associated with the autoclave used for the immobilization material also decreases, as the required volume is lower. The results are reported in Table 3. 10, which shows the comparison between the values of the LCOH for the base case and the improved case, highlighting the variation of the PVA cost and the autoclave cost.

	CAPEX [k€]	OPEX [k€]	PVA cost [k€]	Autoclave cost [k€]	LCOH [€/kg]
Case study (1.5% wt biomass in PVA)	12,770	9,762	5,162	5,582	13.11
Improved case (3% wt biomass in PVA)	10,325	7,190	2,796	3,683	8.49

Table 3. 10: Comparison between base case and optimized case considering the cost of PVA and the resulting LCOH.

3.4 Discussion

The results obtained from the economic analysis of the two different processes highlight the strengths and the critical aspects of each. Regarding the single-stage process, it is found that the most optimal scenario involves the fermentation section for the H_2 production, which is subsequently enriched through the gas upgrading section. On one hand, the separation and purification of the organic acids, which represent the by-products of the process, can partially offset the production costs of biohydrogen. However, this requires very expensive equipment, not only from a construction point of view but also for the installation part, and highly energy-intensive technology. For this reason, in the current study, this strategy does not prove to be economically profitable. Nevertheless, if the liquid by-products separation were to be integrated into the plant, optimized separation methods with less energy requirements should be considered.

In the optimal scenario for the dark fermentation process, the LCOH is approximately 4.40 €/kg, which is significantly lower compared to that obtained for the case a). This pronounced difference is related to the capital costs of the distillation columns and the associated steam consumption in the reboilers. Regarding the dark fermentation section, it is important to consider that the reaction environment requires precise control of temperature and pH, as these operative factors are pivotal for an optimal process performance. In fact, the microorganisms involved in the dark fermentation process are highly sensitive to even slight variations in the operating parameters, which can lead to an inhibition of hydrogen production, making the plant's outcome lower than expected. Therefore, in addition to the cost of the bioreactor, the costs of an efficient control system for these operating variables should be included, which in this study are neglected. In the case of a pH control system, one needs to take into

account the requirement for a neutralizing agent (mainly hydrochloric acid, HCl) which must be added to maintain the solution at the desired setpoint.

Regarding the combined processes plant, the LCOH result (13.11 €/kg) does not appear favourable compared to the value obtained for the single-stage dark fermentation process (4.39 €/kg). The photofermentation process, in fact, presents some limitations primarily related to the light requirements for microorganism growth and especially for the PBRs, as well as the technology adopted for the bacterial immobilization. The light source used consists of LED bulbs with a specific equivalent power compared to halogen bulbs (about 19 W). It is important to consider that LED lights emit a range of wavelengths, which can vary from the violet radiation (about 300 nm) to near-infrared radiation (around 1000 nm). Nevertheless, not all the emitted wavelengths are useful for photosynthetic bacteria to produce hydrogen, meaning that part of this radiation is wasted and diverted from the microorganism activity. For this reason, a light source with an emission spectrum more compatible with that of the photosynthetic microorganism should be considered to better stimulate the hydrogen production activity. In this way, higher values of light conversion efficiency can be achieved, indicating that a larger percentage of the energy provided by the light source is exploited, rather than being scattered and wasted. Another limitation related to the photofermentation process is associated to the immobilization technique used for the photosynthetic microorganisms. In particular, this study revealed that the use of PVA hydrogels constitutes a significant operating cost, both due to the large quantities required and because the unit cost of PVA is quite high. On one hand, it should be considered that the use of an immobilization technique represents a favourable strategy for separating solid- and hydraulic-residence times and allows for continuous operation, thus improving the economic feasibility of large-scale implementation of such biocatalyst. However, the result highlights the need to investigate optimized strategies for the immobilization material adopted. In fact, the sensitivity analysis shows that a higher concentration of biomass entrapped within the beads leads to a reduction of 50% in the PVA-related cost. However, this value cannot be freely increased, as an excessively high concentration of bacteria can inhibit their activity, resulting in a mutual shading effect. Therefore, future laboratory experiments should be carried out to optimize the biomass-to-hydrogel material mass fraction, since it is a key factor in the total PVA consumption and consequently in the biohydrogen production cost.

Moreover, it is important to emphasize that the LCOH results for the DF process are based entirely on the systematic process simulation performed in Aspen Plus, which allowed for the rigorous evaluation of mass and energy balances. In contrast, the results for hydrogen production in the PF process are based on literature data, owing to the lack of a suitable kinetic model. This may have led to a less

rigorous and precise estimation of the cost sources considered for the evaluation of such economic key indicator, resulting in an overestimation of the LCOH. For this reason, the methodology used in the dark fermentation process, which combines the systematic process simulation with the key indicator's evaluation, should be extended to the photofermentation process as well. This would allow for a more appropriate comparison of the results, where the level of accuracy (and consequently, the margin of error) is assessable.

Table 3. 11 illustrates the LCOH values for different technologies associated with green and blue hydrogen production (Mio et al., 2023). These technologies include the SMR both with and without carbon capture and three distinct technologies for water electrolysis. The target for the H_2 production is consistent with the one considered in the current analysis, specifically 33 kg/h. The LCOH for the single-stage dark fermentation process obtained in this study is 4.39 €/kg, which is lower compared to the more conventional processes of steam reforming and water electrolysis. However, when the two-stage dark and photo fermentation processes are considered (13.11 €/kg), the cost of biohydrogen production is even higher than the SMR with the CCS of the fluegas stream.

	SMR	**CCS fluegas**	**AEC**	**PEMEC**	**SOEC**
LCOH [€/kg]	6.50	11.69	6.29	6.79	5.58

Table 3. 11: LCOH values for different technologies for hydrogen production: SMR with and without carbon capture, and water electrolysis (AEC, PEMEC and SOEC) (Mio et al., 2023).

Conclusions

The aim of the current thesis was to perform a techno-economic analysis on two different biological routes for the H_2 production starting from biomass, in order to assess the feasibility and profitability of such processes on a small-medium scale. The two fermentations processes analysed, dark fermentation and photo fermentation, require specific and distinct operating conditions, such as the type of microorganisms involved or the need for a light source. However, there is the possibility of coupling these two processes, since the liquid effluent from the dark fermentation reactions can serve as the substrate for the photo fermentation process. Therefore, these two processes can be combined in order to enhance the hydrogen production.

Initially, the block flow diagrams for the two processes are obtained: the single-stage dark fermentation and the combined dark and photo fermentation processes. As for dark fermentation, a kinetic model adopted to model the anaerobic digestion (modified ADM1) was used to predict the fermentative hydrogen production, which was implemented in MATLAB. This enabled the calculation of preliminary mass balances, which serve as the basis for the process simulation in Aspen Plus. A target for hydrogen production equal to 33 kg/h is assumed, which corresponds to a small to medium-sized plant capacity. Moreover, the results obtained from the kinetic model in terms of hydrogen production rate allowed for the selection of an optimal operating HRT value. A waste activated sludge is assumed as the feedstock for the process, which is recovered from a wastewater treatment plant and contains organic material necessary for the metabolic activity of the microorganisms. The dark fermentation process is simulated on Aspen Plus and it comprises the fermentation section, the gas upgrading section and the separation and purification of the liquid by-products through of a series of distillation columns. This latter stage is considered to assess the potential economic advantages related to the sales of by-products, which could partially offset the overall production costs for hydrogen. The gaseous products are sent to an upgrading section, where reactive absorption and stripping columns are used. From this, a hydrogen-enriched stream is recovered from the top of the absorption column, with CO_2 being separated in a subsequent step.

Regarding the photofermentation process, the lack of a kinetic model has resulted in the prediction of hydrogen production being based on literature data. Thus, the mass balances are obtained on calculations performed on an Excel spreadsheet. It is assumed that an immobilisation technique is employed for the microorganisms using PVA hydrogels, thus they are considered as a constant

biocatalyst within the PBRs. Consequently, the preparation of the inoculum and the immobilization material are considered as steps preceding the photofermentation reactions.

The estimation of an economic key indicator such as the Levelized Cost of Hydrogen (LCOH) for the dark fermentation process lies on the systematic process simulations, allowing for the evaluation of rigorous mass and energy balances. By comparing the indicators' values, it was concluded that the single-stage process is more favourable in economic terms, as it results in a lower biohydrogen production cost, equal to 4.39 €/kg, compared to the two-stage process (13.11 €/kg). However, optimized strategies for the photofermentation process could lead to a lower LCOH value, necessitating further laboratory experiments to improve operational conditions and integrating a rigorous estimation of the economic performance of this process entirely based on systematic simulation.

Appendix A

Modified ADM1

Table A.1: Biochemical rate coefficients ($v_{i,j}$) and kinetic rate equations (ρ_j) for particulate components ($I = 1–12$; $j = 1–19$).

	Component →	1	2	3	4	5	6	7	8	9	10	11	12	
	i	S_{su}	S_{aa}	S_{fa}	S_{va}	S_{bu}	S_{pro}	S_{ac}	S_{h2}	S_{ch4}	S_{IC}	S_{IN}	S_I	
j ↓	Process ↓													Rate (ρ_j, kg COD.m^{-3}.d^{-1})
1	Disintegration												$f_{sI,xc}$	$k_{dis}X_c$
2	Hydrolysis Carbohydrates	1												$k_{hyd,ch}X_{ch}$
3	Hydrolysis of Proteins		1											$k_{hyd,pr}X_{pr}$
4	Hydrolysis of Lipids	$1-f_{fa,li}$		$f_{fa,li}$										$k_{hyd,li}X_{li}$
5	Uptake of Sugars	-1				$(1-Y_{su})\,f_{bu,su}$	$(1-Y_{su})\,f_{pro,su}$	$(1-Y_{su})\,f_{ac,su}$	$(1-Y_{su})\,f_{h2,su}$		$-\sum_{i=1+9,11-24} C_i Y_{i,5}$	$-(Y_{su})\,N_{bac}$		$k_{m,su}\frac{S_{su}}{K_S+S_{su}}X_{su}I_1$
6	Uptake of Amino Acids		-1		$(1-Y_{aa})\,f_{va,aa}$	$(1-Y_{aa})\,f_{bu,aa}$	$(1-Y_{aa})\,f_{pro,aa}$	$(1-Y_{aa})\,f_{ac,aa}$	$(1-Y_{aa})\,f_{h2,aa}$		$-\sum_{i=1+9,11-24} C_i Y_{i,6}$	$N_{aa}-(Y_{aa})\,N_{bac}$		$k_{m,aa}\frac{S_{aa}}{K_S+S_{aa}}X_{aa}I_1$
7	Uptake of LCFA			-1				$(1-Y_{fa})\,0.7$	$(1-Y_{fa})\,0.3$			$-(Y_{fa})\,N_{bac}$		$k_{m,fa}\frac{S_{fa}}{K_S+S_{fa}}X_{fa}I_2$
8	Uptake of Valerate				-1		$(1-Y_{c4})\,0.54$	$(1-Y_{c4})\,0.31$	$(1-Y_{c4})\,0.15$			$-(Y_{c4})\,N_{bac}$		$k_{m,c4}\frac{S_{va}}{K_S+S_{va}}X_{c4}\frac{1}{1+S_{bu}/S_{va}}I_2$
9	Uptake of Butyrate					-1		$(1-Y_{c4})\,0.8$	$(1-Y_{c4})\,0.2$			$-(Y_{c4})\,N_{bac}$		$k_{m,c4}\frac{S_{bu}}{K_S+S_{bu}}X_{c4}\frac{1}{1+S_{va}/S_{bu}}I_2$
10	Uptake of Propionate						-1	$(1-Y_{pro})\,0.57$	$(1-Y_{pro})\,0.43$		$-\sum_{i=1\ 9,11\ 24} C_i Y_{i,10}$	$-(Y_{pro})\,N_{bac}$		$k_{m,pro}\frac{S_{pro}}{K_S+S_{pro}}X_{pro}I_2$
11	Uptake of Acetate							-1		$(1-Y_{ac})$	$-\sum_{i=1+9,11-24} C_i Y_{i,11}$	$-(Y_{ac})\,N_{bac}$		$k_{m,ac}\frac{S_{ac}}{K_S+S_{ac}}X_{ac}I_3$
12	Uptake of Hydrogen								-1	$(1-Y_{h2})$	$-\sum_{i=1+9,11-24} C_i Y_{i,12}$	$-(Y_{h2})\,N_{bac}$		$k_{m,h2}\frac{S_{h2}}{K_S+S_{h2}}X_{h2}I_1$
13	Decay of X_{su}													$k_{dec,Xsu}X_{su}$
14	Decay of X_{aa}													$k_{dec,Xaa}X_{aa}$
15	Decay of X_{fa}													$k_{dec,Xfa}X_{fa}$
16	Decay of X_{c4}													$k_{dec,Xc4}X_{c4}$
17	Decay of X_{pro}													$k_{dec,Xpro}X_{pro}$
18	Decay of X_{ac}													$k_{dec,Xac}X_{ac}$
19	Decay of X_{h2}													$k_{dec,Xh2}X_{h2}$

Inhibition factors (3.7):

$I_1 = I_{pH}I_{IN,lim}$

$I_2 = I_{pH}I_{IN,lim}I_{h2}$

$I_3 = I_{pH}I_{IN,lim}I_{NH3,Xac}$

Table A.2: Biochemical rate coefficients ($v_{i,j}$) and kinetic rate equations (ρ_j) for soluble components (i = 13-24; j = 1–19).

j	Component → / Process ↓	i	13	14	15	16	17	18	19	20	21	22	23	24	Rate (ρ_j, kg COD.m^{-3}.d^{-1})
			X_c	X_{ch}	X_{pr}	X_{li}	X_{su}	X_{aa}	X_{fa}	X_{c4}	X_{pro}	X_{ac}	X_{h2}	X_I	
			Composites (kgCOD m^{-3})	Carbohydrates (kgCOD m^{-3})	Proteins (kgCOD m^{-3})	Lipids (kgCOD m^{-3})	Sugar degraders (kgCOD m^{-3})	Amino acid degraders (kgCOD m^{-3})	LCFA degraders (kgCOD m^{-3})	Valerate and butyrate degraders (kgCOD m^{-3})	Propionate degraders (kgCOD m^{-3})	Acetate degraders (kgCOD m^{-3})	Hydrogen degraders (kgCOD m^{-3})	Particulate inerts (kgCOD m^{-3})	
1	Disintegration		-1	$f_{ch,xc}$	$f_{pr,xc}$	$f_{li,xc}$								$f_{I,xc}$	$k_{dis}X_c$
2	Hydrolysis Carbohydrates			-1											$k_{hyd,ch}X_{ch}$
3	Hydrolysis of Proteins				-1										$k_{hyd,pr}X_{pr}$
4	Hydrolysis of Lipids					-1									$k_{hyd,li}X_{li}$
5	Uptake of Sugars						Y_{su}								$k_{m,su}\frac{S_{su}}{K_S+S_{su}}X_{su}I_1$
6	Uptake of Amino Acids							Y_{aa}							$k_{m,aa}\frac{S_{aa}}{K_S+S_{aa}}X_{aa}I_1$
7	Uptake of LCFA								Y_{fa}						$k_{m,fa}\frac{S_{fa}}{K_S+S_{fa}}X_{fa}I_2$
8	Uptake of Valerate									Y_{c4}					$k_{m,c4}\frac{S_{va}}{K_S+S_{va}}X_{c4}\frac{1}{1+S_{bu}/S_{va}}I_2$
9	Uptake of Butyrate									Y_{c4}					$k_{m,c4}\frac{S_{bu}}{K_S+S_{bu}}X_{c4}\frac{1}{1+S_{va}/S_{bu}}I_2$
10	Uptake of Propionate										Y_{pro}				$k_{m,pr}\frac{S_{pro}}{K_S+S_{pro}}X_{pro}I_2$
11	Uptake of Acetate											Y_{ac}			$k_{m,ac}\frac{S_{ac}}{K_S+S_{ac}}X_{ac}I_3$
12	Uptake of Hydrogen												Y_{h2}		$k_{m,h2}\frac{S_{h2}}{K_S+S_{h2}}X_{h2}I_1$
13	Decay of X_{su}		1				-1								$k_{dec,Xsu}X_{su}$
14	Decay of X_{aa}		1					-1							$k_{dec,Xaa}X_{aa}$
15	Decay of X_{fa}		1						-1						$k_{dec,Xfa}X_{fa}$
16	Decay of X_{c4}		1							-1					$k_{dec,Xc4}X_{c4}$
17	Decay of X_{pro}		1								-1				$k_{dec,Xpro}X_{pro}$
18	Decay of X_{ac}		1									-1			$k_{dec,Xac}X_{ac}$
19	Decay of X_{h2}		1										-1		$k_{dec,Xh2}X_{h2}$

Inhibition factors (3.7):

$I_1 = I_{pH}I_{IN,lim}$

$I_2 = I_{pH}I_{IN,lim}I_{h_2}$

$I_3 = I_{pH}I_{IN,lim}I_{NH\,3,Xac}$

Table A.3: Concentration parameters and the corresponding values at initial conditions. *Unless otherwise stated, the unit of measure is kgCOD m^{-3}.

Parameter	Value	Unit of measure
S_{su}	0.024309	*
S_{aa}	0.010808	*
S_{fa}	0.29533	*
S_{va}	0.02329	*
S_{bu}	0.031123	*
S_{ac}	0.50765	*
S_{H2}	4.9652e-07	*
S_{CH4}	0.055598	*
S_{IC}	0.10258	M
S_{IN}	0.10373	M
S_{I}	3.2327	*
X_{xc}	7.5567	*
X_{ch}	0.074679	*
X_{pr}	0.074679	*
X_{li}	0.11202	*
X_{su}	0.57565	*
X_{aa}	0.43307	*
X_{fa}	0.44433	*
X_{c4}	0.18404	*
X_{pro}	0.087261	*
X_{ac}	0.57682	*
X_{H2}	0.28774	*
X_{I}	18.6685	*
S_{cat}	3.3431e-042	M
S_{an}	1-5293e-0.41	M
S_{hva}	0.023204	*
S_{hbu}	0.031017	*
S_{hpro}	0.043803	*
S_{hac}	0.50616	*
S_{hco3}	0.092928	*
S_{nh3}	0.0021958	*
S_{gasH2}	1.9096e-05	*
S_{gasCH4}	1.5103	*
S_{gasCO2}	0.013766	*
S_{H_ion}	5-3469e-08	kg m^{-3}

Table A.4: Kinetic parameters and rates and their corresponding values at initial conditions.

Parameter	Value	Unit of measure
K_{dis}	0.5	d^{-1}
K_{hyd_ch}	10	d^{-1}
K_{hyd_pr}	10	d^{-1}
K_{hyd_li}	10	d^{-1}
K_{m_su}	30	$kgCOD_S\ kgCOD_X^{-1}\ d^{-1}$
K_{m_aa}	50	$kgCOD_S\ kgCOD_X^{-1}\ d^{-1}$
K_{m_fa}	6	$kgCOD_S\ kgCOD_X^{-1}\ d^{-1}$
K_{m_c4}	20	$kgCOD_S\ kgCOD_X^{-1}\ d^{-1}$
K_{m_pro}	0	$kgCOD_S\ kgCOD_X^{-1}\ d^{-1}$
K_{m_ac}	0	$kgCOD_S\ kgCOD_X^{-1}\ d^{-1}$
K_{m_H2}	0	$kgCOD_S\ kgCOD_X^{-1}\ d^{-1}$
K_{S_IN}	1e-04	$kgCOD_S\ m^{-3}$
K_{s_su}	0.5	$kgCOD_S\ m^{-3}$
K_{S_aa}	0.3	$kgCOD_S\ m^{-3}$
K_{S_fa}	0.4	$kgCOD_S\ m^{-3}$
K_{S_c4}	0.2	$kgCOD_S\ m^{-3}$
K_{S_pro}	0.1	$kgCOD_S\ m^{-3}$
K_{S_ac}	0.15	$kgCOD_S\ m^{-3}$
K_{S_H2}	7e-06	$kgCOD_S\ m^{-3}$
K_{dec_Xsu}	0.02	d^{-1}
K_{dec_Xaa}	0.02	d^{-1}
K_{dec_Xfa}	0.02	d^{-1}
K_{dec_Xc4}	0.02	d^{-1}
K_{dec_Xpro}	0	d^{-1}
K_{dec_Xac}	0	d^{-1}
K_{dec_XH2}	0	d^{-1}
k_La	200	d^{-1}
$k_{A/Bva}$	1e+8	$M^{-1}d^{-1}$
$k_{A/Bbu}$	1e+8	$M^{-1}d^{-1}$
$k_{A/Bac}$	1e+8	$M^{-1}d^{-1}$
$k_{A/BCO2}$	1e+8	$M^{-1}d^{-1}$
$k_{A/BIN}$	1e+8	$M^{-1}d^{-1}$

Table A.5: pH limiting parameters and their corresponding values at initial conditions.

Parameter	Value	Unit of measure
pH_{UL_H2}	6	-
pH_{LL_H2}	5	-
pH_{UL_ac}	7	-
pH_{LL_ac}	6	-
pH_{UL_aa}	5.5	-
pH_{LL_aa}	4	-

Table A.6: Carbon content of various components and their corresponding values at initial conditions. Unit of measure is $kmole_C\ kgCOD^{-1}$.

Parameter	Value
C_{xc}	0.03
C_{sI}	0.03
C_{ch}	0.0313
C_{pr}	0.03
C_{li}	0.022
C_{xI}	0.03
C_{su}	0.0313
C_{aa}	0.03
C_{fa}	0.0217
C_{bu}	0.025
C_{pro}	0.0268
C_{ac}	0.0313
C_{bac}	0.0313
C_{va}	0.024
C_{CH4}	0.0156

Table A.7: Yield of products and biomass on substrates and their corresponding values at initial conditions.

Parameter	Value	Unit of measure
f_{fa_li}	0.95	kgCOD $kgCOD^{-1}$
f_{H2_su}	0.19	kgCOD $kgCOD^{-1}$
f_{bu_su}	0.13	kgCOD $kgCOD^{-1}$
f_{pro_su}	0.27	kgCOD $kgCOD^{-1}$
f_{ac_su}	0.41	kgCOD $kgCOD^{-1}$
f_{H2_aa}	0.06	kgCOD $kgCOD^{-1}$
f_{va_aa}	0.23	kgCOD $kgCOD^{-1}$
f_{bu_aa}	0.26	kgCOD $kgCOD^{-1}$
f_{pro_aa}	0.05	kgCOD $kgCOD^{-1}$
f_{ac_aa}	0.40	kgCOD $kgCOD^{-1}$
f_{sI_xc}	0.1	kgCOD $kgCOD^{-1}$
f_{xI_xc}	0.2	kgCOD $kgCOD^{-1}$
f_{ch_xc}	0.2	kgCOD $kgCOD^{-1}$
f_{pr_xc}	0.2	kgCOD $kgCOD^{-1}$
f_{li_xc}	0.3	kgCOD $kgCOD^{-1}$
Y_{su}	0.1	$kgCOD_S$ $kgCOD_X^{-1}$
Y_{aa}	0.08	$kgCOD_S$ $kgCOD_X^{-1}$
Y_{fa}	0.06	$kgCOD_S$ $kgCOD_X^{-1}$
Y_{c4}	0.06	$kgCOD_S$ $kgCOD_X^{-1}$
Y_{pro}	0.04	$kgCOD_S$ $kgCOD_X^{-1}$
Y_{ac}	0.05	$kgCOD_S$ $kgCOD_X^{-1}$
Y_{H_2}	0.06	$kgCOD_S$ $kgCOD_X^{-1}$

Appendix B

Modified ADM1 - Plots

The results obtained from the modified kinetic model ADM1 implemented in MATLAB are used to predict the H_2 production through DF. The main variables are plotted in the graphs below. In Figure B. 1 the concentration of carbohydrates, proteins and lipids are plotted as a function of the HRT.

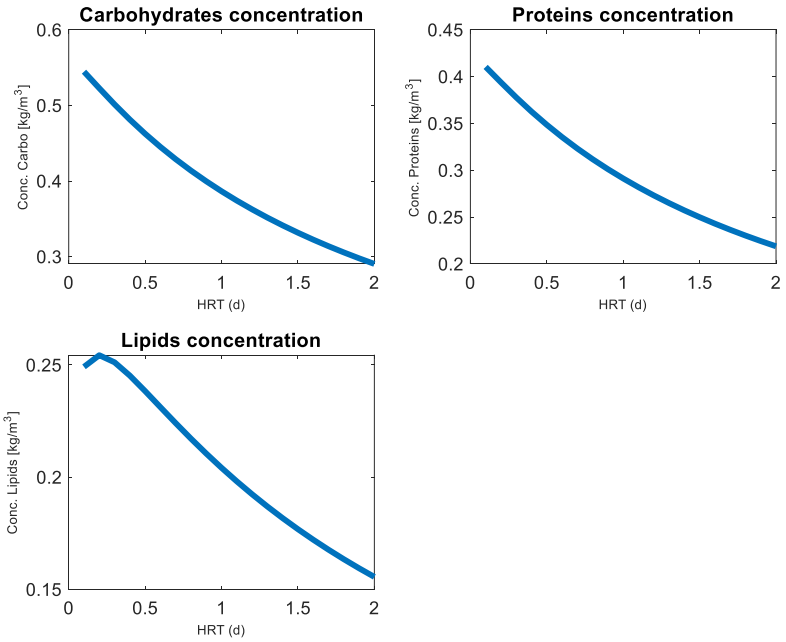

Figure B. 1: Plot of macromolecules (carbohydrates, proteins and lipids) concentration as function of HRT.

The concentration of these macromolecules decreases with an increase in the HRT, since at the beginning of the process the macromolecules are broken down into smaller molecules such as amino acids, sugars and fats that can be more easily degraded by microorganisms. Correspondingly, the concentration of VFAs follows an opposite trend to that of carbohydrates, proteins and lipids, as VFAs are not yet present at low HRT and their levels increase with the degradation of macromolecules (Figure B. 2). Among the three main organic acids that are formed during the DF process, acetic acid has the highest concentration, highlighting that microorganisms primarily produce hydrogen through the acetate metabolic pathway.

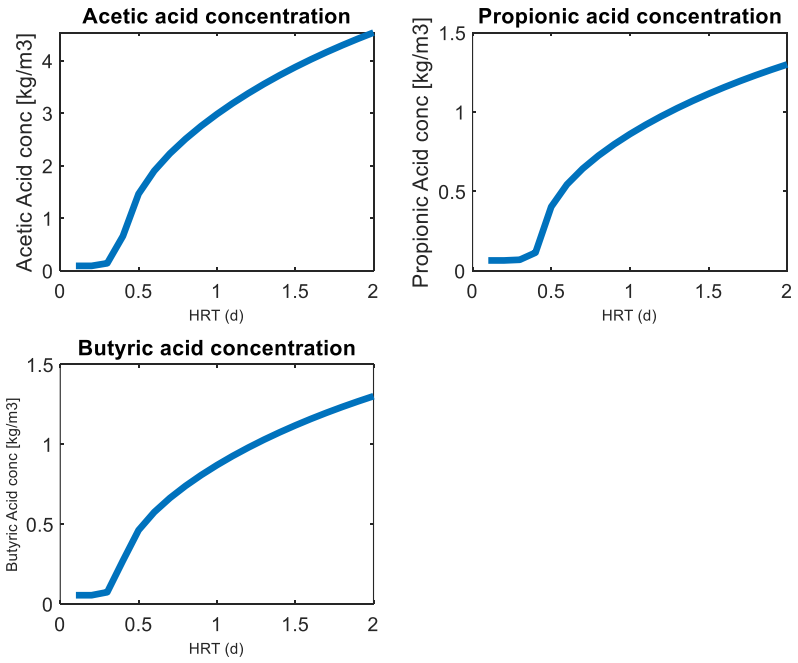

Figure B. 2: Plot of the VFAs (acetic, propionic and butyric acids) concentration as a function of the HRT.

As a reflection of the gradual formation of organic acids, the plot of the system pH (Figure B. 3) represents the transition to a more acidic environment as the HRT increases. In addition, a pH of 5-6 is more suitable for the H_2 production by means of anaerobic bacteria.

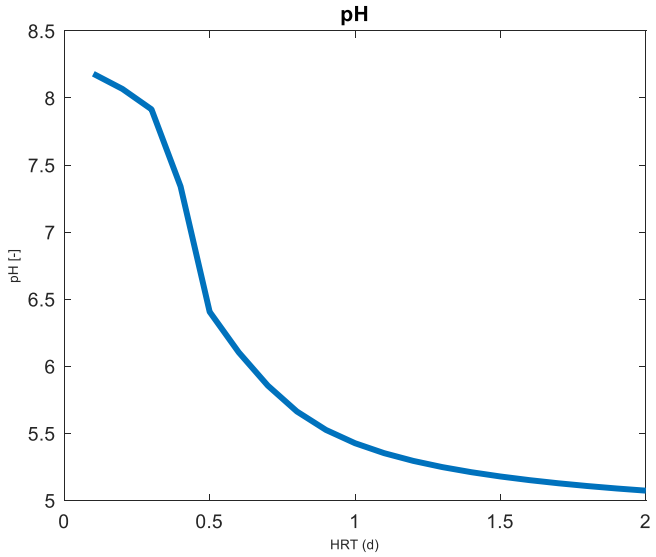

Figure B. 3: Plot of the pH of the system as a function of the HRT.

The molar fraction of H_2 and CO_2 produced in the gas phase are represented in **Errore. L'origine riferimento non è stata trovata.**. The steep variation in the molar fraction for both components occurs at values of HRT that are insufficient for the production of H_2 to start. At low HRT, which corresponds

to shorter residence times of the liquid stream within the reactor, microorganisms are not immediately able to produce H_2 in the liquid phase, which is then transferred to the gas phase.

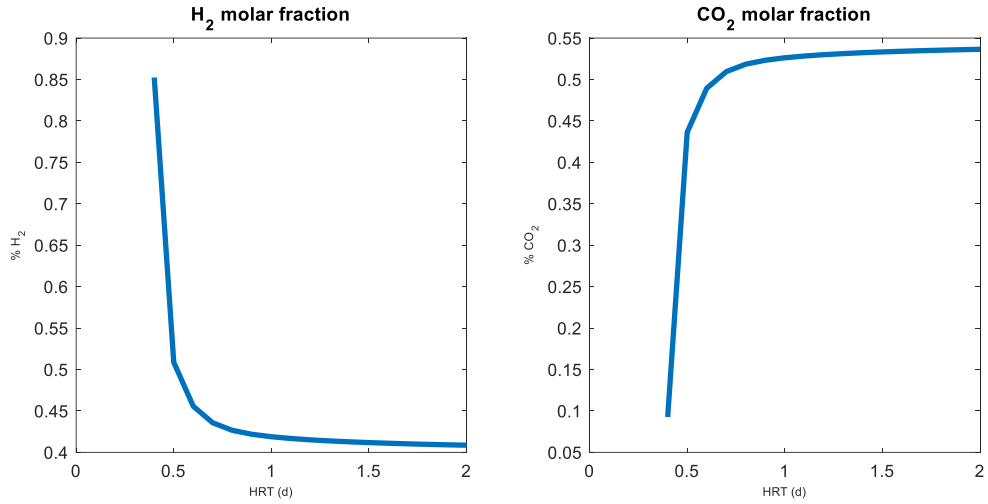

Figure B. 4: Molar fraction of H_2 and CO_2 in the gas phase produced through the DF process predicted by the kinetic model.

- **"*For*" cycle:** the function ADM1_ode is inserted in this cycle to obtain the results of the differential equations at different values of HRT.

```
parfor n=1:nSteps

    HRT(n) = (2/nSteps)*n;
    Q = V_liq / HRT(n);

    [~, x] = ode15s(@(t, x) Adm1_ode(t, x,d,Q), t_span, Xinit);
    xp = x(end,:);
    x1(n,:)=xp;

end
```

Nomenclature

Acronyms

CAPEX = capital cost

CCS = carbon capture and storage

DF = dark fermentation

HRT = hydraulic retention rime

LCE = light conversion efficiency

LCOH = levelized cost of hydrogen

OPEX = operating cost

PBR = photobioreactor

PF = photo fermentation

PNSB = purple non-sulphur bacteria

SMR = steam methane reforming

SRT = solid retention time

OLR = organic loading rate

Bibliography

Abdalla, A.M., Hossain, S., Nisfindy, O.B., Azad, A.T., Dawood, M., Azad, A.K., 2018. Hydrogen production, storage, transportation and key challenges with applications: A review. Energy Conversion and Management 165, 602–627. https://doi.org/10.1016/j.enconman.2018.03.088

Ahmed, M.A., Amin, S., Mohamed, A.A., 2023. Fouling in reverse osmosis membranes: monitoring, characterization, mitigation strategies and future directions. Heliyon 9, e14908. https://doi.org/10.1016/j.heliyon.2023.e14908

Ahmed, S.F., Rafa, N., Mofijur, M., Badruddin, I.A., Inayat, A., Ali, M.S., Farrok, O., Yunus Khan, T.M., 2021. Biohydrogen Production From Biomass Sources: Metabolic Pathways and Economic Analysis. Front. Energy Res. 9, 753878. https://doi.org/10.3389/fenrg.2021.753878

Akkerman, I., Janssen, M., Rocha, J., 2002. Photobiological hydrogen production: photochemical e ciency and bioreactor design. International Journal of Hydrogen Energy.

Appels, L., Baeyens, J., Degrève, J., Dewil, R., 2008. Principles and potential of the anaerobic digestion of waste-activated sludge. Progress in Energy and Combustion Science 34, 755–781. https://doi.org/10.1016/j.pecs.2008.06.002

Barbera, E., Mio, A., Massi Pavan, A., Bertucco, A., Fermeglia, M., 2022. Fuelling power plants by natural gas: An analysis of energy efficiency, economical aspects and environmental footprint based on detailed process simulation of the whole carbon capture and storage system. Energy Conversion and Management 252, 115072. https://doi.org/10.1016/j.enconman.2021.115072

Barbosa, M.J., Rocha, J.M.S., Tramper, J., Wijffels, R.H., 2001. Acetate as a carbon source for hydrogen production by photosynthetic bacteria. Journal of Biotechnology 85, 25–33. https://doi.org/10.1016/S0168-1656(00)00368-0

Batstone, D.J., Keller, J., Angelidaki, I., Kalyuzhnyi, S.V., Pavlostathis, S.G., Rozzi, A., Sanders, W.T.M., Siegrist, H., Vavilin, V.A., 2002. The IWA Anaerobic Digestion Model No 1 (ADM1). Water Science and Technology 45, 65–73. https://doi.org/10.2166/wst.2002.0292

Boran, E., Özgür, E., Van Der Burg, J., Yücel, M., Gündüz, U., Eroglu, I., 2010. Biological hydrogen production by Rhodobacter capsulatus in solar tubular photo bioreactor. Journal of Cleaner Production 18, S29–S35. https://doi.org/10.1016/j.jclepro.2010.03.018

Brown, B., Wilkins, M., Saha, R., 2022. Rhodopseudomonas palustris: A biotechnology chassis. Biotechnology Advances 60, 108001. https://doi.org/10.1016/j.biotechadv.2022.108001

Carlozzi, P., Lambardi, M., 2009. Fed-batch operation for bio-H2 production by Rhodopseudomonas palustris (strain 42OL). Renewable Energy 34, 2577–2584. https://doi.org/10.1016/j.renene.2009.04.016

Chandrasekhar, K., Lee, Y.-J., Lee, D.-W., 2015. Biohydrogen Production: Strategies to Improve Process Efficiency through Microbial Routes. IJMS 16, 8266–8293. https://doi.org/10.3390/ijms16048266

Chen, C., Chen, H., Wu, J., Lin, C., 2008. Fermentative hydrogen production at high sulfate concentration. International Journal of Hydrogen Energy 33, 1573–1578. https://doi.org/10.1016/j.ijhydene.2007.09.042

Chen, C.-Y., Chang, J.-S., 2006. Enhancing phototropic hydrogen production by solid-carrier assisted fermentation and internal optical-fiber illumination. Process Biochemistry 41, 2041–2049. https://doi.org/10.1016/j.procbio.2006.05.005

Clippinger, J., Davis, R., 2019. Techno-Economic Analysis for the Production of Algal Biomass via Closed Photobioreactors: Future Cost Potential Evaluated Across a Range of Cultivation System Designs (No. NREL/TP--5100-72716, 1566806). https://doi.org/10.2172/1566806

Cormos, C.-C., Petrescu, L., Cormos, A.-M., Agachi, S., 2016. Process Design and Integration of Various Carbon Capture Approaches into the Energy Sector and Other Energy-intensive Industrial Applications, in: Computer Aided Chemical Engineering. Elsevier, pp. 265–270. https://doi.org/10.1016/B978-0-444-63428-3.50049-7

Das, D., Khanna, N., Veziroğlu, N., 2008. Recent developments in biological hydrogen production processes. CI&CEQ 14, 57–67. https://doi.org/10.2298/CICEQ0802057D

Dasgupta, C.N., Jose Gilbert, J., Lindblad, P., Heidorn, T., Borgvang, S.A., Skjanes, K., Das, D., 2010. Recent trends on the development of photobiological processes and photobioreactors for the improvement of hydrogen production. International Journal of Hydrogen Energy 35, 10218–10238. https://doi.org/10.1016/j.ijhydene.2010.06.029

De Gioannis, G., Muntoni, A., Polettini, A., Pomi, R., 2013. A review of dark fermentative hydrogen production from biodegradable municipal waste fractions. Waste Management 33, 1345–1361. https://doi.org/10.1016/j.wasman.2013.02.019

Deo, D., Ozgur, E., Eroglu, I., Gunduz, U., Yucel, M., 2012. Photofermentative Hydrogen Production in Outdoor Conditions, in: Minic, D. (Ed.), Hydrogen Energy - Challenges and Perspectives. InTech. https://doi.org/10.5772/50390

Domini, M., Abbà, A., Bertanza, G., 2022. Analysis of the variation of costs for sewage sludge transport, recovery and disposal in Northern Italy: a recent survey (2015–2021). Water Science and Technology 85, 1167–1175. https://doi.org/10.2166/wst.2022.040

El-Gendi, A., Abdallah, H., Amin, A., 2021. Economic study for blend membrane production. Bull Natl Res Cent 45, 126. https://doi.org/10.1186/s42269-021-00584-0

Fan, J.-L., Yu, P., Li, K., Xu, M., Zhang, X., 2022. A levelized cost of hydrogen (LCOH) comparison of coal-to-hydrogen with CCS and water electrolysis powered by renewable energy in China. Energy 242, 123003. https://doi.org/10.1016/j.energy.2021.123003

Ferchichi, M., Crabbe, E., Gil, G.-H., Hintz, W., Almadidy, A., 2005. Influence of initial pH on hydrogen production from cheese whey. Journal of Biotechnology 120, 402–409. https://doi.org/10.1016/j.jbiotec.2005.05.017

Gadhamshetty, V., Arudchelvam, Y., Nirmalakhandan, N., Johnson, D.C., 2010. Modeling dark fermentation for biohydrogen production: ADM1-based model vs. Gompertz model. International Journal of Hydrogen Energy 35, 479–490. https://doi.org/10.1016/j.ijhydene.2009.11.007

Ghimire, A., Frunzo, L., Pirozzi, F., Trably, E., Escudie, R., Lens, P.N.L., Esposito, G., 2015a. A review on dark fermentative biohydrogen production from organic biomass: Process parameters and use of by-products. Applied Energy 144, 73–95. https://doi.org/10.1016/j.apenergy.2015.01.045

Ghimire, A., Frunzo, L., Pirozzi, F., Trably, E., Escudie, R., Lens, P.N.L., Esposito, G., 2015b. A review on dark fermentative biohydrogen production from organic biomass: Process parameters and use of by-products. Applied Energy 144, 73–95. https://doi.org/10.1016/j.apenergy.2015.01.045

Ghosh, D., Sobro, I.F., Hallenbeck, P.C., 2012. Stoichiometric conversion of biodiesel derived crude glycerol to hydrogen: Response surface methodology study of the effects of light intensity and crude glycerol and glutamate concentration. Bioresource Technology 106, 154–160. https://doi.org/10.1016/j.biortech.2011.12.021

Ghosh, S., Chowdhury, R., Bhattacharya, P., 2018. A review on single stage integrated dark-photo fermentative biohydrogen production: Insight into salient strategies and scopes. International Journal of Hydrogen Energy 43, 2091–2107. https://doi.org/10.1016/j.ijhydene.2017.12.018

Gilbert, J.J., Ray, S., Das, D., 2011. Hydrogen production using Rhodobacter sphaeroides (O.U. 001) in a flat panel rocking photobioreactor. International Journal of Hydrogen Energy 36, 3434–3441. https://doi.org/10.1016/j.ijhydene.2010.12.012

GürtekiN, E., n.d. Biological Hydrogen Production Methods.

Hallenbeck, P.C., Ghosh, D., 2009. Advances in fermentative biohydrogen production: the way forward? Trends in Biotechnology 27, 287–297. https://doi.org/10.1016/j.tibtech.2009.02.004

Ham, K., Bae, S., Lee, J., 2024. Classification and technical target of water electrolysis for hydrogen production. Journal of Energy Chemistry 95, 554–576. https://doi.org/10.1016/j.jechem.2024.04.003

Han, W., Liu, Z., Fang, J., Huang, J., Zhao, H., Li, Y., 2016. Techno-economic analysis of dark fermentative hydrogen production from molasses in a continuous mixed immobilized sludge reactor. Journal of Cleaner Production 127, 567–572. https://doi.org/10.1016/j.jclepro.2016.04.055

Hawkes, F., Hussy, I., Kyazze, G., Dinsdale, R., Hawkes, D., 2007. Continuous dark fermentative hydrogen production by mesophilic microflora: Principles and progress. International Journal of Hydrogen Energy 32, 172–184. https://doi.org/10.1016/j.ijhydene.2006.08.014

Howarth, R.W., Jacobson, M.Z., 2021. How green is blue hydrogen? Energy Science & Engineering 9, 1676–1687. https://doi.org/10.1002/ese3.956

Kamran, M., 2021. Bioenergy, in: Renewable Energy Conversion Systems. Elsevier, pp. 243–264. https://doi.org/10.1016/B978-0-12-823538-6.00002-6

Kapdan, I.K., Kargi, F., 2006. Bio-hydrogen production from waste materials. Enzyme and Microbial Technology 38, 569–582. https://doi.org/10.1016/j.enzmictec.2005.09.015

Keet, G., Du Toit, J.P., Pott, R.W.M., 2024. Methods for the separation of hydraulic retention time and solids retention time in the application of photosynthetic microorganisms in photobioreactors: a review. World J Microbiol Biotechnol 40, 100. https://doi.org/10.1007/s11274-024-03909-z

Khraisheh, M., Dawas, N., Nasser, M.S., Al-Marri, M.J., Hussien, M.A., Adham, S., McKay, G., 2020. Osmotic pressure estimation using the Pitzer equation for forward osmosis modelling. Environmental Technology 41, 2533–2545. https://doi.org/10.1080/09593330.2019.1575476

Kim, J.K., Oh, B.R., Chun, Y.N., Kim, S.W., 2006. Effects of temperature and hydraulic retention time on anaerobic digestion of food waste. Journal of Bioscience and Bioengineering 102, 328–332. https://doi.org/10.1263/jbb.102.328

Lee et al. - 2021 - Scenario-Based Techno-Economic Analysis of Steam M.pdf, n.d.

Li, C., Fang, H.H.P., 2007. Fermentative Hydrogen Production From Wastewater and Solid Wastes by Mixed Cultures. Critical Reviews in Environmental Science and Technology 37, 1–39. https://doi.org/10.1080/10643380600729071

Madeddu, C., Errico, M., Baratti, R., 2019. CO2 Capture by Reactive Absorption-Stripping: Modeling, Analysis and Design, SpringerBriefs in Energy. Springer International Publishing, Cham. https://doi.org/10.1007/978-3-030-04579-1

Manish, S., Banerjee, R., 2008. Comparison of biohydrogen production processes. International Journal of Hydrogen Energy 33, 279–286. https://doi.org/10.1016/j.ijhydene.2007.07.026

McKinlay, J.B., Harwood, C.S., 2010. Photobiological production of hydrogen gas as a biofuel. Current Opinion in Biotechnology 21, 244–251. https://doi.org/10.1016/j.copbio.2010.02.012

McKinlay, J.B., Oda, Y., Rühl, M., Posto, A.L., Sauer, U., Harwood, C.S., 2014. Non-growing Rhodopseudomonas palustris Increases the Hydrogen Gas Yield from Acetate by Shifting from the Glyoxylate Shunt to the Tricarboxylic Acid Cycle. Journal of Biological Chemistry 289, 1960–1970. https://doi.org/10.1074/jbc.M113.527515

Meerman, J.C., Hamborg, E.S., Van Keulen, T., Ramírez, A., Turkenburg, W.C., Faaij, A.P.C., 2012. Techno-economic assessment of CO2 capture at steam methane reforming facilities using commercially available technology. International Journal of Greenhouse Gas Control 9, 160–171. https://doi.org/10.1016/j.ijggc.2012.02.018

Mio, A., Barbera, E., Pavan, A.M., Danielis, R., Bertucco, A., Fermeglia, M., 2023. Analysis of the energetic, economic, and environmental performance of hydrogen utilization for port logistic activities. Applied Energy 347, 121431. https://doi.org/10.1016/j.apenergy.2023.121431

Møller, K.T., Jensen, T.R., Akiba, E., Li, H., 2017. Hydrogen - A sustainable energy carrier. Progress in Natural Science: Materials International 27, 34–40. https://doi.org/10.1016/j.pnsc.2016.12.014

Nath, K., Das, D., 2009. Effect of light intensity and initial pH during hydrogen production by an integrated dark and photofermentation process. International Journal of Hydrogen Energy 34, 7497–7501. https://doi.org/10.1016/j.ijhydene.2008.11.065

Özgür, E., Afsar, N., De Vrije, T., Yücel, M., Gündüz, U., Claassen, P.A.M., Eroglu, I., 2010. Potential use of thermophilic dark fermentation effluents in photofermentative hydrogen production by Rhodobacter capsulatus. Journal of Cleaner Production 18, S23–S28. https://doi.org/10.1016/j.jclepro.2010.02.020

Pott, R.W.M., Howe, C.J., Dennis, J.S., 2014. The purification of crude glycerol derived from biodiesel manufacture and its use as a substrate by Rhodopseudomonas palustris to produce hydrogen. Bioresource Technology 152, 464–470. https://doi.org/10.1016/j.biortech.2013.10.094

Rosen, C., Jeppsson, U., n.d. Aspects on ADM1 implementation within the BSM2 framework.

Ross, B.S., Pott, R.W.M., 2022. Investigating and modeling the effect of light intensity on *Rhodopseudomonas palustris* growth. Biotech & Bioengineering 119, 907–921. https://doi.org/10.1002/bit.28026

Ross, B.S., Pott, R.W.M., 2021. Hydrogen production by immobilized Rhodopseudomonas palustris in packed or fluidized bed photobioreactor systems. International Journal of Hydrogen Energy 46, 1715–1727. https://doi.org/10.1016/j.ijhydene.2020.10.061

Shabbani, H.J.K., Othman, M.R., Al- Janabi, S.K., Barron, A.R., Helwani, Z., 2024. H2 purification employing pressure swing adsorption process: Parametric and bibliometric review. International Journal of Hydrogen Energy 50, 674–699. https://doi.org/10.1016/j.ijhydene.2023.11.069

Sharma, A., Dahiya, P., 2023. Characterization of wastewater and effluents remediation through nanotechnology for efficient reclamation and reuse, in: Emerging Technologies in Applied and Environmental Microbiology. Elsevier, pp. 65–83. https://doi.org/10.1016/B978-0-323-99895-6.00009-5

Singh, N., Sarma, S., 2022. Biological routes of hydrogen production: a critical assessment, in: Handbook of Biofuels. Elsevier, pp. 419–434. https://doi.org/10.1016/B978-0-12-822810-4.00021-X

Tao, Y., 2008. Characteristics of a new photosynthetic bacterial strain for hydrogen production and its application in wastewater treatment. International Journal of Hydrogen Energy 33, 963–973. https://doi.org/10.1016/j.ijhydene.2007.11.021

Tian, X., Liao, Q., Zhu, X., Wang, Y., Zhang, P., Li, J., Wang, H., 2010. Characteristics of a biofilm photobioreactor as applied to photo-hydrogen production. Bioresource Technology 101, 977–983. https://doi.org/10.1016/j.biortech.2009.09.007

Turton, R., Shaeiwitz, J.A., Bhattacharyya, D., Whiting, W.B., 2018. Analysis, synthesis, and design of chemical processes, Fifth edition. ed, Prentice Hall international series in the physical and chemical engineering sciences. Prentice Hall, Boston Columbus Indianapolis New York San Francisco Amsterdam.

Uyar, B., Eroglu, I., Yucel, M., Gunduz, U., Turker, L., 2007. Effect of light intensity, wavelength and illumination protocol on hydrogen production in photobioreactors. International Journal of Hydrogen Energy 32, 4670–4677. https://doi.org/10.1016/j.ijhydene.2007.07.002

Van Niel, C.B., 1944. THE CULTURE, GENERAL PHYSIOLOGY, MORPHOLOGY, AND CLASSIFICATION OF THE NON-SULFUR PURPLE AND BROWN BACTERIA. Bacteriol Rev 8, 1–118. https://doi.org/10.1128/br.8.1.1-118.1944

Wang, J., Wan, W., 2009. Factors influencing fermentative hydrogen production: A review. International Journal of Hydrogen Energy 34, 799–811. https://doi.org/10.1016/j.ijhydene.2008.11.015

Wang, Y.-Z., Liao, Q., Zhu, X., Tian, X., Zhang, C., 2010. Characteristics of hydrogen production and substrate consumption of Rhodopseudomonas palustris CQK 01 in an immobilized-cell photobioreactor. Bioresource Technology 101, 4034–4041. https://doi.org/10.1016/j.biortech.2010.01.045

Werber, J.R., Deshmukh, A., Elimelech, M., 2016. The Critical Need for Increased Selectivity, Not Increased Water Permeability, for Desalination Membranes. Environ. Sci. Technol. Lett. 3, 112–120. https://doi.org/10.1021/acs.estlett.6b00050

Xie, G.-J., Liu, B.-F., Xing, D.-F., Ding, J., Nan, J., Ren, H.-Y., Guo, W.-Q., Ren, N.-Q., 2012. The kinetic characterization of photofermentative bacterium Rhodopseudomonas faecalis RLD-53 and its application for enhancing continuous hydrogen production. International Journal of Hydrogen Energy 37, 13718–13724. https://doi.org/10.1016/j.ijhydene.2012.02.168

Lide, D. (2001). CRC Handbook of Chemistry and Physics, 82nd edition. CRC Press, Boca Raton, FL, USA.

Eastman, J.A. and Ferguson, J.F. (1981). Solubilization of particulate organic carbon during the acid phase of anaerobic digestion. J. Wat. Poll. Cont. Fed. 53, 352–366.

Web sites

[1] IPCC. AR6synthesis report: climate change. 2023. n.d, https://www.ipcc.ch/report/sixth-assessment-report-cycle/. (Accessed: 29 August 2024).

[2] IEA. Net zero by 2050 e analysis. n.d, https://www.iea.org/reports/net-zero-by-2050 (Accessed: 29 August 2024).

[3] Chemical Engineering. Plant Cost Index, https://www.chemengonline.com/site/plant-cost-index/ (Accessed: 10 September 2024)

[4] ECHEMI, Acetic acid international price, https://www.echemi.com/pip/acetic-acid-temppid160628000977.html (Accessed: 29 September 2024)

[5] INTRATEC, Propionic acid prices, https://www.intratec.us/chemical-markets/propionic-acid-price (Accessed: 29 September 2024)

[6] ChemAnalyst, Butyric acid prices, https://www.chemanalyst.com/Pricing-data/butyric-acid-1250 (Accessed: 29 September 2024)

[7] OECD, "Effective Carbon Rates 2022.", https://www.oecd.org/content/dam/oecd/en/topics/policy-sub-issues/carbon-pricing-and-energy-taxes/effective-carbon-rates-2021-brochure.pdf (Accessed: September 29, 2024)